Journal of Low Temperature Physics, Vol. 109, Nos. 1/2, 1997

Review

Slip in Quantum Fluids

Dietrich Einzel[1] and Jeevak M. Parpia[2]

[1] *Walther-Meissner-Institut für Tieftemperaturforschung, D-85748 Garching, Germany*
[2] *Department of Physics, Cornell University, Ithaca, NY 14853, U.S.A*

(Received October 16, 1996; revised June 2, 1997)

In this review we describe theoretical and experimental investigations of general slip phenomena in context with the flow of the quantum liquids ^{3}He, ^{4}He and their mixtures at low temperatures. The phenomenon of slip is related to a boundary effect. It occurs when sufficiently dilute gases flow along the wall of an experimental cell. A fluid is said to exhibit slip when the fluid velocity at the wall is not equal to the wall's velocity. Such a situation occurs whenever the wall reflects the fluid particles in a specular-like manner, and/or if the fluid is describable in terms of a dilute ordinary gas (classical fluid) or a dilute gas of thermal excitations (quantum fluid). The slip effect in quantum fluids is discussed theoretically on the basis of generalized Landau–Boltzmann transport equations and generalized to apply to a regime of ballistic motion of the quasiparticles in the fluid. The central result is that the transport coefficient of bulk shear viscosity, which typically enters in the Poiseuille flow resistance and the transverse acoustic impedance, has to be replaced by geometry dependent effective viscosity, which depends on the details of the interaction of the fluid particles with the cell walls. The theoretical results are compared with various experimental data obtained in different geometries and for both Bose and Fermi quantum fluids. Good agreement between experiment and theory is found particularly in the case of pure normal and superfluid ^{3}He, with discrepancies probably arising because of deficiencies in characterization of the experimental surfaces.

1. INTRODUCTION

Slip is a boundary effect in the hydrodynamic flow of fluids, i.e. liquids or gases, that occurs at the border between its microscopic and mesoscopic or macroscopic description. In order to make this explicit we start with a conventional description of hydrodynamic fluid flow by specifying the mass

0022-2291/97/1000-0001$12.50/0

density ρ and the transport coefficient of shear viscosity η. In a typical experimental arrangement that aims at the determination of the shear viscosity, one measures the damping and the period shift of a torsional oscillator due to the presence of the fluid, which is entrained in a flow channel of width d, oscillating at a frequency ω with a velocity v^{ext}. If such an oscillator performs a purely transverse motion, the walls of the cell exert a shear force on a fluid layer with a typical thickness $\delta(\omega) = (2\eta/\rho\omega)^{1/2}$, the viscous penetration or skin depth. The lengths d and δ characterize the bulk features of the experimental arrangement.

The dynamic regimes of fluid motion can be classified according to the ratio of the viscous skin depth δ and the size d of the measuring cell:

(i) If $\delta \gg d$ the fluid is clamped in the flow channel and may at most exhibit a macroscopic velocity field with parabolic profile. Therefore this regime is referred to as the clamped or Poiseuille flow regime. The cross sectional average of the velocity field relative to the walls is known to be directly related to the inverse bulk shear viscosity η via Hagen–Poiseuille's law[1]

$$\langle v \rangle = \frac{\rho d^2}{12\eta}(-i\omega)\, v^{\text{ext}} \tag{1}$$

(ii) In the opposite limit $\delta \ll d$, the so-called open regime, the surfaces of the measuring cell drag along only a fluid layer of thickness δ. In this case one measures the complex transverse surface impedance $Z_\perp(\omega)$, which is defined as the ratio of the shear stress Π_{xz} at the surface and the boundary velocity v^{ext} [2]

$$Z_\perp(\omega) \equiv \frac{\Pi_{xz}(0,\omega)}{v^{\text{ext}}} = R - iX = (1-i)\frac{\eta}{\delta} = (1-i)\sqrt{\frac{\rho\omega\eta}{2}} \tag{2}$$

As can be seen from (1) and (2), both types of experiments allow for the determination of the shear viscosity η. This determination is obscured, however, by a phenomenon which typically occurs in the dilute limit of classical gases and at low temperatures in quantum fluids and which is referred to as the velocity slip effect.

The phenomenon of slip sets in when the fluid acquires the capability of sliding along walls. The importance of slip can be physically expressed in a new length ζ_0, the so called slip length, which in general depends on temperature and the details of the momentum exchange between the fluid particles and the wall. The slip length is the distance at which the velocity field, if extrapolated into the wall, vanishes. In context with phenomenological hydrodynamical theory it is commonly introduced by relating the

component $\mathbf{v}_\perp$ of the macroscopic fluid velocity field along the surface tangent at the wall and its spatial derivative $\mathbf{v}'_\perp$ normal to the surface in a boundary condition[3]

$$\mathbf{v}_\perp(\text{wall}) = \zeta_0 \mathbf{v}'_\perp(\text{wall}) \tag{3}$$

We shall demonstrate in Sec. 4, that the slip length is of the order of the (viscous) transport mean free path λ_η of the fluid particles.

$$\zeta_0 = a\lambda_\eta \tag{4}$$

Hence, if the fluid can be made more and more dilute, a so-called Knudsen layer with a finite thickness of the order of the viscous mean free path λ_η, is formed near the walls. The fluid particles move essentially ballistically in the Knudsen layer. The flow channel then effectively becomes wider which in turn allows the fluid to slip and move with nonvanishing velocity at the wall. In Eq. (4) a is the so-called slip coefficient, which is defined as the ratio of the slip length to the viscous mean free path. In general a contains the information about the interaction of the fluid particles with the wall. For a classical Maxwell–Boltzmann gas and diffuse scattering at the wall $a_d = 1.126$,[4] whereas for a Fermi liquid $a_d = 0.5819$,[5] to give only two examples for the case of diffuse scattering of fluid particles off a flat surface. The importance of slip can be measured by introducing the so-called Knudsen number $\text{Kn} = \lambda_\eta/d$. In a strict hydrodynamic description one would treat the slip length as the smallest length in the problem and neglect it, $\text{Kn} = 0$, which leads to $\mathbf{v}_\perp = 0$ as the standard hydrodynamic boundary condition. In this sense Eq. (3) is a *first order correction* to hydrodynamics with respect to an expansion in small ratios ζ_0/d or ζ_0/δ. This is, however, not the general case. If a fraction $0 \leqslant s < 1$ of fluid particles undergoes specular reflection at the surface, the slip coefficient can be shown to be enhanced with respect to its value for diffuse scattering

$$a(s) = a\frac{1+s}{1-s} \tag{5}$$

the enhancement being described by a phenomenological specularity coefficient s.

From this we may conclude that the phenomenon of slip occurs in two distinct situations:

(i) When fluids can be made more and more dilute. Examples are dilute classical gases such as air, carbon dioxide or hydrogen, or dilute

gases of thermal excitations in quantum liquids in the extreme low temperature limit such as phonons and rotons in superfluid ^{4}He (He–II) or Landau– and Bogoliubov quasiparticles in normal and superfluid ^{3}He.

(ii) When the walls act more and more as mirrors, i.e., when they scatter the fluid particles in a specular–like manner. An example is liquid ^{3}He in a vessel covered with a superfluid ^{4}He film.

The slip effect will be shown below to affect Hagen–Poiseuille's law (Eq. (1)) in that the bulk shear viscosity η gets replaced by an effective viscosity η_{eff}. η_{eff} depends explicitly on the size and geometry of the measuring cell and, as will turn out later, on the details of the fluid–particle–wall scattering process:

$$\langle v \rangle = \frac{\rho d^2}{12\eta_{\text{eff}}}(-i\omega)\, v^{\text{ext}}; \qquad \eta_{\text{eff}} = \eta \frac{d}{d + c\zeta_0} \tag{6}$$

As a consequence of fluid slip, the effective viscosity η_{eff} is, in general, smaller than the bulk viscosity η. The quantity c depends on the geometry of the flow channel ($c = 4$ and 6 for cylinders and parallel plates, respectively).

The complex transverse surface impedance $Z_\perp(\omega)$ (cf. Eq. (2))[2] is affected by slip effects in that the bulk viscous penetration depth changes into an effective (and in general larger) length, which in turn can be expressed by two effective viscosities $\eta_{1\text{eff}}$ and $\eta_{2\text{eff}}$:

$$Z_\perp(\omega) = R - iX = \frac{(1-i)\,\eta}{\delta + (1-i)\,\zeta_0} \equiv \sqrt{\frac{\rho\omega\eta_{1\text{eff}}}{2}} - i\sqrt{\frac{\rho\omega\eta_{2\text{eff}}}{2}}$$

$$\eta_{1\text{eff}} = \eta \frac{(1 + 2(\zeta_0/\delta))^2}{[1 + 2(\zeta_0/\delta) + 2(\zeta_0/\delta)^2]^2}; \qquad \eta_{2\text{eff}} = \eta \frac{1}{[1 + 2(\zeta_0/\delta) + 2(\zeta_0/\delta)^2]^2} \tag{7}$$

The traditional picture of fluid flow with slip developed so far involves effective viscosities only: η_{eff} for the case of Poiseuille flow and $\eta_{1\text{eff}}$, $\eta_{2\text{eff}}$ for the case of the transverse surface impedance, as corrected for the slip length ζ_0, which is calculated from microscopic theory. In the framework of such a theory, all slip effects vanish in the hydrodynamic (low frequency, high temperature) limit. They enter as a first order correction for small but finite Knudsen number Kn. If $\text{Kn} \geqslant 1$, the slip description is no longer adequate and has to be generalized to one that includes all orders in Kn.

In classical gases, it was found already in 1875 by Kundt and Warburg[6] that experiments on oscillating discs could be interpreted correctly only if one assumed that the gas "slips" at the wall. In 1879 Maxwell[7] put forward a kinetic slip theory in which, for the first time, the slip length was related in an approximate way to the mean free path. The slip boundary

condition was used extensively during the development of vacuum technology in the following decades. Knudsen and his collaborators[8] realized that the slip boundary condition, which introduces slip only as a first order correction to hydrodynamics, does not adequately describe the flow of a rarefied gas when the bulk mean free path becomes comparable or considerably larger than the typical dimensions of the vessel in which the flow takes place. Considerable effort was spent in developing more accurate descriptions of the slip phenomenon and the fluid flow of rarefied classical gases. Starting from a model Boltzmann equation and imposing a simple surface scattering boundary condition (such as for purely diffuse scattering), the integral equation for the flow velocity of a rarefied Boltzmann gas was derived[9] and solved approximately or numerically for certain geometrically simple types of flow such as Couette and plane Poiseuille flow. The integral equation for the slip length, in particular, was analyzed by Welander[10] and used by Willis[4] and Albertoni *et al.*[11] to derive the numerical value of the slip coefficient a for a classical Boltzmann gas.

The class of systems which is of particular interest for us is that of liquid helium with its isotopes ^{3}He (Fermi liquid) and ^{4}He (Bose liquid). For these systems, complicated vacuum techniques are not required in order to observe dilute gas behavior because at low temperatures the transport properties of liquid helium are those of a rarefied gas of thermal excitations or quasiparticles, obeying quantum statistics.

Generally speaking, the problem of mean free path effects in quantum liquids has received less attention, despite considerable effort that has been devoted to the transport properties, especially shear viscosity of liquid ^{4}He and ^{3}He. Most experiments in the past have been performed in the regime of low Knudsen numbers. But with lower and lower temperatures becoming available, the effects of boundaries on the flow properties of the helium liquids became increasingly important.

We will demonstrate that in liquid helium the elementary excitations become a dilute gas at low temperature and their the mean free path may be increased in nearly all cases by decreasing the temperature. One can then always reach a regime in which mean free path or finite size effects become important by just lowering the temperature. This is, of course, not always a simple problem to achieve from the cryotechnical point of view, particularly in the case of liquid ^{3}He with the Fermi liquid behavior setting in only well below about 100 mK, and where superfluidity occurs in the region below a few mK. Therefore finite size effects in the quantum superfluid ^{3}He have been studied extensively and systematically only after the early eighties.

In order to deal with quantum fluids such as ^{3}He and ^{4}He at low temperatures, a generalized gas dynamics, applicable to any gas of thermal

excitations that obey any statistics has to be developed. The presence of boundaries will have to be incorporated via a general boundary condition for the scattering of quasiparticles off the wall to ensure that the description is valid at arbitrary Knudsen numbers. The theoretical part of this review deals with precisely this problem, where we focus on the description of normal and superfluid ^{3}He and results for the ^{4}He counterpart can be, at least on the level of a phenomenological description, taken over from these general results.

The review is organized as follows:

In Sec. 2 we summarize results for the shear viscosity associated with elementary excitations from the normal and superfluid Fermi quantum liquids ^{3}He and ^{3}He–B (Landau– and Bogoliubov quasiparticles) and the superfluid Bose quantum liquid ^{4}He (phonons and rotons) on a phenomenological basis. The discussion is restricted to quantum fluids in an infinitely extended volume.

The Secs. 3–6 are devoted to readers interested in theoretical details of the calculation of the bulk shear viscosity of an isotropic Fermi superfluid and the extension of such a calculation to include finite size effects induced by the surfaces of the experimental measuring cell.

In Sec. 3 we establish a quasiclassical description of an isotropic superfluid Fermi system starting from a microscopic Nambu-matrix kinetic equation. The coefficient of bulk shear viscosity for Bogoliubov quasiparticles emerges as a result of this section.

In Sec. 4 we explain why the presence of surfaces induces slip of the fluid velocity whenever the excitation mean free path is finite. The leading order slip correction to the hydrodynamic result for the viscosity is calculated for the simplest law of diffuse boundary scattering. The microscopic calculation of the slip length in Fermi quantum liquids is then extended to incorporate a general class of wall boundary conditions which include specular and backward scattering as well as Andreev scattering in the case of a Fermi superfluid.

In Sec. 5 we discuss the experimental relevance of the slip effect in that we derive and solve the phenomenological equations of hydrodynamic fluid motion amended by a slip boundary condition, which accounts for the mean free path effect in first order only. This description is applied to various experimentally relevant flow geometries.

In Sec. 6 the concept of slip, which only accounts for leading order corrections in ζ_0/d or ζ_0/δ, is generalized to arbitrary Knudsen numbers or ratios of the mean free path and the viscous penetration depth. In order to keep this discussion on a tractable level, we limit ourselves to two cases:

(i) the "clamped" limit $d \ll \delta$, for which we discuss a microscopic treatment of the problem of Poiseuille flow in a Fermi superfluid in a parallel plate geometry. An expression for an effective viscosity, observable in stationary Poiseuille flow experiments, Eq. (6), is generalized so that it is valid at arbitrary Knudsen numbers.

(ii) the "open" limit $d \gg \delta$ for which we discuss the problem of the quantum superfluid bounded by a single oscillating plane. The result is the transverse surface impedance for arbitrary ratios λ_η/δ of the mean free path and the viscous penetration depth, which generalizes Eq. (7), so that it is valid at arbitrary ζ_0/δ.

Sections 7–10 deal with the experimental observations of the slip effect in the ^{3}He and ^{4}He quantum liquids and their mixtures. Both the simple slip effect, represented by Eqs. (6) and (7) as well as observable deviations from it at finite and even large Knudsen numbers will be discussed.

Section 7 is concerned with experimental results that expose the effects of finite mean free path on fluid flow in normal fluid ^{3}He at low temperatures i.e. the slip effect of Landau quasiparticles. In Sec. 8 we treat the comparison of theory and experiment for the superfluid B-phase of ^{3}He. In this case, due to the constant energy gap in the excitation spectrum of Bogoliubov quasiparticles, mean free path and Knudsen flow phenomena are particularly pronounced.

Section 9 reviews the experimental situation in ^{3}He–^{4}He mixtures and in Sec. 10 we finally describe the experimental situation in pure ^{4}He, i.e. the slip-related effects of phonon and roton excitations.

Section 11 is devoted to our summary and conclusions.

2. GAS-KINETIC DESCRIPTION OF ELEMENTARY EXCITATIONS IN QUANTUM LIQUIDS

In this section we discuss the bulk shear viscosity associated with the (dilute) gas of elementary excitations from the quantum Bose liquid ^{4}He and Fermi liquid ^{3}He, which enters the expression for the Poiseuille flow impedance (6) and the transverse surface impedance (7). We focus primarily on the most important thermal excitations, namely the phonons and rotons in ^{4}He, the Landau quasiparticles in normal ^{3}He and the Bogoliubov quasiparticles in superfluid ^{3}He. Starting from their energy dispersion, we calculate the number and normal fluid densities, the mean free paths and deduce a gas–kinetic expression for the bulk shear viscosity.

Let us begin with a description of the quantum liquid ^{4}He at below 4K. Its superfluid phase (He–II) was discovered in 1924 by Heike Kamerlingh Onnes.[12] In context with our general aim we are interested in the properties

of the thermal excitations from He-II, the phonons and the rotons. The phonons characterize the low energy part of the spectrum ε_k of elementary excitations:

$$\varepsilon_k = c_1 \hbar k \tag{8}$$

of the interacting Bose liquid, with c_1 the first sound velocity. The Bose–Einstein statistics of the ^{4}He atoms is reflected in the equilibrium momentum (Planck) distribution function

$$n^0_{\rm ph}(\varepsilon_k) = \frac{1}{\exp(\varepsilon_k / k_{\rm B} T) - 1} \tag{9}$$

from which the mean number density $N_{\rm ph}$ of phonons

$$N_{\rm ph} = \sum_k n^0_{\rm ph}(\varepsilon_k) = \frac{48\pi}{5} \left(\frac{k_{\rm B} T}{2\pi \hbar c_1} \right)^3 \tag{10}$$

can be deduced. The phonons contribute to the local mass current $\mathbf{g}^{\rm n} = \rho^{\rm n} \mathbf{v}^{\rm n}$ through their normal fluid mass density as follows:

$$\rho^{\rm n}_{\rm ph} = \frac{\pi^4}{27} \frac{k_{\rm B} T}{c_1^2} N_{\rm ph} \tag{11}$$

A measure for the mean free path of the phonons is the quantity

$$\lambda_{\rm ph} = c_1 \tau_{\rm ph}; \qquad \tau_{\rm ph} = \frac{1}{(1/\tau_{\rm pr}) + (1/\tau_{\rm pp})} \tag{12}$$

Here $\tau_{\rm pr}$ and $\tau_{\rm pp}$ are the characteristic times for phonon–roton and phonon–phonon collision processes, respectively.[13] Finally, the phononic contribution to the bulk shear viscosity is given by the gas-kinetic expression

$$\eta_{\rm ph} = \frac{1}{5} \rho^{\rm n}_{\rm ph} c_1 \lambda_{\rm ph} = \frac{\pi^4}{135} k_{\rm B} T N_{\rm ph} \tau_{\rm ph} \tag{13}$$

The phonons play a dominant role at temperatures below 0.6 K whereas for $T > 1K$ a second kind of excitation, the so-called rotons, become important. They are characterized by the dispersion near the minimum of Landau's excitation spectrum:

$$\varepsilon_k = \Delta + \frac{\hbar^2 (k - k_0)^2}{2 m_{\rm r}} \tag{14}$$

with m_r the effective roton mass, Δ the roton gap and $p_0 = \hbar k_0$ the momentum characterizing the minimum in the roton dispersion. The equilibrium distribution of rotons $n_r^0(\varepsilon_k)$ is of the form (9) with ε_k taken from (14). In thermal equilibrium the number N_r of rotons is given by

$$N_r = \sum_k n_r^0(\varepsilon_k) = \frac{2p_0^2}{(2\pi)^{3/2}} \frac{\sqrt{m_r k_B T}}{\hbar^3} e^{-\Delta/k_B T} \tag{15}$$

The roton mass current can be expressed by the roton contribution to the normal fluid density

$$\rho_r^n = \frac{2}{3} \frac{p_0^2/2m_r}{k_B T} m_r N_r \tag{16}$$

The mean free path λ_r of rotons can be written as

$$\lambda_r = \bar{v}_r \tau_r; \qquad \bar{v}_r = \sqrt{\frac{k_B T}{m_r}}; \qquad \frac{1}{\tau_r} = \frac{1}{\hbar} \frac{|V_0|^2}{p_0^2/2m_r} N_r k_0^3 \tag{17}$$

Here $\bar{v}_r$ is the root mean square roton velocity, τ_r^{-1} is a collision rate as obtained from elastic roton–roton scattering processes, with an amplitude V_0, which specifies the interaction of the rotons. The rotons contribution to the bulk shear viscosity is a constant due to compensation of exponential factors in the roton number density and the lifetime:

$$\eta_r = \frac{1}{5} \rho_r^n \bar{v}_r \lambda_r = \frac{2}{15} \frac{p_0^2}{2m_r} N_r \tau_r = \frac{2}{15} \frac{\hbar}{k_0^3} \left(\frac{p_0^2/2m_r}{|V_0|} \right)^2 \tag{18}$$

The total bulk viscosity η_n^{tot} of the system of thermal excitations (normal component) from He–II is given by the sum of the phonon and roton contributions

$$\eta_n^{tot} = \eta_{ph} + \eta_r \tag{19}$$

Thus, in ^{4}He, there are two dilute gases which are responsible for momentum transport. The roton contribution is essentially constant at temperatures below about 0.8 of T_c since the number of rotons decreases exponentially with temperature while their mean free path increases exponentially, the two dependencies thus cancel one another, as can be seen from Eq. (18) above. Thus the pure roton contribution to the viscosity is a constant at low temperatures, as can be expected because the dominant scattering mechanism of the rotons is by other rotons.

The phonon contribution gives rise to an approximately exponential increase in the viscosity at low temperatures. This happens because the flux of phonons is mainly scattered by the heavier rotons. Since the phonon number varies as a power law, and the rotons have an exponentially increasing mean free path, the viscosity increases exponentially. The combined behavior of the phonon and roton contributions to the viscosity is summarized in Fig. 1 in which we show a plot of η_n^{tot} vs. temperature. In this figure, experimental determinations of the viscosity from capillary flow can be compared to theoretical results corrected for slip at the walls. The low temperature rise in the viscosity is due to the phononic contribution to η_n^{tot}.

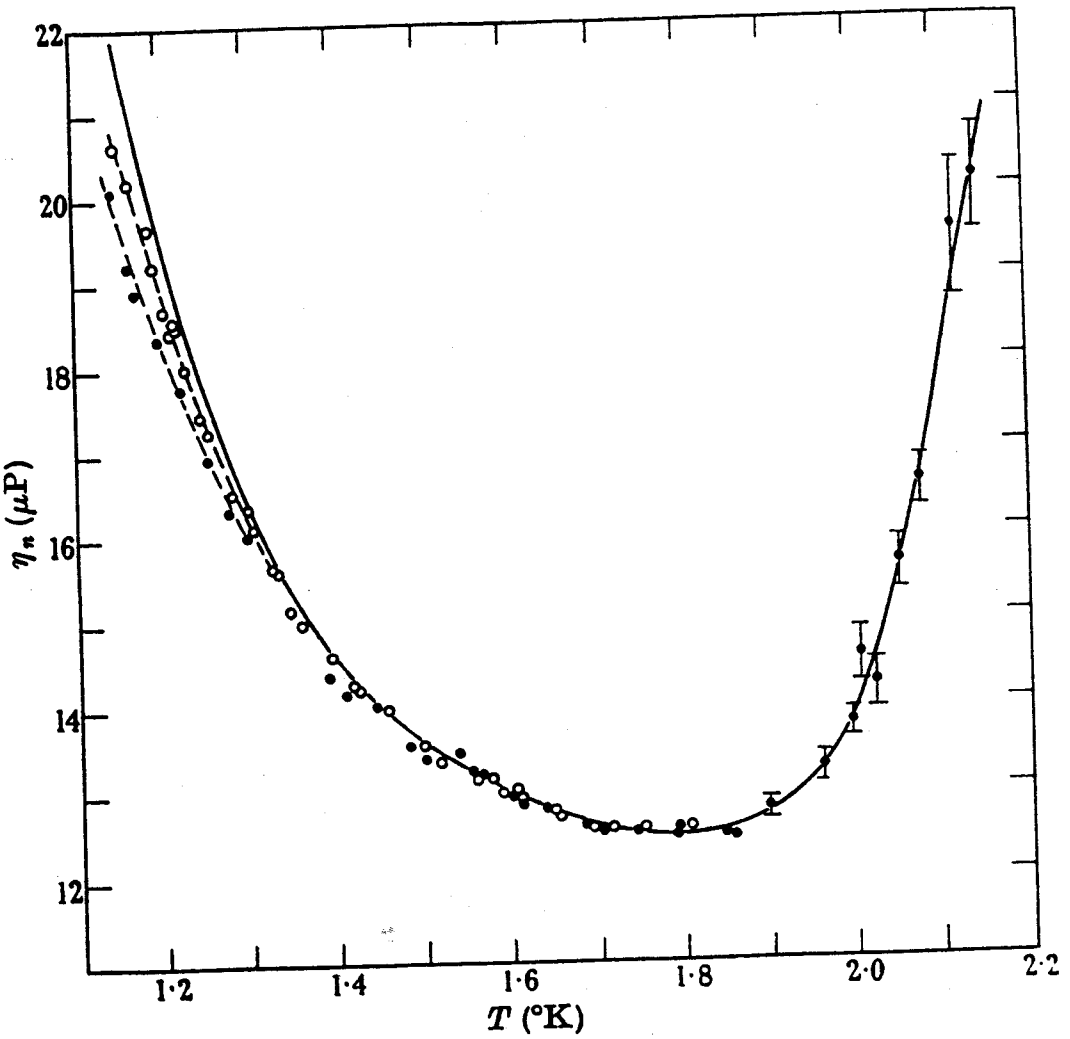

Fig. 1. Viscosity of the normal component of superfluid He–II vs. temperature in K. Shown are the data by Brewer and Edwards (Ref. 112) who measured capillary flow in 52 μm (●) and 107.6 μm diameter capillaries (○). Full line: viscosity corrected for slip.[112]

Next we turn to the Fermi liquid ^{3}He in its normal state. Near the Fermi surface the quasiparticle excitation spectrum is given by

$$\varepsilon_k = \mu + v_F^* \hbar(k - k_F) = \xi_k + \mu \tag{20}$$

with μ the chemical potential, k_F the Fermi wave number, $v_F^* = \hbar k_F / m^*$ the Fermi velocity and m^* the (pressure dependent) effective mass of the Landau quasiparticles.

The thermal equilibrium momentum distribution of the quasiparticles is the Fermi–Dirac function

$$n_k^0 = n^0(\xi_k) = \frac{1}{\exp(\xi_k / k_B T) + 1} \tag{21}$$

from which the total number density follows as the sum

$$n = \sum_{k\sigma} n_k^0$$

The number density n_q of thermal excitations at finite temperature from the Fermi system can be obtained from a Fermi–Dirac function $n^0(|\xi|)$ in which particle- and hole-like branches of the excitation spectrum are taken to have positive energy:

$$n_q(T) = \sum_{k\sigma} n^0(|\xi_k|) = 3n \ln 2 \frac{k_B T}{\mu} \tag{22}$$

The quasiparticle collision rate

$$\frac{1}{\tau_k} = \frac{1}{\tau_N(\xi_k, T)} = \frac{\langle W \rangle_a}{32\hbar} \frac{\xi_k^2 + (\pi k_B T)^2}{\mu} \tag{23}$$

vanishes near the Fermi surface in the zero temperature limit. Here $\langle W \rangle_a$ is the Fermi surface average of the dimensionless scattering cross section for two–particle scattering. A measure of the quasiparticle mean free path is given by

$$\lambda = v_F^* \bar{\tau}; \qquad \bar{\tau} = \frac{1}{\int_{-\infty}^{\infty} d\xi_k \varphi_k / \tau_k} = \frac{3}{4} \tau_N(0, T) \tag{24}$$

Here $\varphi_k = -\partial n_k^0 / \partial \xi_k$ is the derivative of the Fermi function and $\bar{\tau} \propto T^{-2}$ is the energy–average of the quasiparticle lifetime (23), which diverges in

the limit of low temperatures as does the mean free path λ. The shear viscosity of normal liquid ^{3}He can be written as

$$\eta = \frac{1}{5}\left(\rho \frac{m^*}{m}\right) v_F^* \lambda_\eta = \frac{1}{5} n p_F \lambda_\eta \tag{25}$$

Here λ_η is the viscous transport mean free path, which differs from the quasiparticle mean free path λ by (vertex) corrections of $\ell = 2$ (stress tensor) symmetry, as will be shown in Sec. 3. The shear viscosity of liquid ^{3}He can thus become very large at low temperatures and eventually be comparable to that of machine oil.

The transport coefficients for the viscosity of ^{3}He were calculated by many groups[14–16] using a variety of techniques. As it turns out, initial theoretical estimates of the viscosity coefficient were about 75% of the experimental values, but the pressure dependence of the viscosity was very well reproduced. Finite temperature corrections[17] and fluctuation precursors to the superfluid transition[18] were also calculated. Very recently, there have been measurements[19] that show good agreement with the fluctuation theory of Emery and these results will be discussed in Sec. 7. Finite temperature effects (at least of the form predicted in Ref. 17) have not been measured accurately in any experiment to date.

Measurements of the viscosity of ^{3}He were carried out soon after ^{3}He became available for research by Zinoveva,[20] though the temperature range was limited. The viscosity of ^{3}He in the normal phase below 0.1 K was measured over a wide range of temperature by Abel, Anderson, and Wheatley[21] at low pressure. The probe they employed was the attenuation of high frequency sound in the fluid. Similar measurements at higher temperatures were carried out by Betts, Osborne, Welber, and Wilks.[22] These measurements agreed very well with one another and also with the next series of results also at low pressure by Bertinat *et al.*[23] and Black, Hall, and Thompson.[24] The viscosity at higher pressure was inferred from zero sound attenuation measured by Paulson and others at La Jolla.[25] Measurements were also carried out at the melting pressure by Alvesalo *et al.*[26] and by the Cornell group.[27] All of these measurements appeared to follow a weakly pressure-dependent behavior. The pressure dependence which was summarized in the review by Wheatley[28] did not reproduce the dependence calculated from theory. However, theory and experiment did agree at low pressure. It was not until a single viscometer was used to study the entire pressure range that the strongly pressure dependent nature of the viscosity was measured by Parpia, Sandiford, Berthold, and Reppy.[29, 30] It is this result that agrees with pressure dependence predicted

by theory with the exception that the experimental viscosity is always greater than the calculated one by a factor of approximately 1.3.

Finally we turn to the discussion of a neutral pair-correlated superfluid namely superfluid ^{3}He–B. This is one of the superfluid phases of liquid ^{3}He which were discovered by Osheroff, Lee, and Richardson,[31] and for which they were awarded the 1996 Nobel Prize for Physics. In the superfluid phase, the quasiparticle excitation spectrum

$$E_k = \sqrt{\xi_k^2 + \Delta_k \Delta_k^\dagger} \tag{26}$$

is characterized by a pseudoisotropic gap matrix, first discussed by Balian and Werthamer[32]

$$\Delta_{k\sigma_1\sigma_2} = \Delta(T)\{\vec{\tau} i\tau^y\}_{\sigma_1\sigma_2} \cdot \vec{R}[\hat{\mathbf{n}}, \theta] \cdot \hat{\mathbf{k}} \tag{27}$$

Here the matrix $\vec{R}[\hat{\mathbf{n}}, \theta]$ describes a rotation of the orbital relative to the spin degrees of freedom of the order parameter and $\vec{\tau} \equiv \{\tau^x, \tau^y, \tau^z\}$ is the vector formed with the Pauli spin matrices. From (27) one observes that $\Delta_k \Delta_k^\dagger = \Delta^2(T)\,\mathbf{1}$, therefore in this pairing state mean free path effects can be expected to become particularly pronounced because of the constant gap $\Delta(T)$ in the excitation spectrum. The second, so-called A-phase,[33, 34] has an energy gap $\Delta(\hat{\mathbf{k}})$ of axial symmetry, with two point nodes on the Fermi surface. This pairing state will not be considered further.

The equilibrium distribution of Bogoliubov quasiparticles reads

$$v_k^0 = v^0(E_k) = \frac{1}{\exp(E_k/k_B T) + 1} \tag{28}$$

and can be used to compute the average number density of thermally excited quasiparticles:

$$n_q(T) = \sum_{k\sigma} v_k^0 \overset{T \to 0}{=} 3n \ln 2 \frac{k_B T}{\mu} \lim_{T \to 0} Y_0(T) \tag{29}$$

with $Y_0(T)$ the lowest order quasiparticle Yosida function

$$Y_n(T) = \int_{-\infty}^{\infty} d\xi_k \left(-\frac{\partial v_k^0}{\partial E_k} \right) \left| \frac{\xi_k}{E_k} \right|^n \tag{30}$$

The mass current $\mathbf{g}^n = \rho^n \mathbf{v}^n$ of the Bogoliubov quasiparticles is characterized by the normal fluid density (to be derived in Sec. 3)

$$\rho^n(T) = \rho \frac{1 + F_1^s/3}{1 + (F_1^s/3)\, Y_0(T)} Y_0(T) \tag{31}$$

where F_1^s is the Landau interaction parameter which describes the effective mass enhancement $m^*/m = 1 + F_1^s/3$ of the Fermi liquid. The quasiparticle lifetime is complicated in structure and has been discussed in detail by Einzel and coworkers.[35] Its energy dependence can be approximated in the way shown in Appendix 1. Here we give only its asymptotic form in the low temperature limit

$$\lim_{T\to 0} \frac{1}{\tau(E_k, T)} = \frac{1}{\tau_N(T_c)} \cdot \frac{3w_0}{\sqrt{2\pi}} \sqrt{\frac{k_B T \Delta^3}{(k_B T_c)^4}} \exp\left(-\frac{\Delta}{k_B T}\right)$$

$$= \frac{1}{\tau_N(T_c)} \frac{3k_B T \Delta}{(k_B T_c)^2} \lim_{T\to 0} Y_0(T) \tag{32}$$

where $w_0 = O(1)$ is a (only weakly pressure dependent) dimensionless scattering parameter for superfluid ^{3}He–B. The mean free path of the Bogoliubov quasiparticles can be constructed from the root mean square velocity $\bar{V}$ and the energy averaged lifetime $\bar{\tau}$

$$\lambda = \bar{V}\bar{\tau}; \qquad \bar{V} = \sqrt{\frac{\int_{-\infty}^{\infty} d\xi_k (-\partial v_k^0/\partial E_k)(\xi_k^2/E_k^2)\, v_k^2}{\int_{-\infty}^{\infty} d\xi_k (-\partial v_k^0/\partial E_k)}};$$

$$\bar{\tau} = \frac{Y_0(T)}{\int_{-\infty}^{\infty} d\xi_k (-\partial v_k^0/\partial E_k)/\tau(E_k)} \tag{33}$$

The result for the shear viscosity of Bogoliubov quasiparticles can be written similar to the result of kinetic theory for dilute gases (cf. Eqs. (13) and (18)):

$$\eta(T) = \tfrac{1}{5}\rho_0^n \bar{V}\lambda_\eta = \tfrac{1}{5} n p_F Y_2(T)\, \lambda_\eta(T) \tag{34}$$

where $\rho_0^n = \rho(m^*/m)\, Y_0$ and λ_η is the viscous transport mean free path in the superfluid B-phase. Like in the case of the roton viscosity, the viscosity of the gas of Bogoliubov quasiparticles is seen to tend to a constant in the low temperature limit due to a compensation of temperature dependent factors $\rho_0^n \propto T^{-1/2} \exp(-\Delta/k_B T)$, $\bar{V} \propto T^{1/2}$ and $\lambda_\eta \propto \exp(\Delta/k_B T)$:

$$\lim_{T\to 0} \eta(T) = \frac{1}{5} n p_F v_F^* \tau_S; \qquad \tau_S = \frac{2\pi}{3w_0} \left(\frac{k_B T_c}{\Delta(0)}\right)^2 \tau_N(0, T_c) \tag{35}$$

In Fig. 2 we show a plot of the viscosity of Bogoliubov quasiparticles vs. reduced temperature, together with measured values of the viscosity taken with a torsion pendulum and with a vibrating wire all calculated or measured at 20 bar.

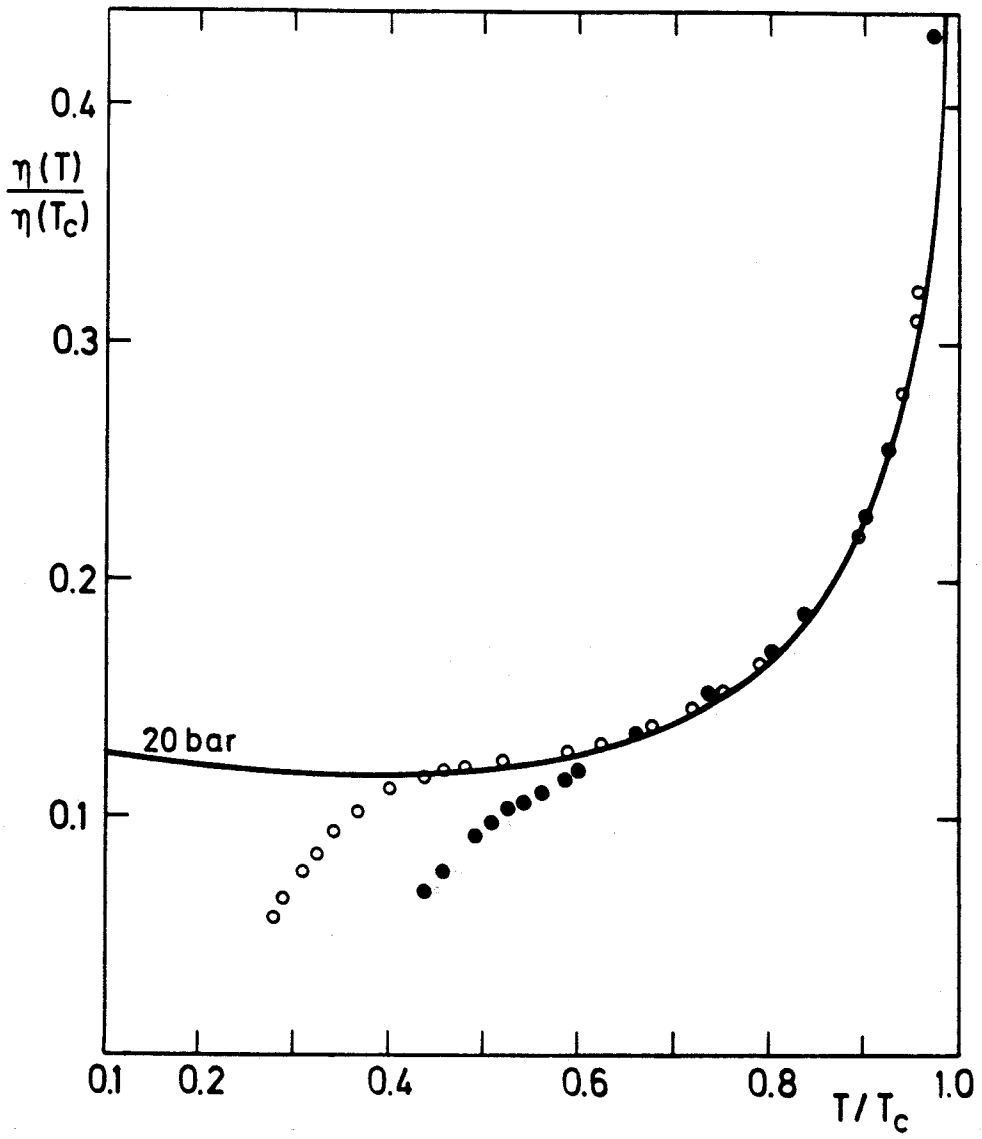

Fig. 2. Normalized shear viscosity of ^{3}He–B at 20 bar pressure vs. reduced temperature T/T_c. Full line: Theory; (●) torsional oscillator data by Archie *et al.*;[41] (○) vibrating wire data by Carless *et al.*[83] Neither set of experimental data has been corrected for slip.

The viscosity of ^{3}He in the B phase near the transition temperature was not measured directly till the work of Berthold *et al.*,[36] though there had been measurements of the heat flow from which the viscosity could be inferred.[37] The earliest measurements of the viscosity in the superfluid A phase were carried out by Alvesalo and co-workers using a vibrating wire at the meting curve pressure.[38] The results of Berthold *et al.* showed that the expected $(1-T/T_c)^{1/2}$ dependence of the reduced viscosity, $1-\eta/\eta_c$, did not hold until a region on the order of 10^{-3} of the reduced temperature. The measurements of Parpia *et al.*[29] extended over a larger pressure range

and were able to approach the transition temperature much more closely. These results showed that the reduced viscosity displayed a dominant $(1 - T/T_c)^{1/2}$ dependence as predicted by theory[39] but had significant contributions due to terms higher order in the gap.

All of these experiments also entered into the regime where a plateau in the viscosity was predicted.[40] The vibrating wire experiments[38] claimed to have observed the predicted increase in viscosity towards zero temperature, though this finding is most likely due to errors in the determination of the superfluid fraction. Subsequent measurements (for example Archie and co-workers[41]) in the B phase could not observe the minimum in the viscosity. The results of the experiments were dominated by the long mean free paths and exhibit the "droop" in the reduced viscosity at low temperatures. This feature will be addressed in some detail in the text that follows.

The situation in the quantum fluids with their dilute excitations and long mean free paths at low temperatures is one in which the Knudsen number can easily exceed unity. This is illustrated in the plot by Morishita *et al.*,[42] Fig. 3, which summarizes the mean free path and the viscous penetration depth in the quantum fluids down to 1 mK. The length scales

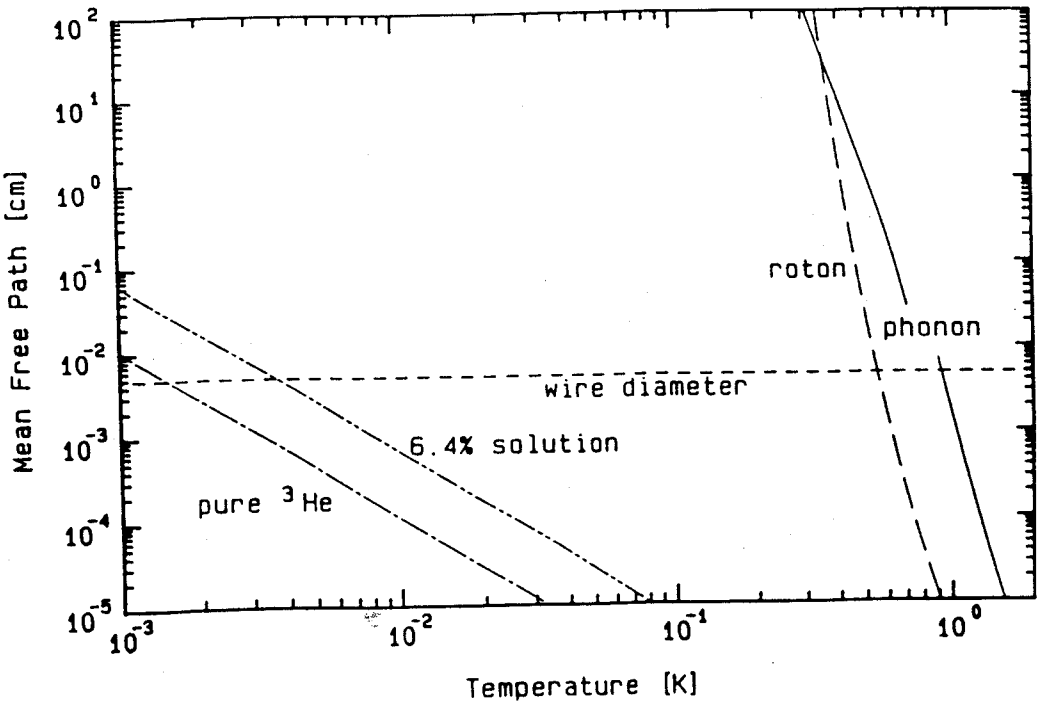

Fig. 3. The mean free path plotted vs. temperature for various quantum fluids. The smallest mean free path is that of pure ^{3}He, followed by the 6.4% solution. The roton and phonon mean free paths are successively longer mean free paths in ^{4}He. The vibrating wire diameter is shown for comparison to these lengths. The figure is taken from Morishita *et al.*[42]

shown in the figure neatly span those which are most experimentally accessible. They also compare these mean free paths to the diameter of their vibrating wire viscometer. It is readily seen that at temperatures on the order of 0.4 K in ^{4}He, the roton and phonon mean free path exceed the wire diameter by orders of magnitude. Therefore ^{4}He is a stringent testing ground for the understanding of Knudsen physics. For ^{3}He and mixtures of ^{3}He and ^{4}He, the characteristic mean free paths can also grow to be significant in comparison to the wire diameter at sufficiently low temperatures. Thus, the need for corrections that account for finite mean free paths is readily apparent, and the first of these corrections, namely slip, is dealt with in Secs. 4 and 5 of this review. Other higher order correction terms, which can be important in many experiments, can only be treated numerically and are discussed in Sec. 6.

3. BULK VISCOSITY IN FERMI QUANTUM FLUIDS

The two fluid description of superfluid ^{4}He, which was derived in a series of papers by Landau and Khalatnikov[43] is now well established. For the Fermion analogue, superfluid ^{3}He, this task has been performed much more recently[44–46] and we would like to devote this section to the description of its derivation.

In this section we describe a kinetic equation approach for calculating the dynamics of pair-correlated Fermi superfluids with the majority of our attention being focused on deriving the flow in restricted geometries from the more generally known transport theory for bulk quantum fluids.

We consider an isotropic Fermi superfluid in which the fermionic states are characterized by a momentum $\hbar\mathbf{k}$, a parabolic energy dispersion $\varepsilon_k = \mu + \xi_k = \hbar^2\mathbf{k}^2/2m^*$ (with μ the Fermi energy and m^* the effective mass), a density of states at the Fermi energy $N_F = m^* p_F/\pi^2\hbar^3$ (both spin projections), a group velocity $\mathbf{v}_k = (1/\hbar)\nabla_k \varepsilon_k$, an energy gap Δ_k, which is a nontrivial 2×2 matrix in spin space, and excitation energies $E_k = (\xi_k^2 + |\Delta_k|^2)^{1/2}$. In global thermodynamic equilibrium such a system is described by a diagonal equilibrium phase space distribution function n_k^0

$$n_k^0 = \langle c_k^\dagger c_k \rangle = u_k^2 v^0(E_k) + v_k^2[1 - v^0(E_k)] = \tfrac{1}{2}[1 - \xi_k \Theta_k] \tag{36}$$

with $\Theta_k = (1/2E_k)\tanh(E_k/2k_B T)$. $v^0(E_k)$ is the Fermi function taken at the Bogoliubov quasiparticle energy E_k (cf. Eq. (28)) and $u_k^2 = \frac{1}{2}[1 + \xi_k/E_k]$ and $v_k^2 = \frac{1}{2}[1 - \xi_k/E_k]$ are the usual coherence factors. In a Fermi superfluid there exists in addition to the (diagonal) average, n_k^0, the (off-diagonal) average, $\mathbf{g}_k^0$

$$\mathbf{g}_k^0 = \langle c_{-k} c_k \rangle = -\Delta_k \Theta_k \tag{37}$$

The pair amplitude $\mathbf{g}_k^0$ describes the structure of the off-diagonal long range order present in the system. It turns out that the quantum-mechanical coupling of the particle-like, hole-like and off-diagonal averages can be conveniently described by combining these quantities into 2×2 matrices in particle-hole space (i.e. 4×4 matrices in particle-hole and spin space), the so-called Nambu-matrices,[47] which will be denoted, in what follows, with an underbar:

$$\underline{n}_k^0 = \begin{pmatrix} n_k^0 & \mathbf{g}_k^0 \\ \mathbf{g}_k^{0\dagger} & -n_{-k}^0 \end{pmatrix} = \frac{1}{2}(\underline{1} - \underline{\varepsilon}_k^0 \Theta_k) \tag{38}$$

Correspondingly, the normal state equilibrium quasiparticle energy ξ_k, together with its hole counterpart $-\xi_k$, has to be amended by the off-diagonal mean fields Δ_k. These may be combined into an equilibrium energy matrix $\underline{\varepsilon}_k^0$:

$$\underline{\varepsilon}_k^0 = \begin{pmatrix} \xi_k & \Delta_k \\ \Delta_k^\dagger & -\xi_k \end{pmatrix} \tag{39}$$

If the pairing interaction is denoted by V_{kp}, the self-consistency (or gap) equation, by which the magnitude of the gap $\Delta(T)$ in Eq. (27), can be determined, is of the form

$$\Delta_k = \sum_p V_{kp} \mathbf{g}_p^0 \tag{40}$$

We have already noted in Sec. 2 that we shall only be interested in solutions of the gap equation (40) for the so-called pseudoisotropic Balian–Werthamer state, cf. Eq. (27),[32] believed to represent the superfluid B-phase of liquid ^{3}He. It should be noted that for numerical calculations of the temperature dependence of the gap for the BW state we have made use of the following very accurate interpolation formula:

$$\Delta(T) = \Delta(0) \tanh\left[\frac{\pi}{\delta_{sc}}\sqrt{\frac{2}{3}\frac{\Delta C}{C_N}\left(\frac{T_c}{T}-1\right)}\right] \tag{41}$$

Here $\delta_{sc} = \Delta(0)/k_B T_c$ and $\Delta C/C_N$ are parameters ($\delta_{sc} = 1.764...$ and $\Delta C/C_N = 1.426...$ in the weak coupling case), which describe the zero temperature gap and the specific heat discontinuity, respectively. They may in principle be taken from experiment, at least at higher pressures where the weak coupling assumption fails.

Let us now turn to the case that a pair correlated Fermi liquid is exposed to the action of external perturbations which vary in time and space. If the variation in space of the external perturbations is of the form

$\propto \exp(i\mathbf{q}\cdot\mathbf{r})$, the nonequilibrium distribution function becomes a momentum matrix $\underline{n}_{p,p'}(t) \equiv \underline{n}_k(\mathbf{q}, t)$, where $\mathbf{p} = \hbar(\mathbf{k} + \mathbf{q}/2)$ and $\mathbf{p}' = \hbar(\mathbf{k} - \mathbf{q}/2)$:

$$\underline{n}_{p,p'}(t) = \underline{n}_k(\mathbf{q}, t) = \underline{n}_k^0 \delta_{\mathbf{q},0} + \delta\underline{n}_k(\mathbf{q}, t); \qquad \delta\underline{n}_k(\mathbf{q}, t) = \begin{pmatrix} \delta\mathbf{n}_k & \delta\mathbf{g}_k \\ \delta\mathbf{g}_k^\dagger & -\delta\mathbf{n}_{-k}^T \end{pmatrix}(\mathbf{q}, t) \tag{42}$$

The quasiparticle energy changes accordingly:

$$\underline{\varepsilon}_{p,p'}(t) = \underline{\varepsilon}_k(\mathbf{q}, t) = \underline{\varepsilon}_k^0 \delta_{\mathbf{q},0} + + \delta\underline{\varepsilon}_k(\mathbf{q}, t); \qquad \delta\underline{\varepsilon}_k(\mathbf{q}, t) = \begin{pmatrix} \delta\varepsilon_k & \delta\Delta_k \\ \delta\Delta_k^\dagger & -\delta\varepsilon_{-k}^T \end{pmatrix}(\mathbf{q}, t) \tag{43}$$

The evolution of the nonequilibrium matrix distribution function in time and space is governed by a matrix-kinetic (von Neumann's) equation[48]:

$$i\hbar \frac{\partial}{\partial t} \underline{n}_{p,p'}(t) = -\frac{1}{\hbar} \sum_{p''} [\underline{n}_{p,p''}, \underline{\varepsilon}_{p'',p'}]_- + i\underline{I}_{p,p'} \tag{44}$$

in which the full quasiparticle energy matrix $\underline{\varepsilon}_{p,p'}$ plays the role of the Hamiltonian of the system. In (44) $\underline{I}_{p,p'}$ represents the matrix collision integral, which we will discuss later. If $\underline{n}_{p,p'}$ is interpreted as a quantum–mechanical Wigner distribution function (the diagonal element of which describes the probability amplitude for the excitation of a particle–hole pair with momenta $\mathbf{p} = \hbar(\mathbf{k} + \mathbf{q}/2)$ (particle) and $\mathbf{p}' = \hbar(\mathbf{k} - \mathbf{q}/2)$ (hole)), the applicability of Eq. (44) extends to external perturbations with frequencies $\omega \ll E_F/\hbar$ and wavevectors $\hbar|\mathbf{q}| \ll p_F$. After linearizing, according to (42) and (43), the matrix-kinetic equation reads

$$i\hbar \frac{\partial}{\partial t} \delta\underline{n}_k(\mathbf{q}, t) + \delta\underline{n}_k \underline{\varepsilon}_{k-}^0 - \underline{\varepsilon}_{k+}^0 \delta\underline{n}_k = \delta\underline{\varepsilon}_k \underline{n}_{k-}^0 - \underline{n}_{k+}^0 \delta\underline{\varepsilon}_k + i\hbar\delta\underline{I}_k \tag{45}$$

As a next step we perform an expansion of (45) with respect to $\hbar\mathbf{v}_k \cdot \mathbf{q}$, by which Planck's constant $\hbar$ is eliminated to leading order. Introducing the Nambu-matrices $\underline{\alpha}^{(s)} = \mathrm{diag}\{1, -s\}$, the linearized form of the matrix kinetic equation can be written in the long wavelength limit (harmonic time dependence $\partial/\partial t \to -i\omega$ assumed):

$$\omega\delta\underline{n}_k(\mathbf{q}, \omega) - \mathbf{q}\cdot\mathbf{v}_k \frac{1}{2} \{\underline{\alpha}^{(+)}, \delta\underline{n}_k(\mathbf{q}, \omega) + \Phi_k \delta\underline{\varepsilon}_k(\mathbf{q}, \omega)\}_+$$

$$= i\delta\underline{I}_k(\mathbf{q}, \omega) - \frac{i}{\hbar} [\underline{\varepsilon}_k^0, \delta\underline{n}_k(\mathbf{q}, \omega) + \Theta_k \delta\underline{\varepsilon}_k(\mathbf{q}, \omega)]_- + \cdots \tag{46}$$

Here we have defined $\Phi_k = -\partial n_k^0/\partial \xi_k = \Theta_k \Delta_k^2/E_k^2 + \varphi_k \xi_k^2/E_k^2$ and $\varphi_k = -\partial v_k^0/\partial E_k$. The coupled equations for the diagonal and the off-diagonal averages describe the dynamics of the superfluid in the whole quasiclassical frequency range $0 < \omega \ll E_F/\hbar$. They have to be amended by the self consistency equations for the diagonal energies (short range Fermi liquid forces, cf. Ref. 49)

$$\{\delta \underline{\varepsilon}_k(\mathbf{q}, \omega)\}_{++} = \delta \varepsilon_k(\mathbf{q}, \omega) = \sum_l \frac{F_l^s}{N_F} \sum_{p\sigma} P_l(\hat{\mathbf{k}} \cdot \hat{\mathbf{p}})\, \delta n_p(\mathbf{q}, \omega) \tag{47}$$

where the set F_l^s denotes the dimensionless spin-symmetric Fermi liquid parameters. A second self–consistency relation holds for the off-diagonal energy (gap equation)

$$\{\delta \underline{\varepsilon}_k(\mathbf{q}, \omega)\}_{+-} = \delta \Delta_k(\mathbf{q}, \omega) = \sum_p V_{kp} \delta \mathbf{g}_p(\mathbf{q}, \omega) \tag{48}$$

of the quasiparticle energy matrix $\delta \underline{\varepsilon}_k$. Equation (48) describes the collective modes of the amplitude and phase of the order parameter. It plays an important role for the gauge invariance of the theory.

One important property of the collision integral in Nambu space should be mentioned at this stage, namely that it has to reflect the conservation properties of the pair-correlated Fermi liquid. Thus, there exists a set of so-called collisional invariants $\underline{A}_k$, with the conservation property[50]

$$2 \sum_k \tfrac{1}{4} \mathrm{tr}[\underline{A}_k \delta \underline{I}_k] = 0 \tag{49}$$

that correspond to the conservation of mass ($\underline{A}_k = m\underline{\alpha}^{(+)}$), momentum ($\underline{A}_k = \mathbf{p}\underline{\alpha}^{(-)}$), and energy ($\underline{A}_k = \underline{\varepsilon}_k^0$).

We are now prepared to attack the problem of deriving conservation laws for macroscopic observable densities from the matrix kinetic equation. As a first step let us note that, as in the normal state, the diagonal part $\delta \mathbf{n}_k$ of the distribution function can be classified according to its parity s with respect to the parity operation $\hat{\mathbf{k}} \to -\hat{\mathbf{k}}$. The diagonal elements of the matrix distribution function $\delta \underline{n}_k$ can be combined to scalar projections

$$\delta n_k^{(s)} = \tfrac{1}{4} \mathrm{tr}[\underline{\alpha}^{(s)} \delta \underline{n}_k] = \tfrac{1}{2}[\delta n_k + s \delta n_{-k}] \tag{50}$$

Here tr denotes the trace over 2×2 matrices in particle–hole space. The parity projected scalar distribution function $\delta n_k^{(s)}$ obeys a scalar kinetic

equation which is reminiscent of the normal state Landau–Boltzmann–Silin[49] equation:

$$\omega\delta n_k^{(s)} - \mathbf{q}\cdot\mathbf{v}_k\left[\delta n_k^{(-s)} - \frac{\partial n_k^0}{\partial\xi_k}\delta\varepsilon_k^{(-s)}\right] = \delta P_k^{(s)} + \frac{i}{4}\,\mathrm{tr}_4[\underline{\alpha}^{(s)}\delta\underline{I}_k] \tag{51}$$

Here $\delta P_k^{(s)}$ is a term, which vanishes for $s=+1$ upon summation over $\mathbf{k}$ as a consequence of the self–consistency relation (48), reflecting the gauge invariance of the theory. The parity-projected kinetic Eq. (51) can now be used to determine the macroscopic observable densities and currents and their conservation properties. The mass density is defined as

$$\delta\rho = m\sum_{k\sigma}\delta n_k \tag{52}$$

Summing Eq. (51) on $\mathbf{k}$ generates the continuity equation:

$$\omega\delta\rho - \mathbf{q}\cdot\mathbf{g} = 0 \tag{53}$$

and a mass current density can be identified as

$$\mathbf{g} = m\sum_{k\sigma}\mathbf{v}_k[\delta n_k + \Phi_k\delta\varepsilon_k] \tag{54}$$

The equation of motion for the mass current or momentum density is known as the Navier Stokes equation:

$$\omega g_i - q_j\Pi_{ij} = 0 \tag{55}$$

and we can identify as the stress tensor the quantity

$$\Pi_{ij} = \sum_{k\sigma} p_i v_{kj}[\delta n_k + \Phi_k\delta\varepsilon_k] \tag{56}$$

In order to proceed further, we restrict our considerations to the case of purely transverse flow. That is, we assume from now on that the current $\mathbf{g}$ only has a component in the x-direction and that spatial variations take place only in the z-direction:

$$\mathbf{g} = \begin{pmatrix} g_x \\ 0 \\ 0 \end{pmatrix}; \qquad \mathbf{q} = \begin{pmatrix} 0 \\ 0 \\ q_z \end{pmatrix} \tag{57}$$

In such a case the continuity Eq. (53) predicts that there are no mass density fluctuations ($\delta\rho = 0$) coupled to the transverse flow. The gauge

mode, emerging as a solution of an integral equation for the quantity $\delta\Delta_k^{(-)}$, is known to couple only to longitudinal degrees of freedom, such as density fluctuations, and is therefore irrelevant in the case of purely transverse flow.

A convenient short-hand notation for momentum sums will be used in what follows:

$$\langle \cdots \rangle \equiv \sum_{k\sigma} \cdots \tag{58}$$

Doing the summations over momentum, we shall encounter the following special averages:

$$\begin{aligned} \langle \Phi \rangle &= N_F \\ \left\langle \varphi \left| \frac{\xi}{E} \right|^n \right\rangle &= N_F Y_n(T) \end{aligned} \tag{59}$$

The quantities $Y_n(T)$ represent the set of generalized Yosida functions which describes the temperature dependence of the response functions and which have already been introduced in Sec. 2 (cf. Eq. (30)). In Fig. 4 we show a plot of the first five Yosida functions vs. reduced temperature.

The two relevant macroscopic observables describing the dynamics are the mass current g_x

$$g_x = m\langle v_x[\delta n + \Phi\delta\varepsilon]\rangle \tag{60}$$

and the shear component of the stress tensor Π_{xz}

$$\Pi_{xz} = \langle p_x v_z[\delta n + \Phi\delta\varepsilon]\rangle \tag{61}$$

As an important step towards the description of transverse flow of thermal excitations we now have to decompose the distribution δn_k, which determines the physical observables such as the density, current and stress tensor into their quasiparticle and condensate contributions. This can be achieved by performing a Bogoliubov–Valatin transformation which is defined as the unitary transformation that diagonalizes the equilibrium matrix energy:

$$\underline{U}_k \underline{\varepsilon}_k^0 \underline{U}_k^\dagger = E_k \underline{\alpha}^{(+)} \tag{62}$$

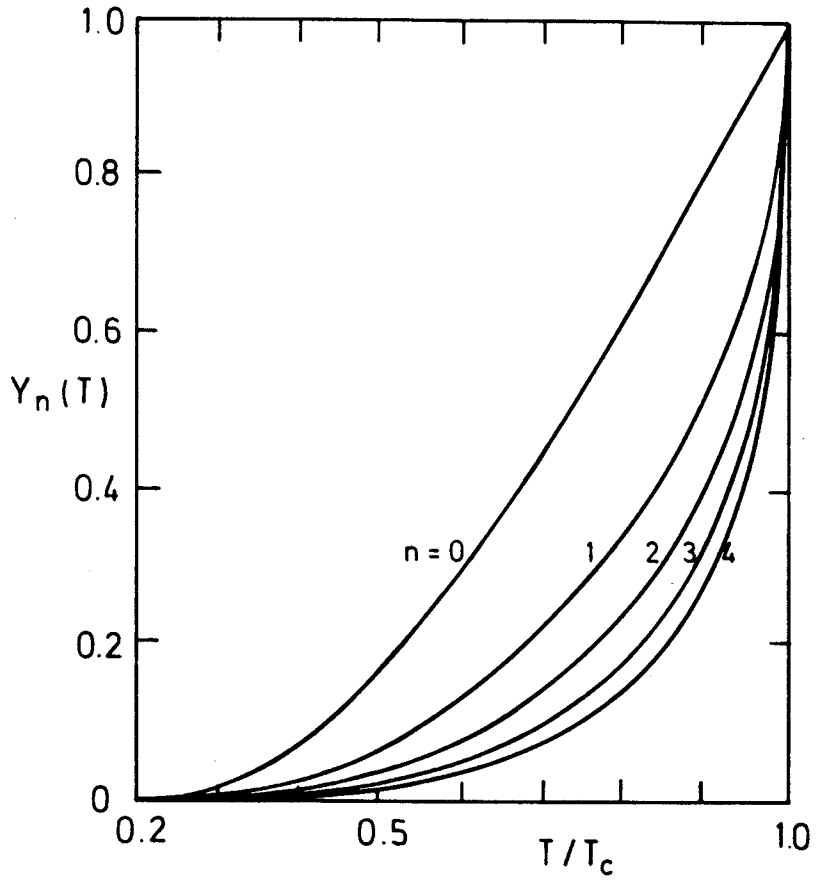

Fig. 4. The generalized Yosida functions $Y_n(T)$ (see Eqs. 30 and 59 in the text) for isotropic pair-correlated superfluids in the weak coupling limit as a function of reduced temperature T/T_c for $n=0, 1, 2, 3, 4$.

where

$$\underline{U}_k = \begin{pmatrix} u_k & \mathbf{v}_k \\ -\mathbf{v}_k^\dagger & u_k \end{pmatrix}$$

with $u_k = \sqrt{(1+\xi_k/E_k)/2}$ and $\mathbf{v}_k = (\Delta_k/|\Delta_k|)\sqrt{(1-\xi_k/E_k)/2}$. The presence of external perturbations induce a nonequilibrium quasiparticle distribution matrix:

$$\delta\underline{\nu}_{p,p'} = \underline{U}_p \delta\underline{n}_{p,p'} \underline{U}_{p'}^\dagger = \begin{pmatrix} \delta\nu_{p,p'} & \delta\gamma_{p,p'} \\ \delta\gamma_{p,p'}^\dagger & -\delta\nu^T_{-p',-p} \end{pmatrix} \tag{63}$$

The Bogoliubov transformation of the nonequilibrium quasiparticle energy matrix is defined to have the matrix elements

$$\delta\underline{E}_{p,p'} = \underline{U}_p \delta\underline{\varepsilon}_{p,p'} \underline{U}_{p'}^\dagger = \begin{pmatrix} \delta E_{p,p'} & \delta\mathbf{D}_{p,p'} \\ \delta\mathbf{D}_{p,p'}^\dagger & -\delta E_{-p',-p} \end{pmatrix} \tag{64}$$

One may now perform a Bogoliubov transformation to the matrix kinetic equation (45) by multiplying from the left with $\underline{U}_p$ and from the right with $\underline{U}_{p'}$. After a subsequent expansion in small $\hbar \mathbf{v}_k \cdot \mathbf{q}$ one obtains the following set of coupled kinetic equations for the new distribution functions δv_k and $\delta \gamma_k$:

$$\omega \delta v_k - q_z V_{kz} [\delta v_k + \varphi_k \delta E_k] = i\delta \mathbf{I}_{k++} \tag{65}$$

$$\omega \delta \gamma_k - \frac{2E_k}{\hbar} [\delta \gamma_k + \Theta_k \delta \mathbf{D}_k] = i\delta \mathbf{I}_{k+-} \tag{66}$$

In (65) $V_{kz} = \partial E_k / \partial \hbar k_z = (\xi_k / E_k)\, v_{kz}$ denotes the z-component of the quasiparticle group velocity, which vanishes at the Fermi surface. We are interested in solutions of these coupled kinetic equations (65) and (66) in the so-called macroscopic limit, $\omega \ll \Delta(T)/\hbar$. An inspection of Eq. (66) immediately shows that in this limit the distribution function $\delta \gamma_k$, which describes the Cooper pair response, has the local equilibrium form

$$\delta \gamma_k(q_z, \omega) = -\Theta_k \delta \mathbf{D}_k(q_z, \omega) + O\left(\frac{\hbar\omega}{\Delta(T)}, \frac{\hbar v_F |\mathbf{q}|}{\Delta(T)}, \frac{\hbar}{\tau_{+-}\Delta(T)}, \ldots\right) \tag{67}$$

where τ_{+-} is a relaxation time characterizing the off-diagonal component $\delta \mathbf{I}_{k+-}$ of the transformed collision integral. Splitting off contributions of the order $O(\hbar\omega/\Delta)$ also in the quasiparticle kinetic equation (65) leaves us with

$$\begin{aligned} \delta v_k(q_z, \omega) = & -\varphi_k \delta E_k(q_z, \omega) + h_k(q_z, \omega) \\ & + O\left(\frac{\hbar\omega}{\Delta(T)}, \frac{\hbar v_F |\mathbf{q}|}{\Delta(T)}, \frac{\hbar \tau_{++}}{\Delta(T)}, \ldots\right) \\ (\omega - q_z V_{kz})\, h_k(q_z, \omega) = & \omega \varphi_k \delta E_k(q_z, \omega) + i\delta I_k^{++}(q_z, \omega) \end{aligned} \tag{68}$$

Here the new quasiparticle distribution function $h_k = O(\omega\tau_k, \mathbf{V}_k \cdot \mathbf{q}\tau_k, \ldots)$ and $\tau_k \equiv \tau_{k++}$ is a time scale which specifies the diagonal component of the collision integral; it will be discussed in detail later. In the macroscopic regime $\omega \ll \Delta(T)/\hbar$ the quasiparticle distribution function δv_k has a local equilibrium contribution $\delta v_k^{\mathrm{loc}} = -\varphi_k \delta E_k$, but, unlike the Cooper pair part $\delta \gamma_k$, it also has a contribution h_k, which describes the deviation from local equilibrium. We shall see below that the distribution function h_k exclusively describes the dynamics of the *normal component* in the macroscopic limit.

We are now able to decompose the distribution function $\delta n_k^{(s)}$ into its quasiparticle and condensate contribution by writing

$$\delta n_k^{(s)} = \tfrac{1}{4}\,\mathrm{tr}_4[\underline{U}_k \underline{\alpha}^{(s)} \underline{U}_k^{\dagger} \delta \underline{\nu}_k] \tag{69}$$

A two fluid description of superfluid Fermi liquids emerges from (65)–(68) if one associates the local contributions $\delta v_k^{\mathrm{loc}}$ and $\delta\gamma_k$ with the local condensate response whereas the normal component is represented by the distribution function $\mathbf{h}_k$. The normal–superfluid decomposition can then be summarized as follows: Defining distribution functions of definite parity through

$$\begin{aligned} \delta v_k^{(s)} &= \frac{1}{2}\,[\delta v_k + s\delta v_{-k}] \\ \delta\gamma_k^{(s)} &= \frac{1}{2\,|\Delta_k|}\,[\delta\gamma_k \Delta_k^{\dagger} + s\Delta_k \delta\gamma_k^{\dagger}] \end{aligned} \tag{70}$$

one may decompose $\delta n_k^{(s)}$ and $\delta g_k^{(s)}$ into

$$\begin{pmatrix} \delta n_k^{(s)} \\ \delta g_k^{(s)} \end{pmatrix} = \begin{pmatrix} q_k^{(s)} & -p_k^{(s)} \\ p_k^{(s)} & q_k^{(s)} \end{pmatrix} \begin{pmatrix} \delta v_k^{(s)} \\ \delta\gamma_k^{(s)} \end{pmatrix} \tag{71}$$

Through the solutions of the pair of kinetic equations (65) and (66) one may express δv and $\delta\gamma$ by δE and δD

$$\begin{pmatrix} \delta E_k^{(s)} \\ \delta D_k^{(s)} \end{pmatrix} = \begin{pmatrix} q_k^{(s)} & p_k^{(s)} \\ -p_k^{(s)} & q_k^{(s)} \end{pmatrix} \begin{pmatrix} \delta\varepsilon_k^{(s)} \\ \delta\Delta_k^{(s)} \end{pmatrix} \tag{72}$$

where $\delta g_k^{(s)}$, $\delta D_k^{(s)}$ and $\delta\Delta_k^{(s)}$ have been defined in analogy to (70). The quantities $q_k^{(s)}$ and $p_k^{(s)}$ are quasiparticle and pair coherence factors, respectively

$$\begin{aligned} q_k^{(s)\,2}(\mathbf{q}) &= (u_{k+}u_{k-} - s v_{k+}v_{k-})^2 \\ &\overset{\mathbf{q}\to 0}{=} \frac{1+s}{2}\frac{\xi_k^2}{E_k^2}\left(1 - \frac{(\mathbf{v}_k\cdot\mathbf{q})^2}{2E_k^2}\frac{|\Delta_k|^2}{E_k^2}\right) \\ &\quad + \frac{1-s}{2}\left(1 - \frac{(\mathbf{v}_k\cdot\mathbf{q})^2}{4E_k^2}\frac{|\Delta_k|^2}{E_k^2}\right) \\ p_k^{(s)\,2}(\mathbf{q}) &= (u_{k+}v_{k-} + s v_{k+}u_{k-})^2 \\ &\overset{\mathbf{q}\to 0}{=} \frac{1+s}{2}\frac{|\Delta_k|^2}{E_k^2}\left(1 + \frac{(\mathbf{v}_k\cdot\mathbf{q})^2}{2E_k^2}\frac{\xi_k^2}{E_k^2}\right) \\ &\quad + \frac{1-s}{2}\frac{(\mathbf{v}_k\cdot\mathbf{q})^2}{4E_k^2}\frac{|\Delta_k|^2}{E_k^2} \end{aligned} \tag{73}$$

They obey the following general sum rule:

$$q_k^{(s)\,2} + p_k^{(s)\,2} = 1; \qquad s = \pm 1$$

It is worth noting at this stage, that the off–diagonal energies $\delta\Delta_k^{(s)}$ represent the contribution from the collective modes of the order parameter. These can be split off into amplitude modes ($\delta\Delta_k^{(+)}$) with characteristic frequency $\omega_\Delta \propto \Delta/\hbar$ and phase modes ($\delta\Delta_k^{(-)}$) with characteristic frequency $\omega_\phi \propto \mathbf{c}\cdot\mathbf{q}$, where $\mathbf{c}$ is a typical sound or spin–wave velocity. The amplitude modes are irrelevant in the macroscopic limit $\omega \ll \Delta/\hbar$ which we are primarily interested in. The phase mode, relevant for the transport of mass, is the ordinary gauge- or Anderson–Bogoliubov mode, the treatment of which is necessary to maintain gauge invariance of the theory.[51] For our purposes it is sufficient to note that

$$\delta\Delta_k^{(-)}(q_z, \omega) = i\,|\Delta_k|\,\delta\phi(q_z, \omega) \tag{74}$$

with $\delta\phi$ the phase of the nonequilibrium order parameter $\delta\Delta_k$. In context with hydrodynamic flow, the phase $\delta\phi$ may be interpreted to act as a velocity potential for the superflow velocity v_x^s:

$$v_x^s(q_z, \omega) = \frac{\hbar}{2m} iq_z \delta\phi(q_z, \omega) \to \frac{\hbar}{2m}\frac{\partial\delta\phi(z, \omega)}{\partial z} \tag{75}$$

In what follows we shall assume that the coupling of the transverse motion of the walls to the condensate fraction is negligible and the superfluid component is at rest, i.e. $v_x^s \equiv 0$. The final result for the diagonal distribution function $\delta n_k^{(s)}$, needed to generate expressions for the density, current and the stress tensor, reads then:

$$\delta n_k^{(s)} + \Phi_k \delta\varepsilon_k^{(s)} = q_k^{(s)} h_k^{(s)} + \frac{1-s}{2}(\Phi_k - \varphi_k)\,\delta\varepsilon_k^{(-)} \tag{76}$$

To solve the scalar kinetic equation for the diagonal distribution δv_k for Bogoliubov quasiparticles, it is helpful to split the collision integral δI_k into an in-scattering contribution, characterized by the quasiparticle relaxation time τ_k, and an out–scattering contribution, characterized by the collision operator B_{kp}:

$$\delta I_k = -\frac{1}{\tau_k}(h_k - \varphi_k \delta C_k); \qquad \delta C_k = \sum_{p\sigma} B_{kp} h_p \tag{77}$$

with B_{kp} the collision operator for Bogoliubov quasiparticles representing inelastic two-particle collisions, which will be specified later. Defining $z_k = \omega + i\Gamma_k$ with $\Gamma_k = 1/\tau_k$, we may rewrite the kinetic equation (68) for $h_k^{(s)}$ in the following compact form

$$h_k^{(s)} = \Xi_k \left[\delta F_k^{(s)} + \frac{q_z V_{kz}}{z_k} \delta F_k^{(-s)} \right] \tag{78}$$

where δF_k is a collection of collisional and Fermi liquid vertex corrections, which guarantee an appropriate treatment of the conservation and relaxation properties together with the collective modes of the interacting Fermi system:

$$\delta F_k = \delta C_k - i\omega\tau_k \delta E_k$$

and Ξ_k is a response kernel

$$\Xi_k = \varphi_k \frac{i\Gamma_k z_k}{z_k^2 - (q_z V_{kz})^2} = \frac{\varphi_k}{1 - i\omega\tau_k} \frac{1}{1 - (iq_z\lambda_{kz})^2}$$

with $\lambda_{kz} = V_{kz}\tau_k/(1 - i\omega\tau_k)$ a complex mean free path. If one recalls that iq_z corresponds to the gradient operator $\partial/\partial z$ in real space, one can interpret Eq. (78) as the result of a straightforward gradient expansion

$$\begin{aligned} h_k^{(s)} &= \frac{\varphi_k}{1 - i\omega\tau_k} \frac{\delta F_k^{(s)} - iq_z\lambda_{kz}\delta F_k^{(-s)}}{1 - (iq_z\lambda_{kz})^2} \\ &= \frac{\varphi_k}{1 - i\omega\tau_k} \hat{D}_k \left(\delta F_k^{(s)} - \lambda_{kz} \frac{\partial}{\partial z} \delta F_k^{(-s)} \right) \qquad (79) \\ \hat{D}_k &= \sum_{\mu=0}^{\infty} \left(\lambda_{kz} \frac{\partial}{\partial z} \right)^{2\mu} \end{aligned}$$

In order to proceed further, we have to specify both the quasiparticle energy δE_k describing Fermi liquid effects, and the quantity δC_k which is the backscattering contribution of the collision integral. In the case of transverse flow, the expansion of the Fermi liquid interaction (47), if restricted to include only the $\ell = 1, 2$ components, assumes the simple form

$$\delta\varepsilon_k = \sum_{\mu=1}^{2} \frac{F_\mu^s}{2\mu + 1} \frac{v_{kx} v_{kz}^{\mu-1}}{\langle \Phi v_x^2 v_z^{2\mu-2} \rangle} \langle v_x v_z^{\mu-1} \delta n \rangle \tag{80}$$

We may, with the aid of Eq. (76) express δn_k through h_k with the result

$$\delta\varepsilon_k = \frac{(F_2^s/5)}{1+(F_2^s/5)} \frac{v_{kx}v_{kz}}{\langle \Phi v_x^2 v_z^2\rangle} \langle v_x v_z q^{(+)} h^{(+)}\rangle + \frac{(F_1^s/3)\ Y_0}{1+(F_1^s/3)\ Y_0} \frac{v_x}{\langle \Phi v_x^2\rangle} \langle v_x q^{(-)} h^{(-)}\rangle \tag{81}$$

Using (81) we arrive at the following thermal excitation gas picture that relates the observables g_x and Π_{xz} to the quasiparticle distribution functions $h_k^{(+)}$ and $h_k^{(-)}$:

$$g_x = m \frac{1+F_1^s/3}{1+(F_1^s/3)\ Y_0} \langle v_x h^{(-)}\rangle \equiv \rho^{\mathrm{n}}(T)\, v_x^n; \qquad \rho^{\mathrm{n}} = \rho \frac{(1+F_1^s/3)\ Y_0}{1+(F_1^s/3)\ Y_0} \tag{82}$$

This is the result (31) anticipated in the previous section. We can therefore identify the *normal velocity field* from (82):

$$v^n(z) = \frac{\langle v_x h^{(-)}\rangle}{nY_0} = \frac{\langle p_x h^{(-)}\rangle}{nm^* Y_0} \tag{83}$$

The stress tensor is written as

$$\Pi_{xz}(z) = \langle p_x V_z h^{(+)}\rangle \tag{84}$$

This is the hydrodynamic result for velocity and stress tensor for the case of purely transverse flow. A comprehensive review of the two-fluid description of the mass and spin dynamics of superfluid Fermi liquids has been given by one of the authors.[46]

The quasiparticle energy change δE_k can be written in terms of the observables $v_x^n(z)$ and $\Pi_{xz}(z)$ as

$$\delta E_k^{(s)} = \frac{1+s}{2} \frac{(F_2^s/5)\ Y_2}{1+F_2^s/5} \frac{p_x \lambda_{kz}}{\langle \varphi p_x^2 V_z \lambda_z\rangle} \Pi_{xz} + \frac{1-s}{2} \frac{(F_1^s/3)\ Y_0}{1+(F_1^s/3)\ Y_0} p_x v_x^n \tag{85}$$

Since we plan to consider the influence of surfaces on the flow properties of the Fermi quantum fluids, we will be forced to use approximations for the collisional contributions to h_k^s in (78). We shall, in what follows, make use of a relaxation time approximation, which is consistent with the conservation of momentum of the Bogoliubov quasiparticles (scattering parameter $\lambda_1 \equiv 1$) and with the relaxation of the stress tensor on the scale of the appropriate viscous transport time (pressure dependent scattering

parameter $\lambda_2 \neq 1$). In this approximation, the energy dependent relaxation rate Γ_k is replaced by its thermal average $\bar{\Gamma}$

$$\bar{\Gamma} = \frac{1}{\bar{\tau}} = \frac{\langle \varphi \Gamma \rangle}{\langle \varphi \rangle} \tag{86}$$

Then the collision operator B_{kp} in $\delta C_k = \langle B_{kp} h_p \rangle_p$ assumes the simple form of a two relaxation time model[52]:

$$B_{kp}^{(s)} = q_k^{(s)} q_p^{(s)} \sum_{\mu=1}^{2} \lambda_\mu \frac{1+(-1)^\mu s}{2} \frac{v_{kx} v_{kz}^{\mu-1} v_{px} v_{pz}^{\mu-1}}{\langle \varphi v_x^2 v_z^{2\mu-2} \rangle} \tag{87}$$

and δC_k can be related to the observables v_x^n and Π_{xz} in a manner similar to δE_k:

$$\delta C_k^{(s)} = \frac{1+s}{2} \lambda_2 \frac{p_x \lambda_{kz}}{\langle \varphi p_x^2 V_z \lambda_z \rangle} \Pi_{xz} + \frac{1-s}{2} \lambda_1 p_x v_x^n \tag{88}$$

Therefore

$$\begin{aligned}
\delta F_k^{(s)} &= (1 - i\omega\bar{\tau}) \left\{ \frac{1+s}{2} a_2 \frac{p_x \lambda_{kz}}{\langle \varphi p_x^2 V_z \lambda_z \rangle} \Pi_{xz} + \frac{1-s}{s} a_1 p_x v_x^n \right\} \\
a_2 &= a_2(\omega) = \frac{1}{1 - i\omega\bar{\tau}} \left\{ \lambda_2 \frac{Y_2}{Y_0} - i\omega\bar{\tau} \frac{(F_2^s/5)\, Y_2}{1 + F_2^s/5} \right\} \overset{\omega \to 0}{=} \lambda_2 \frac{Y_2}{Y_0} \\
a_1 &= a_1(\omega) = \frac{1}{1 - i\omega\bar{\tau}} \left\{ \lambda_1 - i\omega\bar{\tau} \frac{(F_1^s/3)\, Y_0}{1 + (F_1^s/3)\, Y_0} \right\} \overset{\omega \to 0}{=} \lambda_1 \equiv 1
\end{aligned} \tag{89}$$

We are now prepared to calculate the shear viscosity of a bulk Fermi superfluid. The shear viscosity can be identified from the constitutive relation between the stress tensor and the gradient of the normal velocity field, which is obtained from Eq. (84) as:

$$\Pi_{xz}(q_z, \omega) = -\eta(q_z, \omega)\, i q_z v_x^n(q_z, \omega) \tag{90}$$

with $\eta(q_z, \omega)$ the dynamic shear viscosity of our model which is given by

$$\begin{aligned}
\eta(q_z, \omega) &= \frac{(1 - i\omega\bar{\tau})\, a_1 \langle \varphi p_x^2 V_z \lambda_z / 1 - (i q_z \lambda_z)^2 \rangle}{1 - a_2 \dfrac{\langle \varphi p_x^2 V_z \lambda_z / (1 - (i q_z \lambda_z)^2] \rangle}{\langle \varphi p_x^2 V_z \lambda_z \rangle}} \overset{q_z \to 0}{=} \frac{(1 - i\omega\bar{\tau})\, a_1}{1 - a_2} \langle \varphi p_x^2 V_z \lambda_z \rangle \\
&\overset{\omega \to 0}{=} \frac{\langle \varphi p_x^2 V_z \lambda_z \rangle}{1 - \lambda_2 (Y_2 / Y_0)}
\end{aligned} \tag{91}$$

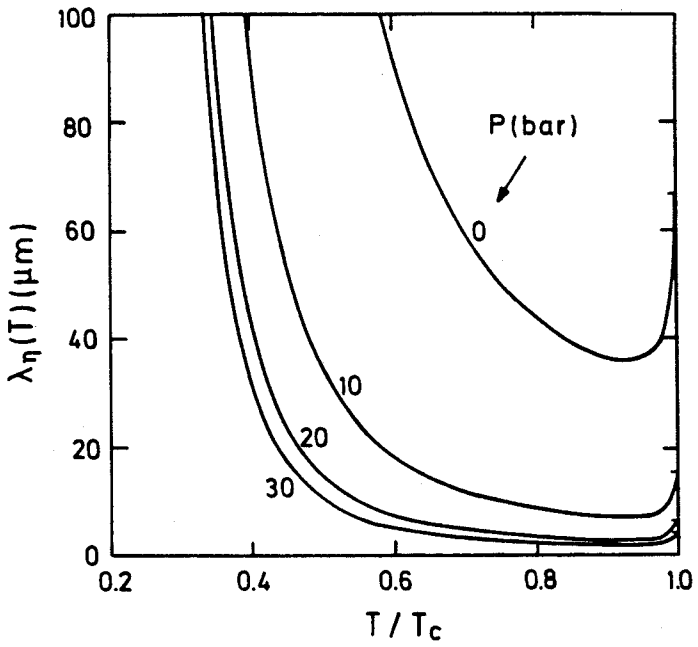

Fig. 5. Viscous mean free path of Bogoliubov quasiparticles in ^{3}He–B at four different pressures vs. reduced temperature.

The latter equality in Eq. (91) corresponds to the stationary limit of the leading order gradient expansion and leads to the final result for the shear viscosity of Bogoliubov quasiparticles, which may be cast into the simple form (34) reminiscent of gas-kinetic theory

$$\eta(T)=\frac{1}{5}\rho_0^{\mathrm{n}}\bar{V}\lambda_\eta;\qquad \lambda_\eta=\bar{V}\tau_\eta$$
$$\bar{V}=v_{\mathrm{F}}\sqrt{\frac{\langle\varphi V_z^2\rangle}{\langle\varphi v_z^2\rangle}};\qquad \tau_\eta=\frac{\bar{\tau}}{1-\lambda_2 Y_2/Y_0} \tag{92}$$

with $\bar{V}$ a root mean square averaged velocity and λ_η the viscous transport mean free path. In Fig. 5 we show a plot of λ_η for superfluid ^{3}He–B at different pressures vs. reduced temperature. This clearly shows that the bulk result for η is only valid in a regime of temperatures where λ_η is the smallest length in the problem. This ceases to be the case at lower temperatures where λ_η diverges exponentially and exceeds typical sizes of the measuring cell. In the next section we deal with the consequences of long mean free paths.

4. THE SLIP EFFECT

In this section we aim at re-deriving the constitutive relation (90) between the current and the gradient of the velocity field for the case in

which the fluid is constrained to the half space $z>0$ and bounded by an infinite plane wall at $z=0$, which is assumed to scatter quasiparticle excitations in different ways ranging from diffuse to specular.

We start by rewriting Eq. (68) by changing over from the (q_z, ω)—to a (z, ω)—representation:

$$\left(\frac{1}{\lambda_{kz}}+\frac{\partial}{\partial z}\right) h_k(z,\omega)=\varphi_k p_x q_k(z,\lambda_{kz}) \tag{93}$$

$$q_k(z,\lambda_{kz})\equiv\frac{1}{p_x\lambda_{kz}}\frac{\delta F_k}{1-i\omega\bar{\tau}}=\frac{a_2\Pi_{xz}}{\langle\varphi p_x^2 V_z\lambda_z\rangle}+\frac{1}{\lambda_{kz}}a_1 v_x^{\mathrm{n}}$$

This integro-differential equation can be formally inverted to read:

$$h_k(z)=\mathrm{e}^{-(z/\lambda_{kz})}C_k+\varphi_k p_x\int_0^z dz'\, q_k(z',\lambda_{kz})\,\mathrm{e}^{(z'-z)/\lambda_{kz}} \tag{94}$$

Inside a layer of thickness $\propto\lambda_\eta$ (the so-called Knudsen layer) where the quasiparticles move essentially ballistically, the surface is capable of *distinguishing* incoming quasiparticle excitations (negative group velocities $V_{kz}<0$) from those that are re-emitted (positive group velocities $V_{kz}>0$) from it, at least if the reflection is not specular. To see this, we decompose the distribution function $h_k(z)$ into contributions from $V_{kz}<0$ and $V_{kz}>0$

$$h_k(z,V_{kz})=h_k^<(z)\,\Theta(-V_{kz})+h_k^>(z)\,\Theta(V_{kz}) \tag{95}$$

where Θ denotes the Heaviside step function. The unknown integration constant C_k is determined from the boundary conditions for $h_k^>(z)$ at the wall $(z=0)$ and for $h_k^<(z)$ far away from the wall $(z\to\infty)$. The latter boundary condition then simply reads

$$\lim_{z\to\infty} h_k^<(z)=\lim_{z\to\infty}\left\{\mathrm{e}^{z/|\lambda_{kz}|}C_k^<+\varphi_k p_x\int_0^z dz'\, q_k(z',-|\lambda_{kz}|)\,\mathrm{e}^{(z-z')/|\lambda_{kz}|}\right\}=0 \tag{96}$$

and reflects the simple fact that the presence of the wall is not felt at an infinite distance away from it. A simple form for the boundary condition for $h_k^>(0)$ at the wall is that of *diffuse boundary scattering*, where one assumes that the quasiparticles leave the wall with the local equilibrium distribution characterized by the wall velocity v_x^{ext}:

$$h_k^>(0)=C_k^>=\varphi_k p_x v_x^{\mathrm{ext}} \tag{97}$$

and will be extended later to apply to a class of more general wall scattering laws. The formal solution to Eq. (93) for incoming and reflected quasiparticles may be written as

$$h_k^{>}(z) = \varphi_k p_x \left\{ v_x^{\text{ext}} \mathrm{e}^{-(z/\lambda_{kz})} + \int_0^z dz'\, q_k(z', \lambda_{kz})\, \mathrm{e}^{(z'-z)/\lambda_{kz}} \right\}$$
$$h_k^{<}(z) = -\varphi_k p_x \int_z^{\infty} dz'\, q_k(z', -|\lambda_{kz}|)\, \mathrm{e}^{-(z'-z)/|\lambda_{kz}|} \tag{98}$$

Clearly the new physics introduced by the presence of the wall originates from the distribution function $h_k^{>}(0)$ in (98) which describes local equilibrium with respect to the surface in contrast to the bulk distribution representing the incoming excitations. Taking the moments according to (83) and (84)

$$v_x^n(z) = \frac{1}{nY_0} \langle v_x (h^{>} + h^{<}) \rangle_+ \tag{99}$$
$$\Pi_{xz} = \langle p_x V_z (h^{>} - h^{<}) \rangle_+$$
$$\langle \cdots \rangle_+ = \sum_{\substack{\mathbf{k}\sigma \\ V_{kz} > 0}} \cdots$$

one arrives at coupled integral equations for this pair of observables which we will discuss later. In order to make connection with the gradient expansion presented in the previous section, we proceed by performing a partial integration of the terms containing the normal velocity field $v_x^{\mathrm{n}}(z)$:

$$h_k^{>}(z) = \varphi_k p_x \left\{ a_1 v_x^{\mathrm{n}}(z) - \Delta v_x \mathrm{e}^{-(z/\lambda_{kz})} + \int_0^z dz'\, G(z')\, \mathrm{e}^{(z'-z)/\lambda_{kz}} \right\}$$
$$h_k^{<}(z) = \varphi_k p_x \left\{ a_1 v_x^{\mathrm{n}}(z) - \int_z^{\infty} dz'\, G(z')\, \mathrm{e}^{-(z'-z)/|\lambda_{kz}|} \right\} \tag{100}$$
$$G(z) = \frac{a_2 \Pi_{xz}(z)}{2\langle \varphi p_x^2 v_z \lambda_z \rangle_+} - a_1 \frac{\partial v_x^{\mathrm{n}}}{\partial z}(z)$$
$$\Delta v_x \equiv a_1 v_x^{\mathrm{n}}(0) - v_x^{\text{ext}}$$

The quantity Δv_x represents the *finite* velocity difference of the relative motion of the excitation gas and the plane surface, the so-called velocity-*slip*. It will turn out to be of central importance for the discussion of mean

free path effects to follow. Since $G(z) \propto \partial v_x^n(z)/\partial z$, Eq. (100) becomes particularly simple if the velocity field profile is close to linear like in the case of Couette flow which we will discuss later. In such a case one may carry out the partial integration procedure repeatedly and obtain a gradient expansion for the stress tensor Π_{xz}.

$$\begin{aligned}
&\int_0^z dz'\, \mathrm{e}^{(z'-z)/\lambda_{kz}} G(z') = \lambda_{kz} \sum_{n=0}^{\infty} (-1)^n \lambda_{kz}^n [G^{(n)}(z) - G^{(n)}(0)\, \mathrm{e}^{-(z/\lambda_{kz})}] \\
&\int_z^{\infty} \mathrm{e}^{-(z'-z)/|\lambda_{kz}|} G(z') = |\lambda_{kz}| \sum_{n=0}^{\infty} |\lambda_{kz}|^n G^{(n)}(z)
\end{aligned} \tag{101}$$

Here $G^{(n)}(z)$ denotes the n-th derivative of the function $G(z)$ with respect to the variable z. Evaluating Π_{xz} with (101) leads to moments of the general form

$$L_n(z) \equiv \langle \varphi p_x^2 V_z \lambda_z^{n-1} \rangle_+ \operatorname{sgn}(z)^{n-1} \tag{102}$$

Note that the ratios L_{n+1}/L_n are of the order of the quasiparticle mean free path. The result for $\Pi_{xz}(z)$ reads

$$\begin{aligned}
\Pi_{xz}(z) &= -L_1(z)\, \Delta v_x + 2 \sum_{n=0}^{\infty} L_{2n+2}(0)\, G^{(2n)}(z) \\
&\quad - \sum_{n=0}^{\infty} (-1)^n L_{n+2}(z)\, G^{(n)}(0) \\
&= -L_1(z)\, \Delta v_x + 2L_2(0)\, G^{(0)}(z) - L_2(z)\, G^{(0)}(0) + \cdots
\end{aligned} \tag{103}$$

Far away from the surface one recovers the bulk result (91) of the preceding section:

$$\Pi_{xz}(z \to \infty) = 2L_2(0)\, G^{(0)}(z) = -\eta(\omega) \frac{\partial v_x^n}{\partial z}(z)$$

$$\eta(\omega) = \frac{a_1}{1-a_2} 2L_2(0) = \frac{a_1}{1-a_2} 2\langle \varphi p_x^2 V_z \lambda_z \rangle_+ \tag{104}$$

In contrast to the calculation in Sec. 3, the gradient expansion involves, via the boundary condition (97), the velocity gradient $\partial(v_x^n/\partial z)(0) \propto G(0)$ as well as the velocity slip Δv_x. Evaluating (103) at the surface ($z=0$) leads to the condition

$$\Pi_{xz}(0) = L_2(0)\, G^{(0)}(0) - L_1(0)\, \Delta v_x \tag{105}$$

which relates velocity slip Δv_x and velocity gradient. Δv_x may be estimated by assuming stationary ($\omega \to 0$) Couette flow with a linear velocity profile

$$v_x^{\mathrm{n}}(z) = v_x^{\mathrm{n}}(0) + v_x^{\mathrm{n}\prime} z$$

Equating $\Pi_{xz}(z) = -\eta v_x^{\mathrm{n}\prime} = \Pi_{xz}(0)$ leads to Maxwell's velocity slip boundary condition[7]:

$$\begin{aligned} \Delta v_x &= v_x^{\mathrm{n}}(0) - v_x^{\mathrm{ext}} = \zeta_0 v_x^{\mathrm{n}\prime} \\ \zeta_0 &= \frac{1}{1-\lambda_2(Y_2/Y_0)} \frac{L_2(0)}{L_1(0)} = \frac{1}{1-\lambda_2(Y_2/Y_0)} \frac{\langle \varphi p_x^2 V_z \lambda_z \rangle_+}{\langle \varphi p_x^2 V_z \rangle_+} \end{aligned} \tag{106}$$

The quantity ζ_0 has the dimension of a length and can be interpreted as the distance *behind* the wall, at which the velocity field extrapolates to zero. It is therefore referred to as the *slip length*. Eq. (106) can be interpreted as a surface boundary condition for the macroscopic velocity field $v_x^{\mathrm{n}}(z)$ which generalizes the well-known hydrodynamic "stick" boundary condition $v_x^{\mathrm{n}}(0) = v_x^{\mathrm{ext}}$ to include mean free path effects in leading order. With the result (106) we have given a microscopic derivation of Eq. (3) in the introduction. Figure 6 illustrates the shape of the (normal) fluid velocity profile near a plane wall at $z = 0$. It turns out that in a realistic situation the velocity profile acquires a positive curvature within the Knudsen layer, which is sketched in Fig. 6. Such profiles result, for example, from an exact treatment of the transport equation in the case of diffuse boundary scattering, for details of which we defer to Ref. 5. We will make use of Eq. (106) in Sec. 5 in context with the phenomenological description of hydrodynamical fluid flow. Working out the integral on the r.h.s. of Eq. (106), one finds in the hydrodynamic limit $\omega\bar{\tau} \to 0$

$$\frac{L_2(0)}{L_1(0)} = \frac{8}{15} v_{\mathrm{F}} \bar{\tau} \frac{Y_2}{Y_1}$$

Using the definition (92) one observes that in the hydrodynamic limit $\omega\bar{\tau} \to 0$ the slip length scales with the viscous mean free path λ_η of the quasiparticles as stated in Eq. (4) of the introduction:

$$\zeta_0 = a\lambda_\eta; \qquad a = \frac{8}{15}\sqrt{\frac{Y_0 Y_2}{Y_1^2}} \tag{107}$$

Note that the form of the slip coefficient a in (107) is limited to the case of diffuse boundary scattering.

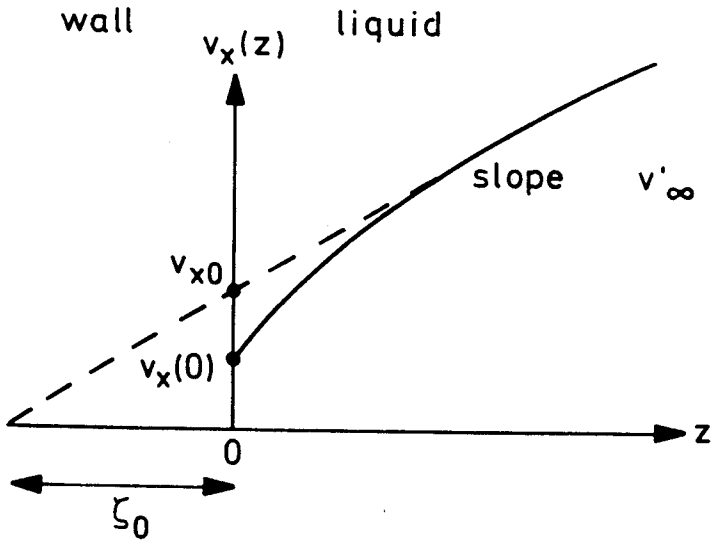

Fig. 6. Velocity profile for the transverse flow of a (quasiparticle) gas past a plane wall.

As a next step, the above calculation of the normal velocity slip length ζ_0 is (i) generalized to a more general class of wall scattering events and is (ii) estimated in a more accurate fashion as compared to the simple Maxwell treatment presented above. A form for the wall boundary condition (97) which is not restricted to the case of diffuse quasiparticle scattering can be written down by relating incoming and outgoing quasiparticle partial currents through a general elastic wall scattering probability $W_{kk'}$:

$$|V_{kz}|\,\delta\nu_k^{>}(0) = 2 \sum_{\substack{k' \\ V_{k'z}<0}} W_{kk'}\,|V_{k'z}|\,\delta\nu_k^{<}(0) \tag{108}$$

The quantity $W_{kk'}$ is the probability that a particle hitting the wall with momentum $\hbar\mathbf{k}'$ leaves it in a quantum state $\hbar\mathbf{k}$. It represents a large class of *elastic* wall scattering laws which are thought to be superimposed on the diffuse scattering processes. $W_{kk'}$ is therefore assumed to have the property

$$W_{kk'} = \tilde{W}_{kk'}\,\delta(E_k - E_{k'}) \tag{109}$$

Furthermore, we consider only the case when the scattering preserves particle number. This can be expressed as a normalization condition

$$2 \sum_{\substack{k \\ V_{kz}>0}} W_{kk'} = 1 \tag{110}$$

Finally, the global equilibrium distribution v_k^0 must obey (110). A sufficient condition for that is

$$|V_{k'z}|\, W_{kk'} v_{k'}^0 = |V_{kz}|\, W_{-k'-k} v_k^0 \qquad \text{for} \quad V_{kz} > 0; \qquad V_{k'z} < 0 \tag{111}$$

This is the reciprocity relation for boundary scattering (cf. Ref. 3). In the case of purely diffuse boundary scattering, the wall scattering probability $W_{kk'}$ is an azimuthally isotropic function of $\hat{k}$ and $\hat{k}'$ which averages to zero upon integration with the weight function p_x, characteristic for transverse flow. Special cases of elastic scattering events may include

(i) specular scattering

$$W_{kk'} = s\delta(V_{kz} - V_{k'z})\, \delta_{\mathbf{k}^*, \mathbf{k}'} \tag{112}$$

where s is a phenomenological specularity factor and $\mathbf{k}^*$ is a vector with components $\{k_x, k_y, -k_z\}$, and

(ii) elastic backward scattering

$$W_{kk'} = -r\delta(V_{kz} - V_{k'z})\, \delta_{\mathbf{k}, -\mathbf{k}'} \tag{113}$$

Here r is the corresponding backward scattering parameter. In pair correlated Fermi liquids a further elastic scattering process of quantum-mechanical origin is known to exist. It is called Andreev scattering[53] or particle–hole conversion and is caused by a reduction of the (triplet) order parameter components near the boundary. This leads to a conversion of an incoming Bogoliubov quasiparticle into a "retro-flected" hole-like excitation which has all components of the group velocity reversed. The transverse momentum, transferred to the wall in this process, however, is negligibly small, eventually leading to a temperature dependent reduction of the frictional force of the normal fluid component on the surface. For a comprehensive review of Andreev scattering we refer to the work of Kurkijärvi and Rainer.[54] Near surfaces, the order parameter representing the B-phase of superfluid ^{3}He splits into components parallel and perpendicular with respect to the surface normal. These components have different spatial gradients. However, for simplicity, we restrict the discussion to an order parameter profile which drops from its bulk value to zero near the surface. Such a step-like order parameter profile serves to provide an upper bound for the estimate of Andreev scattering effects, because it leads to the maximum possible reflection probability $R(E_k)$[53]:

$$R(E_k) = \frac{E_k - \sqrt{E_k^2 - \Delta^2}}{E_k + \sqrt{E_k^2 - \Delta^2}} \tag{114}$$

The corresponding scattering probability $W_{kk'}$ reads in the case of

(iii) Andreev scattering

$$W_{kk'} = R(E_k)\,\delta(V_{kz} + V_{k'z})\,\delta_{\mathbf{k},\mathbf{k}'} \tag{115}$$

Let us now aim at a derivation of coupled integral equations for the observables v_x^n and Π_{xz} for the general set of boundary conditions (108) which can also be written in terms of the distribution functions $h_k^>$ and $h_k^<$:

$$h_k^>(0) = \varphi_k\, p_x v_x^{\text{ext}} + 2 \sum_{\substack{k' \\ V_{k'z}<0}} W_{kk'} \frac{|V_{k'z}|}{|V_{kz}|} [h_{k'}^<(0) - \varphi_{k'}\, p'_x v_x^{\text{ext}}] \tag{116}$$

In deriving expressions for the observables, one generates the moments $L_n(z)$ (see Eq. (102)) of the mean free path λ_{kz} which correspond to the diffuse part of the scattering process, and new moments K_{mn} which account for elastic contributions:

$$K_{mn}(z, z') = \sum_{\substack{k \\ V_{kz}>0}} \sum_{\substack{k' \\ V_{k'z}>0}} \varphi_k\, p_x p'_x V_{k'z} \lambda_{kz}^{m-1} \lambda_{k'z}^{n-1} W_{k-k'} \mathrm{e}^{-(z/\lambda_z)-(z'/\lambda_{k'z})} \tag{117}$$

The integral equations for the observables v_x^n and Π_{xz} can, with the use of (102) and (117) be written in the compact form:

$$\begin{aligned} &2L_0(0)\, v_x^n(z) - a_1 \int_0^\infty dz' [L_{-1}(|z-z'|) - K_{00}(z, z')]\, v_x^n(z') \\ &\quad = [L_0(z) + K_{01}(z, 0)]\, v_x^{\text{ext}} + \frac{a_2}{2L_2(0)} \int_0^\infty dz' [L_0(z-z') \\ &\qquad + K_{01}(z, z')]\, \Pi_{xz}(z') \end{aligned} \tag{118}$$

$$\begin{aligned} &\Pi_{xz}(z) - \frac{a_2}{2L_2(0)} \int_0^\infty dz' [L_1(|z-z'|) + K_{11}(z, z')]\, \Pi_{xz}(z') \\ &\quad = [L_1(z) + K_{11}(z, 0)]\, v_x^{\text{ext}} + a_1 \int_0^\infty dz' [L_0(z-z') - K_{01}(z, z')]\, v_x^n(z') \end{aligned}$$

where the coefficients a_ℓ have been defined through relation (89). The coupling of the observables v_x^n and Π_{xz} is described by the nonlocal integral operators $L_n(|z-z'|)$ and $K_{mn}(z, z')$. The treatment of the problem in Sec. 3 corresponds to the local limit $\lambda_{kz} \to 0$ in L_n and K_{mn}, its generalization to

finite mean free paths requires the full treatment represented by the system of integral equations (118). We come now back to the case of stationary Couette flow which is obtained as a special case ($\omega\bar{\tau} \to 0$) from the second of the coupled integral equations (118):

$$\Pi_{xz}(z) = -\eta(T)\frac{\partial v_x^{\mathrm{n}}(z)}{\partial z} = -\eta(T)\, v_x^{\mathrm{n}\prime}[1+\psi(z)] \tag{119}$$

$$= -[L_1(z) + K_{11}(z,0)]\,\Delta v_x - \frac{1}{1-\lambda_2(Y_2/Y_0)}\int_0^\infty dz'[L_1(|z-z'|) + K_{11}(z,z')]\frac{\partial v_x^{\mathrm{n}}(z')}{\partial z'}$$

Here $\psi(z) = [\partial v_x^{\mathrm{n}}(z)/\partial z - v_x^{\mathrm{n}\prime}]/v_x^{\mathrm{n}\prime} > 0$ is a measure of the curvature of the velocity profile. From (119) one may derive an integral equation for the slip length $\zeta_0 = \Delta v_x / v_x^{\mathrm{n}\prime} + \int_0^\infty dz\,\psi(z)$:

$$\zeta_0\{L_1(z) + K_{11}(z,0)\} - \{L_2(z) - K_{12}(z,0)\}$$

$$= \int_0^\infty dz'\,\psi(z')\{[L_1(z) + K_{11}(z,0)] - [L_1(|z-z'|) + K_{11}(z,z')]\} \tag{120}$$

Now we put $z = 0$. Assuming the three expressions in curly brackets as well as the quantity $\psi(z)$ to be positive one may derive positive bounds for the slip length ζ_0 from (120):

(i) lower bound (Maxwellian slip, $\psi(z) \equiv 0$):

$$\zeta_0^{\mathrm{LB}} > \frac{1}{1-\lambda_2(Y_2/Y_0)}\frac{L_2(0) - K_{12}(0,0)}{L_1(0) + K_{11}(0,0)} \tag{121}$$

Note that this is a generalization of the estimate (106) for the slip length to include elastic wall scattering processes.

(ii) From an integration of Eq. (120) over z from 0 to ∞ one may derive an upper bound:

$$\zeta_0^{\mathrm{UB}} < \frac{1}{1-\lambda_2(Y_2/Y_0)}\frac{L_3(0) - K_{22}(0,0)}{L_2(0) + K_{21}(0,0)} \tag{122}$$

(iii) Finally it is possible to derive an improved lower bound for the slip length:

$$\zeta_0^{\mathrm{ILB}} > \frac{1}{1-\lambda_2(Y_2/Y_0)} \times \frac{[L_2(0)-K_{21}(0,0)]^2+[L_1(0)+K_{11}(0,0)][L_3(0)-K_{22}(0,0)]}{2L_2(0)[L_1(0)+K_{11}(0,0)]} \tag{123}$$

These bounds have, for the case of diffuse scattering ($K\equiv 0$), first been derived by Jensen *et al.*[55] Let us discuss this special case first. Applying the results (121)–(123) to the case of purely diffuse scattering, the slip length of a normal Fermi liquid is bounded by

$$\tfrac{8}{15}\lambda_\eta < \zeta_0 < \tfrac{5}{8}\lambda_\eta; \qquad \zeta_0 > \tfrac{1}{2}[\tfrac{8}{15}+\tfrac{5}{8}]\,\lambda_\eta = 0.579\ldots\lambda_\eta \tag{124}$$

In a superfluid Fermi liquid the ratio of the slip length to the mean free path varies slightly with temperature in the case of diffuse scattering as can be seen from the (Maxwell) result for the lower bound (107) and which is shown in part a) of Fig. 7 for ^{3}He–B at 20 bar pressure. The three bounds (LB, UB, ILB, dashed lines) are shown together with the result of an exact treatment (EX, full line).[5]

The improved lower bound for the slip length is seen to be an excellent approximation in the case of diffuse scattering. It can be anticipated to

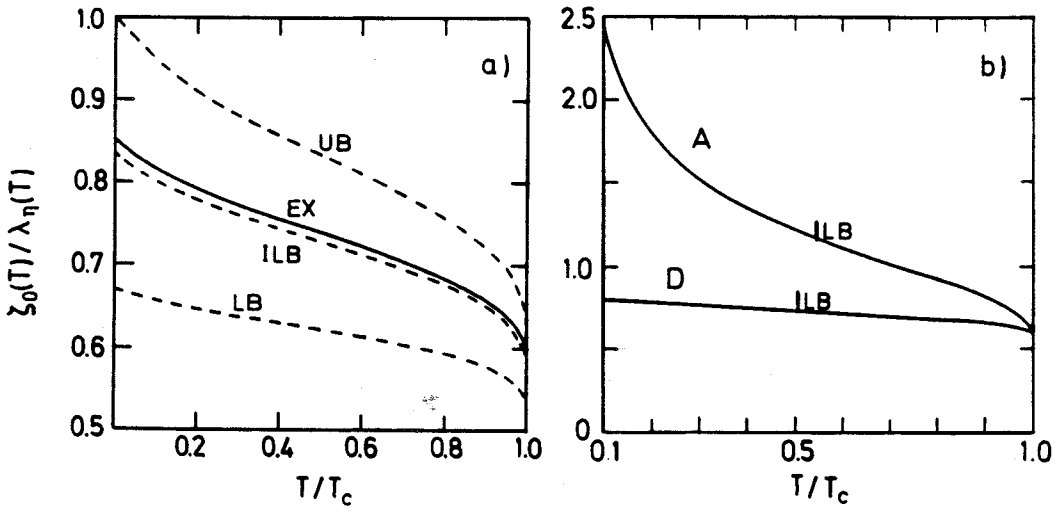

Fig. 7. (a) Slip length ζ_0 of an isotropic Fermi superfluid, normalized to the viscous mean free path λ_η. Dashed lines: bounds on the slip length; full line: exact result (see text). (b) Comparison of the slip lengths normalized to the viscous mean free path for the cases of diffuse (D) and Andreev (A) scattering (step profile).

work as well in the more general case of additional elastic wall scattering processes, which will now be discussed. Inserting the scattering probabilities (112), (113) into the mean free path moments (118) one finds that

$$K_{mn}(z, z') = -tL_{m+n-1}(z+z') \tag{125}$$

where $t=s$ in the case of specular scattering and $t=-r$ in the case of elastic backward scattering. The lower bound for the slip length in these cases has the form

$$\zeta_0^{\mathrm{LB}}(t) = \zeta_0^{\mathrm{LB}}(0)\frac{1+t}{1-t} \tag{126}$$

and is hence seen to be enhanced for specular scattering and reduced for elastic backscattering. The case of Andreev scattering in a Fermi superfluid has to be discussed separately because the functions $K_{mn}(z, z')$ have to be evaluated with the amplitude $R(E_k)$ for particle–hole conversion:

$$K_{mn}(z, z') = -\langle \varphi p_x^2 V_z \lambda_z^{m+n-2} R(E)\, \mathrm{e}^{-(z+z')/\lambda_z}\rangle_+ \equiv -R_{m+n-1}(z+z') \tag{127}$$

Inserting this into the result (121) for the Maxwellian slip length one finds that Andreev scattering leads to an enhancement of the slip length over its value for purely diffuse scattering:

$$\zeta_0^{\mathrm{LB}}(R) = \zeta_0^{\mathrm{LB}}(0)\frac{1+R_2(0)/L_2(0)}{1-R_1(0)/L_1(0)} \tag{128}$$

For the special case of a step-like order parameter profile near the wall $\Delta(z)=\Delta(T)\,\Theta(z-z_0)$ one may show from (128) that the ratio $\zeta_0^{\mathrm{LB}}(R)/\zeta_0^{\mathrm{LB}}(0)$ diverges as $\propto T^{-1/2}$ in the low temperature limit. The temperature dependence of the slip enhancement in the presence of Andreev scattering over that for diffuse scattering is illustrated in part b) of Fig. 7. The dramatic increase which is visible there has been termed the "quantum slip effect" because it is the quantum–mechanical scattering of Bogoliubov quasiparticles which is responsible for the loss of transverse momentum transfer to the container walls.

Being aware of the fact that the length ζ_0 enters the description of fluid flow as an additional temperature dependent parameter and being able to compute it for various wall scattering probabilities, we now have to investigate in detail where the slip length enters the hydrodynamic description of fluid flow as a finite size correction. This will be the topic of the next section.

5. PHENOMENOLOGICAL THEORY OF FLOW IN RESTRICTED GEOMETRY

In this section we deal with the incorporation of experimental finite size constraints on the determination of the shear viscosity. These considerations will be restricted to certain classes of torsional oscillator and sound propagation experiments which use a parallel plate geometry. The treatment will be entirely on a phenomenological level. A phenomenological treatment of mean free path effects, i.e., the incorporation of the slip length ζ_0 into the theory, can be achieved by postulating a boundary condition for the macroscopic velocity field v_x^n at the container wall, which allows for velocity slip. Such a boundary condition is particularly simple in the case of one ideally plane wall, located at $z=0$, which confines the fluid to the half space $z>0$, as discussed in the previous section. For such a geometry we obtain a simple slip boundary condition for transverse flow (cf. Eq. (106)):

$$\Delta v_x \equiv v_x^n(0) - v_x^{ext} = \zeta_0 \frac{\partial v_x^n}{\partial z}(0) \tag{129}$$

It should be noted that the use of the boundary condition (129) amounts to accounting for the slip effect as a first order mean free path correction to the hydrodynamic treatment. It will be shown in the next section how this description may be generalized to arbitrary Knudsen numbers.

Let us first consider an experimental arrangement which is typical for the determination of the shear viscosity, namely the torsional oscillator.

5.1. Torsion Oscillator Experiments

A typical torsional oscillator cell's geometry consists of two circular parallel plates of radius R, a distance d apart, located at $z=\pm d/2$ at the top and bottom, and a cylindrical sidewall. The influence of the sidewall is negligible if $R \gg d$ and turns out to be trivial for $R \approx d$ and will therefore be omitted in the calculations to follow. This cell entrains the Fermi liquid under investigation and is assumed to oscillate with a frequency ω about the cylinder axis. In such a geometry the macroscopic velocity field is purely azimuthal

$$v_\phi^n(r, z, t)$$

where r measures the distance from the cylinder axis and $-d/2 < z < d/2$. The hydrodynamic form of the momentum current then reads (cf. (104)):

$$\Pi_{\phi z}(r, z, t) = -\eta(T) \frac{\partial v_\phi^n(r, z, t)}{\partial z} \tag{130}$$

Splitting off the harmonic time dependence of the velocity field

$$v_\phi^n(r, z, t) = v_\phi^n(r, z)\, e^{-i\omega t} \tag{131}$$

one may write the Navier–Stokes equation in cylindrical coordinates as

$$-i\omega\rho^n v_\phi^n(r, z) = \eta \left[\frac{\partial^2}{\partial r^2} + \frac{1}{r}\frac{\partial}{\partial r} - \frac{1}{r^2} + \frac{\partial^2}{\partial z^2} \right] v_\phi^n(r, z) \tag{132}$$

Dividing (132) by the viscosity η one observes that the length scale for the spatial variation in r and z is set by the quantity

$$\delta(\omega) = \sqrt{\frac{2\eta}{\rho^n \omega}} \tag{133}$$

which is called the viscous penetration (or skin) depth, and which characterizes the thickness of the fluid layer that is dragged along by the motion of the wall. In Fig. 8 we have plotted the viscous penetration depth for

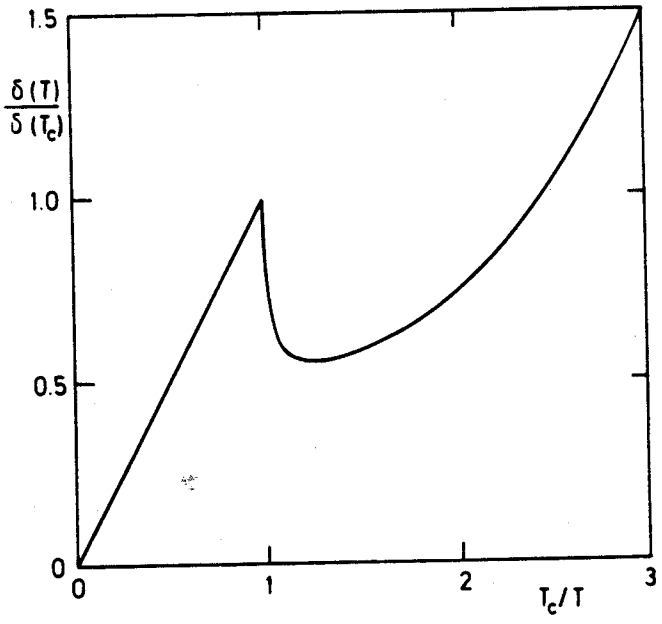

Fig. 8. The viscous penetration depth δ of normal and superfluid ^{3}He(–B) at 0 bar pressure, normalized to its value at T_c vs. inverse reduced temperature, T_c/T.

normal and superfluid ^{3}He–B at 0 bar pressure, normalized to its value at the transition, as a function of the inverse reduced temperature T_c/T.

Depending on the frequency of the oscillator, the viscous penetration depth specifies different regimes of viscous confinement. If $\delta \gg d$, the fluid is "clamped" and moves as a whole with the oscillator whereas in the opposite limit $\delta \ll d$, only a sheet of thickness δ is dragged along by the surfaces. The purpose of the following considerations is to study the fluid response to oscillations of the confining walls in the whole range of parameters d/δ. Defining a complex wavenumber $k = (1+i)/\delta$, the differential equation for the velocity field assumes the form:

$$\left[\frac{\partial^2}{\partial r^2} + \frac{1}{r}\frac{\partial}{\partial r} - \frac{1}{r^2} + \frac{\partial^2}{\partial z^2} + k^2\right] v_\phi^n(r, z) = 0 \tag{134}$$

The r and z dependence of the solution of (134) factorizes

$$v_\phi^n(r, z) = \left[ar + \frac{b}{r}\right] \cos kz \tag{135}$$

and only the choice $b = 0$ for the second integration constant guarantees the regular behavior of the solution at the origin. The remaining integration constant is fixed by the slip boundary condition (129), which, applied to the double plate geometry, reads

$$v_\phi^n\left(r, \pm\frac{d}{2}\right) - \dot{\Theta} r = \mp\zeta_0 \frac{\partial v_\phi^n}{\partial z}\left(r, \pm\frac{d}{2}\right) \tag{136}$$

where $\dot{\Theta}$ denotes the angular frequency of the torsional oscillator. Inserting the solution for the velocity field (135) into the boundary condition (129) fixes the integration constant a:

$$a = \frac{\dot{\Theta}}{\cos(kd/2) - k\zeta_0 \sin(kd/2)} \tag{137}$$

For the torsional oscillator experiment it turns out that two quantities are important:

(i) the cross sectional average of the velocity field v_ϕ^n

$$\langle v_\phi^n \rangle_z \equiv \frac{1}{d}\int_{-d/2}^{d/2} dz\, v_\phi^n(r, z) = \dot{\Theta} r \left\{\frac{2}{kd}\frac{\tan(kd/2)}{1 - k\zeta_0 \tan(kd/2)}\right\} \tag{138}$$

and (ii) the viscous shear force on the walls which reads for the upper wall

$$\Pi_{\phi z}\left(r, \frac{d}{2}\right) = \dot{\Theta} r \eta \frac{k^2 d}{2} \left\{ \frac{2}{kd} \frac{\tan(kd/2)}{1 - k\zeta_0 \tan(kd/2)} \right\} \tag{139}$$

The physics of both quantities is governed by the function in curly brackets which determines the amount of viscous coupling of the fluid to the surfaces in the presence of slip:

$$F = F(d, \delta, \zeta_0) = \frac{2}{kd} \frac{\tan(kd/2)}{1 - k\zeta_0 \tan(kd/2)} \tag{140}$$

It is useful to evaluate the viscous coupling function F in the limits where the viscous penetration depth is either large or small with respect to the plate spacing d:

$$\begin{aligned} \lim_{\delta \gg d} F(d, \delta, \zeta_0) &= 1 + \frac{i}{3}\left(\frac{d}{\delta}\right)^2 \left[1 + 6\frac{\zeta_0}{d} \right] + \cdots \\ \lim_{\delta \ll d} F(d, \delta, \zeta_0) &= (1+i)\frac{\delta}{d}\left[1 - (1-i)\frac{\zeta_0}{\delta} \right] + \cdots \end{aligned} \tag{141}$$

The behavior of the real and imaginary parts of the viscous coupling function for arbitrary values of the parameter d/δ is shown in the insert of Fig. 9 for two different ratios ζ_0/d of the slip length with respect to the plate spacing.

From the viscous shear force (139) on the plates one may now compute the torque that the fluid exerts on the top and bottom plates:

$$M = 2\int_0^R dr\, r(2\pi r)\, \Pi_{\phi z}(r, z) = \frac{\pi}{2} R^4 \eta \dot{\Theta} k^2 d\, F(d, \delta, \zeta_0) \tag{142}$$

The complex viscous torque $M(z)$ specifies the influence of the quasiparticle gas on the equation of motion of the torsional oscillator

$$I_s \ddot{\Theta} + \left[\frac{M}{\dot{\Theta}} + N \right] \dot{\Theta} + \kappa\Theta = D_0 e^{-i\omega t} \tag{143}$$

in which I_s denotes the moment of inertia of the empty cell, N is the nuisance damping, κ the torsion constant and D_0 the driving force. Calling

$$I_f = \tfrac{1}{2}\pi R^2\, d\rho \cdot R^2$$

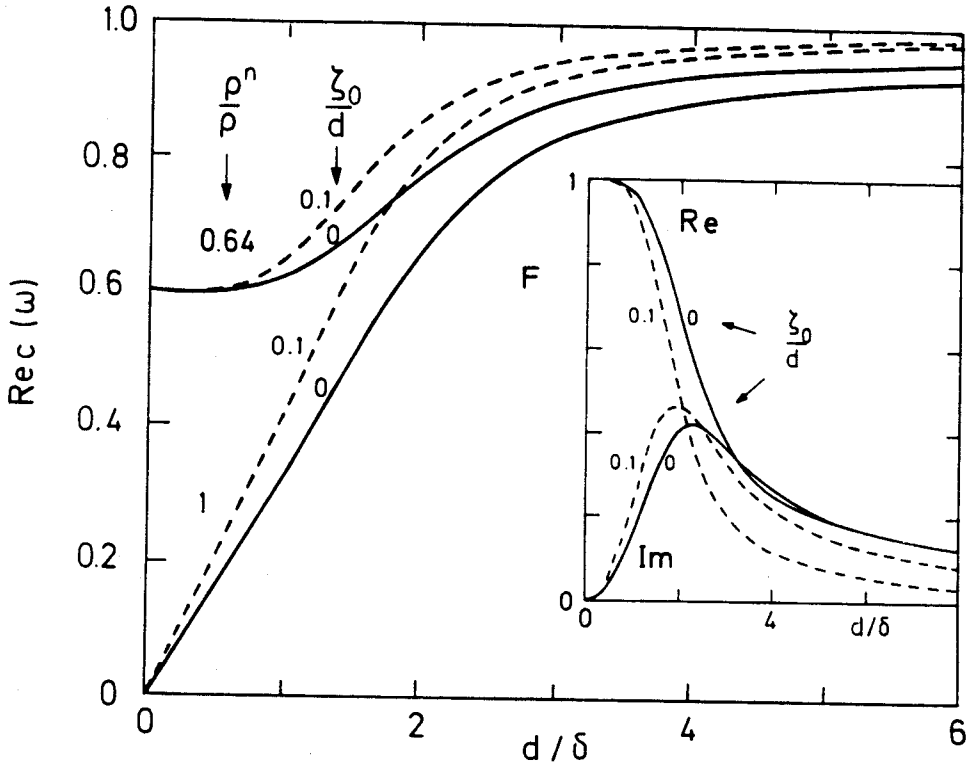

Fig. 9. The transition from fourth to first sound in a parallel plate resonator for two values of ρ^n/ρ and ζ_0/d as a function of d/δ (after Ref. 56). The insert shows real and imaginary part of the viscous confinement function F as a function of d/δ for two values of ζ_0/d.

the fluid moment of inertia, the characteristic frequency of the oscillator can be found to be

$$\omega = \omega_0 \left\{ 1 + \frac{1}{2} \frac{\rho^n}{\rho} \frac{I_f}{I_s} F(d, \delta, \zeta_0) + \frac{iN}{2I_s\omega_0} \right\} \tag{144}$$

where $\omega_0^2 = \kappa/I_s$ is the resonant frequency of the oscillator. From the result (144) for the complex characteristic frequency, one may obtain the dissipation as the imaginary part

$$Q^{-1} = 2 \operatorname{Im}\left(\frac{\omega}{\omega_0}\right) = \frac{N}{I_s\omega_0} + \frac{\rho^n}{\rho} \frac{I_f}{I_s} \operatorname{Im} F(d, \delta, \zeta_0) \tag{145}$$

Using the asymptotic behavior (141) of the F-function one may evaluate the dissipation in the limits of small and large values of the viscous confinement parameter d/δ

$$\lim_{\delta \gg d} Q^{-1} = \frac{N}{I_s \omega_0} + \frac{\rho^n}{\rho} \frac{I_f}{I_s} \frac{\rho^n \omega d^2}{12\eta} \left[1 + 6 \frac{\zeta_0}{d} \right]$$
$$\lim_{\delta \ll d} Q^{-1} = \frac{N}{I_s \omega_0} + \frac{\pi R^4}{I_s \omega_0} \operatorname{Re} Z_\perp(\omega; \zeta_0) \tag{146}$$

The frequency (or period) shift of the oscillator is obtained as the real part of the complex characteristic frequency:

$$2 \frac{\Delta\omega}{\omega_0} = \frac{\rho^n}{\rho} \frac{I_f}{I_s} \operatorname{Re} F(d, \delta, \zeta_0) \tag{147}$$

which again can be treated in the two asymptotic limits

$$2 \lim_{\delta \gg d} \frac{\Delta\omega}{\omega_0} = \frac{\rho^n}{\rho} \frac{I_f}{I_s} \left[1 + O\left(\frac{\delta^4}{d^4} \right) \right]$$
$$2 \lim_{\delta \ll d} \frac{\Delta\omega}{\omega_0} = \frac{\pi R^4}{I_s \omega_0} \operatorname{Im} Z_\perp(\omega; \zeta_0) \tag{148}$$

The above calculations may be summarized as follows: There are two quantities which emerge from a torsional oscillator measurement in the limits of small and large d/δ: In the "clamped" limit $\delta \gg d$ the experiment sees an effective viscosity

$$\eta_{\text{eff}}(T) = \eta(T) \frac{d}{d + 6\zeta_0(T)} \tag{149}$$

in the dissipation, with the normal fluid density ratio that can be obtained from simultaneous measurements of the frequency shift. In the opposite limit, $\delta \ll d$, the same experiment measures the complex transverse surface (or shear) impedance $Z_\perp$:

$$Z_\perp(\omega; \zeta_0) = \frac{\Pi(0)}{v^{\text{ext}}} = \frac{(1-i)\,\eta(T)}{\delta(T) + (1-i)\,\zeta_0(T)} \tag{150}$$

The equations (149) and (150) for the effective viscosity and the transverse surface impedance are the central results of this section and provide the justification of Eqs. (6) and (7) in the introduction. They show that both quantities are affected by mean free path effects which, in our phenomenological treatment, enter as first order slip corrections to the hydrodynamic results for infinitely extended systems. In the case of the effective viscosity the importance of the slip correction is given by the ratio ζ_0/d, i.e.,

essentially the Knudsen number Kn, whereas in the case of the surface impedance the importance of the slip effect scales with ζ_0/δ, i.e., with the inverse of the frequency dependent viscous penetration depth $\delta^{-1} \propto \omega^{1/2}$. Therefore the slip correction to the transverse surface impedance vanishes in the hydrodynamic limit $\omega \to 0$.

5.2. Sound Propagation Experiments

Let us now consider another kind of a clean experimental arrangement for the determination of viscous transport as influenced by mean free path effects. It is a parallel plate sound resonator, which is discussed, to some extent, along the lines of the treatment by Højgaard Jensen *et al.*[56] Consider the idealized case of a parallel plate flow channel with height d in which sound is generated on the one side, propagates in the x-direction and is detected at the other end. The relevant two-fluid hydrodynamic equations for this case are the continuity equation

$$\frac{\partial \rho}{\partial t} + \rho^{\mathrm{n}} \frac{\partial v_x^{\mathrm{n}}}{\partial x} + \rho^{\mathrm{s}} \frac{\partial v_x^{\mathrm{s}}}{\partial x} = 0 \tag{151}$$

the Navier–Stokes equation

$$\rho^{\mathrm{n}} \frac{\partial v_x^{\mathrm{n}}}{\partial t} + \rho^{\mathrm{s}} \frac{\partial v_x^{\mathrm{s}}}{\partial t} = -\frac{\partial \delta P}{\partial x} + \eta \left[\frac{4}{3} \frac{\partial^2}{\partial x^2} + \frac{\partial^2}{\partial z^2} \right] v_x^{\mathrm{n}} \tag{152}$$

and the acceleration equation for the superfluid

$$\frac{\partial v_x^{\mathrm{s}}}{\partial t} = -\frac{1}{\rho} \frac{\partial \delta P}{\partial x} + \zeta_3 \frac{\partial^2}{\partial x^2} [g_x - \rho v_x^{\mathrm{n}}] \tag{153}$$

The dispersion of sound can be studied by differentiating the continuity equation with respect to time and inserting the Navier–Stokes equation. Assuming a spatial variation in the x-direction $\propto \exp(iqx)$, expressing the pressure variation by the mass density change $\delta P = c_1^2 \delta \rho$ via the first sound velocity $c_1 = (\rho\kappa)^{-1} = (1 + F_0^{\mathrm{s}})(1 + F_1^{\mathrm{s}}/3)\, v_{\mathrm{F}}^2/3$, and going over to quantities averaged over the cross section of the flow channel, one eventually arrives at the following equation for the dispersion of sound:

$$\left[\frac{\partial^2}{\partial t^2} - c_1^2 \frac{\rho^{\mathrm{s}}}{\rho} \frac{\partial^2}{\partial x^2} \right] \langle \delta \rho \rangle_z = -\rho^{\mathrm{n}} \frac{\partial^2}{\partial x\, \partial t} \langle v_x^{\mathrm{n}} \rangle_z + \cdots \tag{154}$$

In the derivation of (154), terms of the order $O(q\delta)$ have been ignored for the moment. Let us first assume that the viscous confinement parameter

d/δ is very small so that the right hand side of Eq. (154) is negligible, i.e., that the normal fluid velocity field is clamped. Then we obtain from (154) a dispersion relation of fourth sound with a complex frequency

$$c_4^2(\omega) = (c_4^0)^2 \left[1 - \frac{i}{Q_4} \right] \tag{155}$$

from which one identifies the fourth sound velocity

$$c_4^0 = c_1 \sqrt{\frac{\rho^s}{\rho}} \tag{156}$$

and the damping or Q-factor

$$Q_4^{-1} = \frac{\rho\omega}{c_1^2} \zeta_3 \tag{157}$$

Here ζ_3 is the coefficient of bulk (second) viscosity, which governs the longitudinal degrees of freedom introduced by the longitudinal sound.[57] Let us next relax the assumption of small d/δ and investigate the dispersion relation for arbitrary d/δ. For this purpose we need the normal fluid velocity profile v_x^n which is calculated from the differential equation

$$\left[\frac{\partial^2}{\partial z^2} + k^2 \right] v_x^n(z) = \frac{\rho^n}{\rho} \frac{iq}{\eta} c_1^2 \delta\rho \tag{158}$$

to be of the form

$$v_x^n(z) = \frac{q}{\rho\omega} c_1^2 \delta\rho [1 + A \cos kz] \tag{159}$$

As in the torsional oscillator problem, the slip boundary condition fixes the integration constant A and after a straightforward calculation we arrive at the desired result for the cross sectional average of the velocity field

$$\langle v_x^n \rangle_z = \frac{q}{\omega} \frac{c_1^2}{\rho} \delta\rho [1 - F(d, \delta, \zeta_0)] \tag{160}$$

This result, when inserted into the r.h.s. of Eq. (154) leads to the following general expression for the dispersion of sound in a parallel plate geometry:

$$c^2(\omega) = c_1^2 \left\{ \frac{\rho^s}{\rho} \left[1 - \frac{i\omega\rho\zeta_3}{c_1^2} \right] + \frac{\rho^n}{\rho} \left[1 - \frac{4i\omega\eta(\omega)}{3\rho^n c_1^2} - F(d, \delta, \zeta_0) \right] \right\} \tag{161}$$

Here $\eta(\omega) = 2L_2(0)\, a_1(\omega)/[1 - a_2(\omega)]$ is the dynamic shear viscosity which characterizes the constitutive relation (90) for the dissipative part of the stress tensor at finite frequencies. Not surprisingly, it is the viscous coupling function F that also governs the finite size effects on the dispersion of sound in a parallel plate geometry. Here the limiting cases of small and large viscous confinement parameter d/δ correspond to the propagation of fourth ("clamped" regime) and first ("open" regime) sound, respectively. Let us discuss the two limits separately. The dispersion of fourth sound is obtained from (161) in the limit $d/\delta \to 0$ as

$$c_4^2(\omega) = c_1^2 \frac{\rho^s}{\rho} \left\{ 1 + \frac{1}{30} \frac{\rho^n}{\rho^s} \left(\frac{d}{\delta} \right)^4 \left[1 + 10 \frac{\zeta_0}{d} \right] - \frac{i}{Q_4} \right\} \tag{162}$$

The imaginary part in the dispersion relation (162) has now acquired a surface contribution, which, as in the torsional oscillator case, is characterized by the inverse effective (i.e. slip-corrected) viscosity:

$$Q_4^{-1} = \omega \frac{\rho \zeta_3}{c_1^2} + \frac{\rho^n}{\rho^s} \frac{\rho^n \omega d}{12\eta} \left[1 + 6 \frac{\zeta_0}{d} \right] \tag{163}$$

In the opposite limit, $d/\delta \gg 1$ Eq. (161) describes the dispersion of first sound

$$c_1^2(\omega) = c_1^2 \left\{ 1 - i \frac{4\omega\eta(\omega)}{3\rho c_1^2} - i \frac{2Z_\perp(\omega)}{\rho \omega d} \right\} \tag{164}$$

from which one finds the velocity of first sound

$$\operatorname{Re} c_1(\omega) = c_1 \left\{ 1 + \frac{2\omega \operatorname{Im} \eta(\omega)}{3\rho c_1^2} + \frac{\operatorname{Im} Z_\perp(\omega)}{\rho \omega d} \right\} \tag{165}$$

and the attenuation

$$\alpha(\omega) = \operatorname{Im} \left(\frac{\omega}{c_1(\omega)} \right) = \frac{2\omega^2 \operatorname{Re} \eta(\omega)}{3\rho c_1^2} + \frac{\operatorname{Re} Z_\perp(\omega)}{\rho d c_1} \tag{166}$$

The transition from fourth to first sound in a resonator with parallel plate geometry as a function of d/δ is shown in Fig. 9 for two different temperatures (corresponding to two values for ρ^n/ρ) and two different slip lengths. An inspection of the frequency dependence shows that the surface contributions to the sound dispersion relations dominate the bulk ones in the hydrodynamic limit. It should be noted that similar dispersion relations

for fourth and first sound hold in the case that the shape of the flow channel cross section is arbitrary. If the cross section is characterized by an area S and a circumference L one simply has to replace $d/2$ by S/L. For cylindrical flow channels of radius R, for example, this implies the replacement $d \to R$.

6. POISEUILLE FLOW AND SURFACE IMPEDANCE

In the previous section we have shown that the flow channel width d or the viscous penetration depth δ, typical sizes characterizing fluid flow experiments, are length scales on which effects of finite quasiparticle mean free path may become important. The slip length ζ_0 appears as an additional temperature dependent parameter of the theory which renormalizes the shear viscosity and the transverse surface impedance and turns them into an effective viscosity and an effective surface impedance, respectively, both of which explicitly depend on the geometry of the experimental arrangement for its measurement.

This geometry dependence of the viscosity and surface impedance manifests itself so far, however, only through a *first order* correction in the mean free path (we are in the so-called *slip regime*) and, under certain circumstances, will have to be extended to larger mean free paths λ_η which may increase to being of the same order as d or δ. In order to illustrate this restriction introduced by considering only the slip regime, we have shown in Fig. 10 various regimes of viscous penetration depths and mean free paths. The *slip regime* appears in this figure as the left vertical strip corresponding to small Knudsen numbers, within which one may describe phenomenologically the Poiseuille flow and surface impedance limit of the parallel plate torsional oscillator as well as the transition from fourth to first sound (see previous section).

Two possible extensions of the *slip regime* will be discussed below:

(i) The regime of large values of the viscous penetration or "skin" depth δ ("clamped regime," lower horizontal strip), and *arbitrary* Knudsen numbers. It will be described theoretically using the microscopic Boltzmann equation for (Bogoliubov) quasiparticles as introduced in Sec. 3. The result will be expressed as an effective viscosity of the Poiseuille flow problem η_{eff} valid for arbitrary Knudsen numbers Kn.

(ii) The description of the regime of small δ, on the other hand, ("open regime, upper horizontal strip) is governed by the full microscopic result for the transverse surface impedance $Z_\perp(\omega)$ for arbitrary λ_η/δ, which will also be derived below.

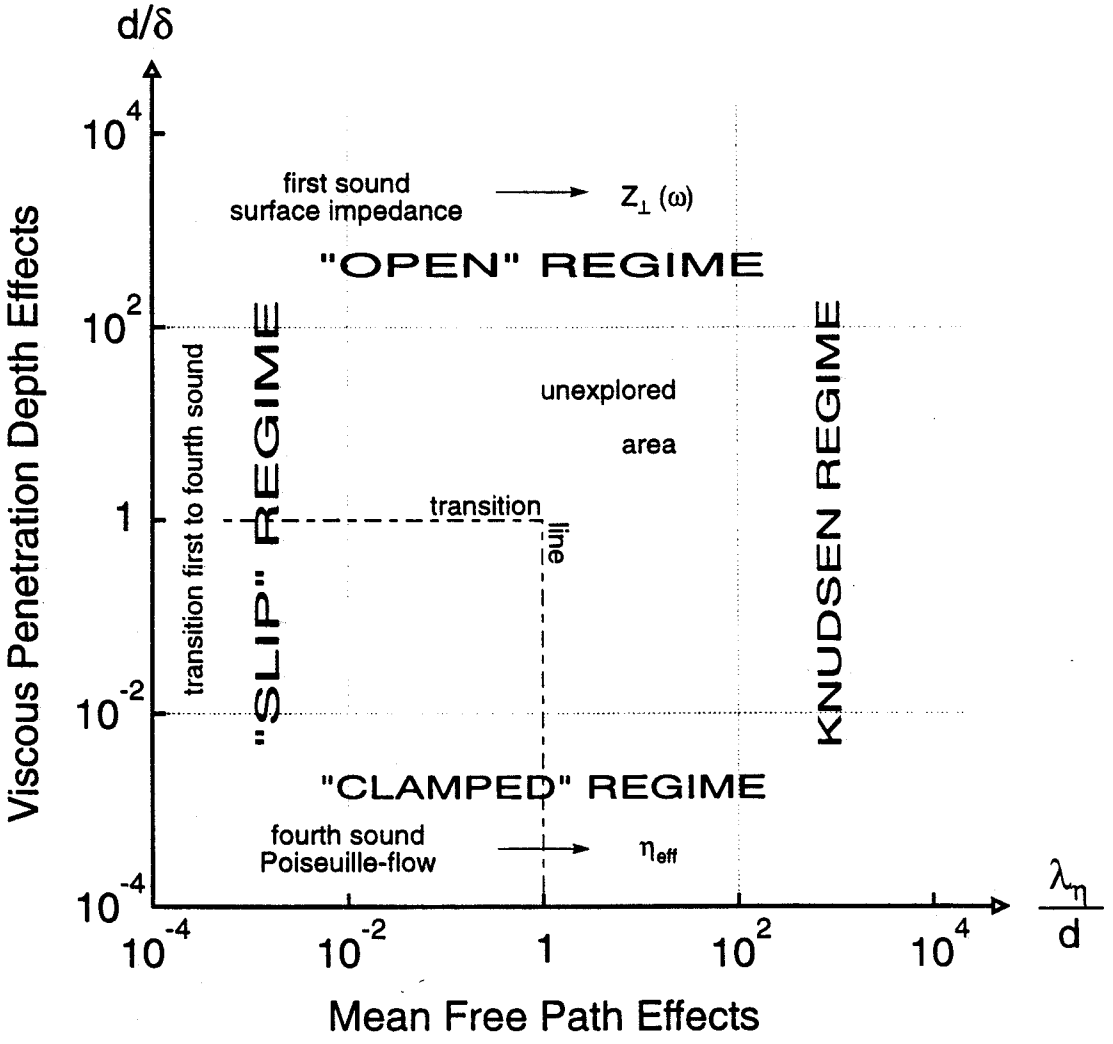

Fig. 10. Dynamic regimes for Fermi superfluids in the $d/\delta - \lambda_\eta/d$ plane.

Finally there is the "Knudsen regime" at high Kn (right vertical strip) in which surface scattering processes dominate the physics for various values of δ. We shall discuss numerical results for the effective Poiseuille flow viscosity and the surface impedance in the Knudsen regime.

The dashed transition line in Fig. 10 marks the complicated and therefore so far unexplored behavior at $d/\delta \sim 1$ and $\lambda_\eta/d \sim 1$.

6.1. Shear Viscosity and Knudsen Flow

It is the aim of this section to calculate the effective viscosity, as determined in a parallel plate geometry in the limit $d/\delta \to 0$, from the scalar Landau–Boltzmann equation for quasiparticles at arbitrary Knudsen numbers $\mathrm{Kn} = \lambda_\eta/d$. We start by applying the Landau–Boltzmann equation (93) for the distribution function h_k to the case of stationary flow of a fluid,

which is confined to the space $-d/2 \leqslant z \leqslant d/2$ between two plane walls at $z = \pm d/2$ (double plane boundary problem):

$$\left(\frac{\partial}{\partial z} + \frac{1}{\lambda_{kz}}\right) h_k = \varphi_k p_x \left\{\frac{\lambda_2 \Pi_{xz}}{2L_2(0)} + \frac{1}{\lambda_{kz}} v_x^{\mathrm{n}} + \frac{\bar{\tau} F_x^{\mathrm{ext}}}{\lambda_{kz} m(1 + (F_1^s/3)\, Y_0)}\right\} \tag{167}$$

Here $\lambda_{kz} = V_{kz}\bar{\tau}$ is the $\omega \to 0$ limit of the k-dependent quasiparticle mean free path. The external force F_x^{ext} appearing in (167) can be thought of as originating from a time-dependent wall velocity (cf. torsional oscillator) or, equivalently, from a pressure gradient (stationary Poiseuille flow):

$$\frac{F_x^{\mathrm{ext}}}{m} = -i\omega v_x^{\mathrm{ext}} \equiv \frac{1}{\rho^{\mathrm{n}}} \frac{\partial \delta P}{\partial x}$$

This external force term appears also in the conservation law for the quasiparticle momentum (Navier–Stokes equation)

$$-i\omega v_x^{\mathrm{n}}(z) + \frac{\partial \Pi_{xz}(z)}{\partial z} = \rho^{\mathrm{n}} \frac{F_x^{\mathrm{ext}}}{m}$$

The effect of the stress tensor term in (167) is essentially to turn the averaged quasiparticle lifetime $\bar{\tau}$ into the appropriate viscous transport time τ_η. In what follows, we shall therefore omit the stress tensor term from the kinetic equations and replace $\bar{\tau}$ by τ_η at the end of the calculation. The kinetic equation can be formally integrated to yield

$$h_k(z) = C_k \mathrm{e}^{-(z/\lambda_{kz})} + \frac{\varphi_k p_x}{\lambda_{kz}} \int_{-d/2}^{z} dz' \left[v_x^{\mathrm{n}}(z') + \frac{\bar{\tau} F_x^{\mathrm{ext}}}{m}\right] \mathrm{e}^{-(z-z')/\lambda_{kz}} \tag{168}$$

The values of the distribution function h_k at the boundaries $z = \pm d/2$, required in Eq. (168) are taken from the boundary condition (cf. (116)):

$$|V_{kz}|\, h_k^{\gtrless}\left(\mp\frac{d}{2}\right) = 2 \sum_{\substack{k' \\ V_{k'z} < 0}} W_{kk'}\, |V_{k'z}|\, h_k^{\lessgtr}\left(\mp\frac{d}{2}\right) \tag{169}$$

We proceed now by deriving an integral equation for the quasiparticle velocity field v_x^{n}. The integral operators $L_n(|z-z'|)$, (cf. Eq. (102)), which describe nonlocal effects in the case of purely diffuse scattering, are amended in the special cases of specular, backward and Andreev scattering by integrals of the form

$$R_n(z, z') = \left\langle \varphi p_x^2 V_z \lambda_z^{n-1} \frac{2R\, \mathrm{e}^{-d/\lambda_z}}{1 - R\, \mathrm{e}^{-d/\lambda_z}} \cosh\left(\frac{z}{\lambda_z}\right) \cosh\left(\frac{z'}{\lambda_z}\right)\right\rangle_+ \tag{170}$$

where $R = R_k = s$, $-r$ and $R = R(E_k)$ in the cases of specular, backward and Andreev scattering, respectively. With the definition (170) the desired integral equation for the velocity field reads

$$v_x^n(z) = \frac{1}{2L_0(0)} \int_{-d/2}^{d/2} dz' [L_{-1}(|z-z'|) + R_{-1}(z, z')] \left[v_x^n(z') + \frac{\bar{\tau} F_x^{ext}}{m} \right] \tag{171}$$

If one introduces a dimensionless velocity field $w(z)$

$$v_x^n(z) = \frac{\bar{\tau} F_x^{ext}}{m} [w(z) - 1] \tag{172}$$

and the integral kernel

$$H(z, z') = \delta(z-z') - \frac{1}{2L_0(0)} [L_{-1}(|z-z'|) + R_{-1}(z, z')] \tag{173}$$

the integral equation can be rewritten in the compact form

$$Hw \equiv \int_{-d/2}^{d/2} dz'\, H(z, z')\, w(z') = 1 \tag{174}$$

An inspection of Eq. (173) shows that the integral operator $H(z, z')$ is symmetric

$$H(z, z') = H(z', z)$$

and positive semidefinite

$$(\phi, H\phi) \equiv \int_{-d/2}^{d/2} dz\, \phi(z) \int_{-d/2}^{d/2} dz'\, H(z, z')\, \phi(z') \geqslant 0$$

This allows us to use a variational procedure for the solution of (174): For a set of trial functions $\lambda\phi$ with amplitudes λ one may use the positivity of

$$(w - \lambda\phi, H[w - \lambda\phi]) \geqslant 0$$

for an estimate of the cross sectional average of the quasiparticle flow velocity field $\langle v_x^n \rangle_z$. This can be expressed through the variational functional of ϕ in the following way:

$$\langle v_x^n \rangle_z = \frac{\bar{\tau} F_x^{ext}}{m} [(w, Hw) - 1] \geqslant \frac{\bar{\tau} F_x^{ext}}{m} \left[\frac{(\phi, 1)^2}{(\phi, H\phi)} - 1 \right] \tag{175}$$

As a final step one may write the averaged velocity field $<v_x^n>_z$ in the form of a generalization of Hagen–Poiseuille's law

$$\langle v_x^n \rangle = \frac{\rho^n d^2 F_x^{ext}}{12m} \frac{1}{\eta_{eff}\{\mathrm{Kn}; \phi, W\}} \tag{176}$$

and hence express it through an effective shear viscosity functional, which depends on the Knudsen number $\mathrm{Kn} = \lambda_\eta / d$, on the choice of the trial function ϕ and on the details of the wall scattering processes, described by the probability $W_{kk'}$:

$$\eta_{eff}\{\mathrm{Kn}; \phi, W\} = \eta(T) \frac{d}{d + 6a\{\mathrm{Kn}; \phi, W\}\, \lambda_\eta(T)} \tag{177}$$

Our general result (177) for the effective viscosity is of a form reminiscent of the slip corrected viscosity (cf. Eq. (149)). It is, in fact, a generalization of it to arbitrary Knudsen numbers Kn. The Knudsen coefficient a is a functional of ϕ and the wall scattering probability $W_{kk'}$:

$$a\{\mathrm{Kn}; \phi, W\} = \frac{2}{5} \mathrm{Kn}^0 \left[\frac{(\phi, 1)^2}{(\phi, H\phi)} - 1 \right] - \frac{1}{6\mathrm{Kn}^0} \tag{178}$$

Here Kn^0 is the Knudsen number evaluated with $\lambda_2 = 0$. It is well known from exact solutions of the kinetic equation for classical gases that the velocity profile is quadratic in z for small Kn and essentially flat in the Knudsen limit.[3] This suggests the use of the simplest set of trial functions of the form

$$\phi(z) = A - z^2$$

that allows a numerical treatment of the integrals in (178) for arbitrary Knudsen numbers. In the limit of small Kn an analytical result for the Knudsen coefficient can be obtained:

$$\lim_{\mathrm{Kn} \to 0} a\{\mathrm{Kn}; A - z^2, W\} = \frac{\zeta_0^{ILB}}{\lambda_\eta} \tag{179}$$

with ζ_0^{ILB} the improved lower bound for the slip length (cf. (123)) derived in Sec. 4. The variational treatment therefore reproduces the best estimate for the slip length in the presence of elastic wall scattering processes. The full result for the effective viscosity of superfluid ^{3}He–B at 20 bar pressure normalized to its value at the transition, is plotted on a logarithmic scale vs. inverse reduced temperature T_c/T in Fig. 11. The dashed line shows the

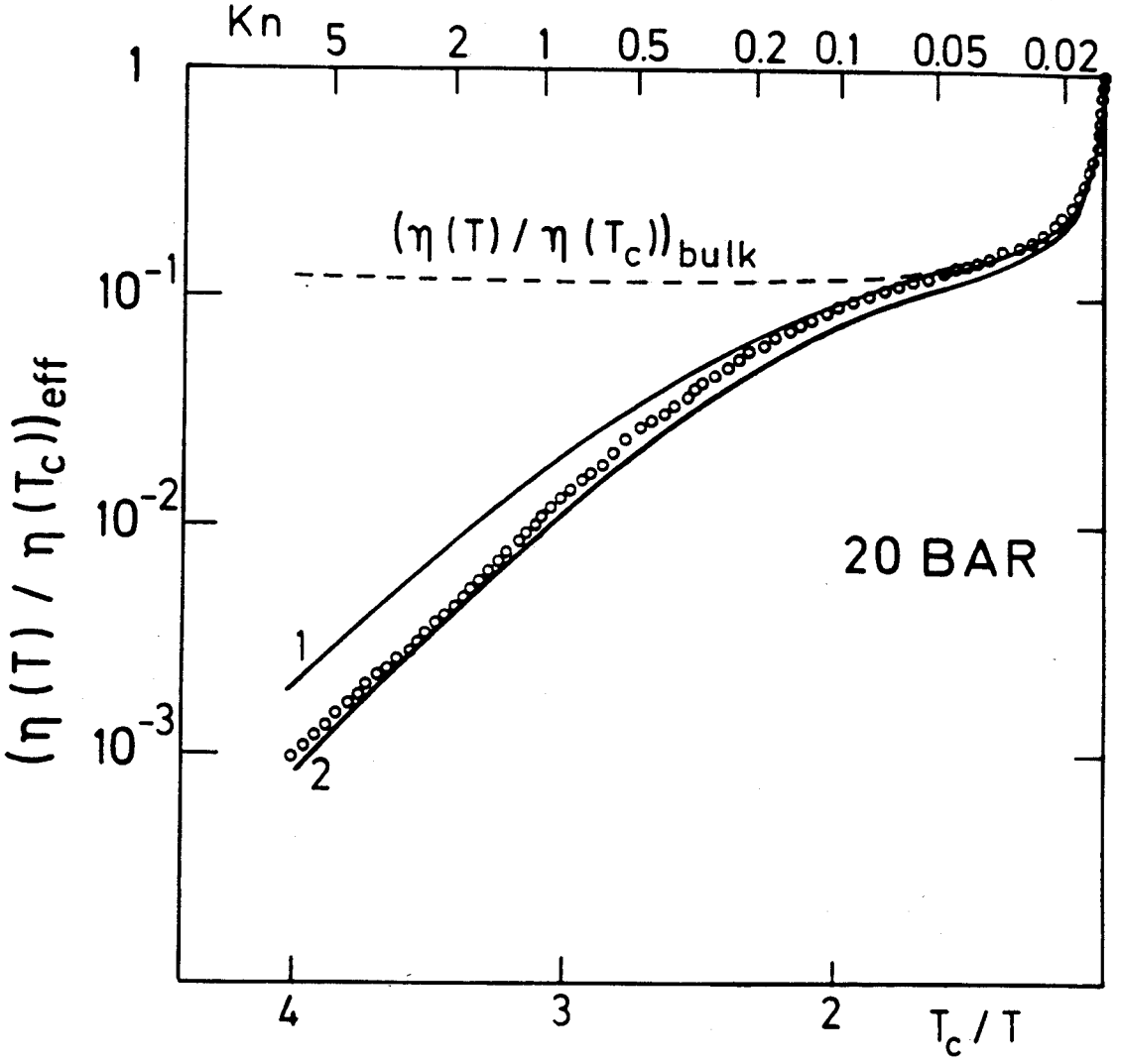

Fig. 11. Normalized effective shear viscosity of superfluid ^{3}He–B at 20 bar pressure vs. reduced inverse temperature, T_c/T. The dashed line represents the bulk theoretical result (cf. Eq. (92)). The solid lines are evaluated for diffuse (1) and diffuse + Andreev (2) scattering (order parameter step). The experimental data from a 135 μm torsional oscillator[58] are shown as circles.

bulk result. The upper of the pair of full lines (1) has been evaluated with the assumption of purely diffuse scattering of quasiparticles off the wall. The lower of these curves (2) has been evaluated by assuming in addition Andreev scattering from a step-like order parameter variation near the wall. This assumption overestimates the effects of Andreev scattering and serves as to give a lower bound to the effective viscosity. The circles are torsional oscillator data taken at Texas A&M.[58] As one should expect, the data points lie between the two bounds set for diffuse and Andreev scattering and hence form an experimental manifestation of what has been called the "quantum slip effect". It should be noted, however, that the

agreement is less good at the lowest pressure as will be shown in Fig. 22 and the discussion accompanying it in Sec. 8.

It should be mentioned here that there have been attempts to solve this problem by describing the process of diffuse quasiparticle scattering off flat walls. This was formulated in a microscopic model put forward by Zhang and Kurkijärvi.[59] In addition, surface roughness on mesoscopic length scales has been treated in the work of Einzel, Panzer, and Liu[60] and by Zwicknagel and Toepffer.[61] The role of mesoscale roughness is discussed in Sec. 9. Although these results lead to a slight improvement of the description, they cannot resolve the discrepancy between theory and experiment that is apparent at the lowest pressure.

6.2. Transverse Surface Impedance

As already explained in Sec. 5.1, a torsional oscillator experiment determines the shear viscosity directly only if the viscous penetration depth δ is large compared to the size d of the flow channel. In the opposite limit, one can detect a viscous force, acting on the surfaces of the container, which is exerted by a fluid layer of thickness δ only. The ratio of this viscous force and the wall velocity v_x^{ext} is called the *transverse surface impedance* $Z_\perp$ of the quasiparticle gas:

$$Z_\perp(\omega) = \frac{\Pi_{xz}(0)}{v_x^{\text{ext}}} \tag{180}$$

The aim is to generalize the result (150) for the transverse surface impedance in the slip approximation to arbitrary values of $\omega\bar{\tau}$ and ratios ζ_0/δ as well as to include the elastic wall scattering events represented by the probability $W_{kk'}$. For this purpose it is sufficient to examine just one oscillating plane wall, which we assume to be located at $z=0$, and restrict the fluid to be confined to the half space $z>0$. This is, however, precisely the geometry that has been treated in Sec. 4, namely the frequency dependent single plane boundary problem. The result was the set (118) of coupled integral equations for the velocity field v_x^{n} and the stress tensor component Π_{xz}. The method of solution of these integral equations, again a variational one, is largely along the lines of the preceding treatment of the effective shear viscosity and will therefore not be discussed in detail. The interested reader may see Ref. 52 for a comprehensive treatment of the problem. At this stage only a few important points will be emphasized. In contrast to the Poiseuille flow case, the trial functions for velocity and stress tensor are chosen to decay exponentially away from the surface,

$$v_x^{\text{n}}(z) = A_v e^{-qz}; \qquad \Pi_{xz}(z) = A_\Pi e^{-qz}$$

characterized by a complex wave number q, which, besides the amplitudes $A_\perp$ and A_Π serves as a variational parameter. The general form of the resulting surface impedance functional is rather complicated and will be omitted here. However, there are a few limits in which the resulting expressions for the variational surface impedance are simple. The first of these is the hydrodynamic limit for which $q \propto \omega^{1/2} \to 0$. The wavenumber q^{var} that emerges after optimization can be written as

$$\lim_{\omega\bar{\tau}\to 0} q^{\mathrm{var}} = \frac{1-i}{\delta}\left[1+\frac{1-i}{\delta}\frac{1}{1-\lambda_2(Y_2/Y_0)} \times \frac{L_3-K_{22}+(K_{12}^2-L_2^2)/(L_1+K_{11})}{L_2}\right]$$

Here we have used the shorthand notation $L_\mu = L_\mu(0)$ and $K_{\mu\nu} = K_{\mu\nu}(0,0)$. In the limit $\delta \to \infty$, q^{var} is just the wavenumber of the diffusive shear mode, present in all gases.

Not unexpectedly, the impedance turns out to be of the slip corrected form

$$\lim_{\omega\bar{\tau}\to 0} Z_\perp(\omega) = (1-i)\frac{\eta}{\delta}\left[1-(1-i)\frac{\zeta_0^{\mathrm{ILB}}}{\delta}\right] \tag{181}$$

with the improved lower bound result for the slip length emerging again from the variational treatment (cf. Eqs. (123) and (179)).

In order to obtain some information about the situation at arbitrary $\omega\bar{\tau}$ one has to restrict oneself to the special cases (112), (113) and (115) for the elastic scattering laws. An approximation for the wavenumber q^{var} is then obtained as

$$q^{\mathrm{var}}(\omega) = \frac{1-i}{\delta}\sqrt{\frac{1-i\omega\bar{\tau}}{1-i\omega\bar{\tau}b(T)}\left(1-i\omega\frac{\tau_\eta(T)}{\phi_2(T)}\right)}$$

where $b(T) = [F_1^s Y_0/3 + L_0(0)\, L_2(0)/L_1^2(0)]/[1+F_1^s Y_0/3]$ and $\phi_2(T) = [1+F_2^s/5]/[1+F_2^s(1-Y_2)/5]$. The corresponding approximate form of the variational impedance then reads

$$Z_\perp(\omega) = \frac{q^{\mathrm{var}}(\omega)}{1+q^{\mathrm{var}}(\omega)\,\zeta_0^{\mathrm{LB}}(1+t)/(1-t) - i\omega\tau_\eta(T)/\phi_2(T)} \tag{182}$$

The dependence on inverse reduced temperature, T_c/T, of the transverse surface impedance $Z_\perp(\omega)$ of normal and superfluid ^{3}He–B at 0 bar

pressure, is shown for a frequency of 100 kHz in Fig. 12. Only the initial linear increase of $\mathrm{Re}\, Z_\perp$ and $\mathrm{Im}\, Z_\perp$ at the high temperature side of the normal phase indicates hydrodynamic behavior. At lower temperatures a deviation from hydrodynamic behavior sets in. As the elastic scattering processes become visible exclusively through the slip correction to the impedance, they can be detected only in the deviations from hydrodynamic behavior which is seen to be amplified by specular (dashed line, $s = 0.5$) and Andreev scattering (dotted line, step profile) and reduced by backward scattering (dashed-dotted line, $r = 0.5$). Surface contributions to the propagation of first sound have been detected in an experiment by Eska *et al.*[62] where they enter most prominently in the sound velocity change (cf. (165)). The change in the velocity of first sound as a function of inverse temperature T^{-1}, as expected from (165) together with (182) in the cases of diffuse (D) and Andreev (D + A) scattering is compared with this data in

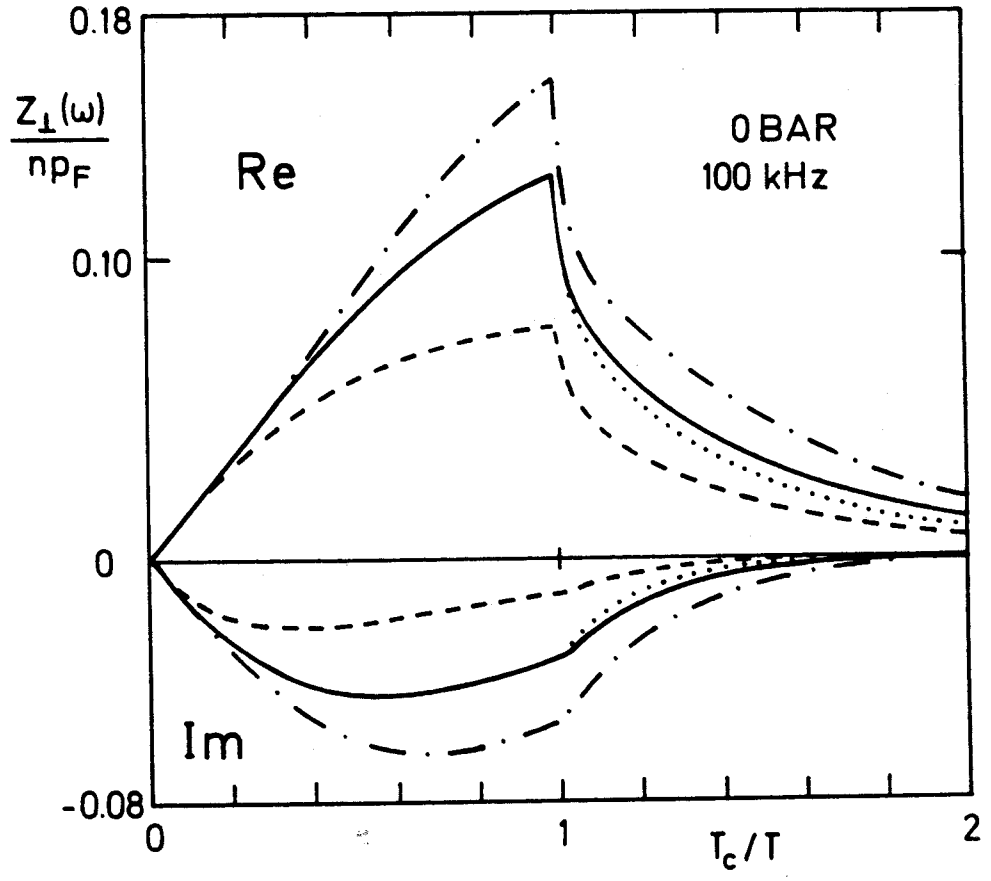

Fig. 12. Real and imaginary parts of the normalized transverse surface impedance $Z_\perp(\omega)/np_F$ of normal and superfluid ^{3}He(–B) at 0 bar pressure and 100 kHz vs. inverse reduced temperature T_c/T for different elastic scattering laws. Full lines: diffuse scattering; dashed lines: specular scattering ($s = 0.5$); dashed-dotted lines: backward scattering ($r = 0.5$); and dotted lines: Andreev scattering from a step–like order parameter profile.

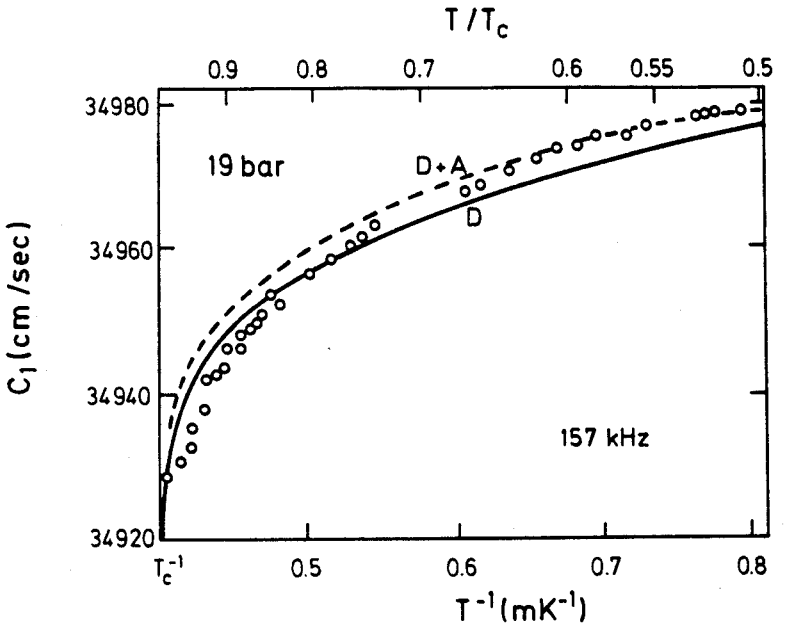

Fig. 13. The first sound velocity c_1 of superfluid ^{3}He–B at 19 bar and 157 kHz (open circles) from the paper by Eska *et al.*,[62] plotted against the inverse temperature. The solid line represents the theoretical result for diffuse scattering alone. The dashed line includes the effects due to Andreev scattering from a step profile variation of the order parameter. Except near T_c, the data are in qualitative agreement with the presence of Andreev scattering at the surface.

Fig. 13. The comparison of experiment and theory seems to indicate that this experiment has most probably seen the effects of Andreev scattering on the transverse surface impedance. The data of Ref. 62, however, only offer a qualitative conclusion in this direction. A quantitative analysis would become possible only on the basis of data with much higher resolution in the superfluid phase.[63]

7. EXPERIMENTAL RESULTS: SLIP IN NORMAL ^{3}He

Historically, finite size effects are difficult to observe in Fermi liquids. This is especially so in the range of temperatures where slip effects are a dominant contribution namely below a few mK. A real constraint in exposing these slip related phenomena was the rather poor footing of the temperature scale more than 10 years after the discovery of superfluidity in ^{3}He.[64]

It is generally true that slip phenomena have played a part in the early experiments carried out on the superfluid phases. The first of these (though not recognized as such) were the experiments on fourth sound in ^{3}He by Kojima *et al.*,[65, 66] and also Yanof and Reppy.[67] These will be discussed in

a later section. Slip related phenomena may have also been responsible for the non-T^{-2} dependent behavior in the regime where $\lambda_\eta \sim d$ in the experiment by Parpia *et al.*[29] in a 100 μm slab geometry torsional oscillator. However, temperature scale problems confuse the issue in this experiment and it will not be discussed further. It should also be noted that similar non-T^{-2} behavior has been recently reported in the literature[19] where it is fitted to a theory[18] of fluctuations above T_c. This work will be discussed later in this section.

The first systematic investigation of slip was carried out by Eisenstein *et al.*[69] at Berkeley. They constructed an apparatus consisting of several reservoirs connected via different cylindrical flow channels to a single central reservoir. The experiments were constrained to be carried out at the saturated vapor pressure. In the experiment, a potential is applied to a particular reservoir connected to a flow channel and the fluid is drawn up into the appropriate reservoir and then released. Unlike the case for ^{4}He in which the motion of the fluid is only lightly damped, the oscillation is overdamped for ^{3}He. They measured the time constant $\tau(T)$ of the helium level as it flowed out of a reservoir following a change in the applied potential.

Accounting for geometrical parameters they apply Eqs. (6) and (149) and write

$$\frac{1}{\tau(T)} = \frac{2\rho g}{ZA}\frac{1}{\eta_{\text{eff}}(T)} = \frac{2\rho g}{ZA}\frac{1}{\alpha}\left(T^2 + c\frac{\beta}{d}\right) \tag{183}$$

where ρ is the mass density, g is the local acceleration due to gravity, A is the cross-sectional area of the reservoirs and $Z = 128L/\pi d^4$ is the flow impedance of the channel with length L, diameter d. $\alpha = \eta T^2$ and $\beta = \lambda_\eta T^2$ are temperature independent constants to be determined from experiment. A plot of the inverse time constant to the square of the temperature should yield a straight line for the expected Fermi liquid behavior. Since the diameter of the flow tubes is much greater than the viscous mean free path, the contribution of the effective viscosity enters in only as the first order correction and modifies the bulk terms with a temperature independent contribution. Eisenstein and collaborators defined the constant c as $c = 8\zeta_0/\lambda_\eta = 4.64$ where the improved lower bound to the slip length (cf. Eq. (123)) has been used. From the slope of Fig. 14 they find $\eta(T_c) = \alpha T_c^{-2} = 2.47$ Poise (for the largest tube) and find $\lambda_\eta(T_c) = \beta T_c^{-2} = 82\,\mu$m, somewhat lower than the expected value of 90 μm obtained from the slope and diffuse quasiparticle scattering from the walls. Thus the experimental value of the slip parameter, c for their largest tube is approximately 10% smaller than the expected value for purely diffuse scattering.

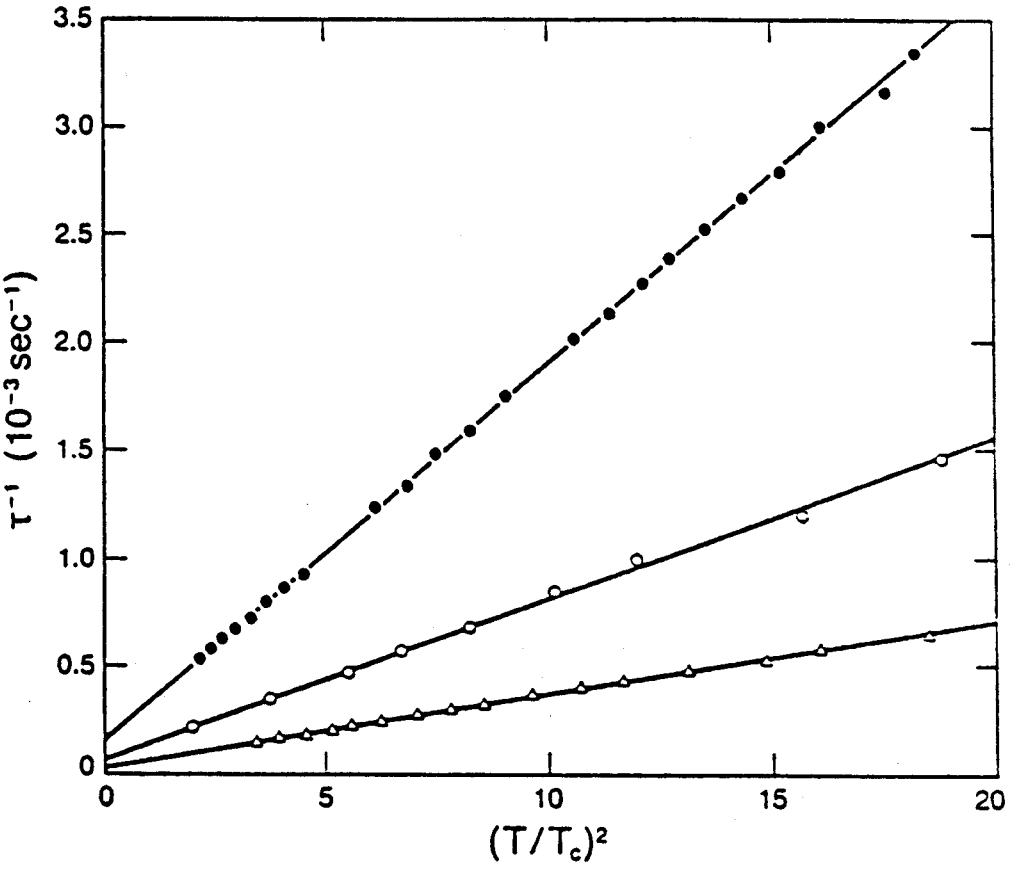

Fig. 14. The inverse time constant for relaxation of the pressure head for pure ^{3}He plotted against $(T/T_c)^2$ for the 454 μm diameter tube (△), 354 μm diameter tube (●) and 252 μm diameter tube (□). The intercept for the largest tube corresponds to a value for the slip that is about 10% smaller than that expected for perfectly diffuse scattering. The data shown is from Ref. 69.

Despite the discrepancy in the slip parameter, this appearance of a temperature independent viscosity was a striking confirmation that the boundary condition of a Fermi liquid at a nominally rough surface is not one where the velocity goes to zero. Further, the linearity of the graph is a confirmation that the slip length and mean free path are closely linked.

The experiments were carried out with three different flow channels. All of the flow geometries show the temperature independent contribution. However, the magnitude of the temperature independent offsets, once scaled for different diameters, are different from the results expected for purely diffuse scattering at the walls. They calculate the mean free path at T_c from the measured viscous flow and assuming the diffuse scattering result of Ref. 55. We have used these values (cf. Eq. (126)) to determine the fraction of elastic backscattering assuming that the surfaces are diffuse scatterers. These numbers are listed in the last column of Table I.

TABLE I

Numerical Results for all Three Tubes. The Second to Last Column is the Mean Free Path at T_c Using the Predictions of Jensen *et al.*, and the Slope of the Lines in Fig. 14. The Last Column Gives t, the Back Scattering Parameter Required to Account for the Smaller Slip Observed in the Experiment (See Eq. (137)

d (μm)	M (10^{-5} s^{-1})	B (10^{-5} s^{-1})	Bd/M (μm)	αT_c^{-2} (P)	βT_c^{-2} (μm)	t
454	17.52	15.38	399 ± 19	2.47 ± 0.10	82 ± 4	-0.047
354	7.49	6.56	310 ± 28	2.28 ± 0.11	67 ± 6	-0.146
252	3.32	3.75	285 ± 23	2.64 ± 0.14	62 ± 5	-0.184

Parpia and Rhodes[70] also carried out experiments in the normal fluid using a torsional oscillator with a more constrained geometry. The $d = 45$ μm thick slab of ^{3}He was sufficiently small so that a Knudsen number $\mathrm{Kn} = \lambda_\eta / d$ of nearly 2 could be achieved in this experiment in the normal phase. In addition to the expected offset term measured in the Berkeley experiment, higher order correction terms were also observed. At long mean free paths the effective viscosity is further modified as the velocity profile in the parallel plate geometry begins to differ from a parabola with a finite velocity offset at the walls to one where the velocity profile is nearly flat together with a finite velocity offset at the walls (see the discussion associated with Fig. 10). The large amount of slip that this experiment was designed to probe shows up as a temperature independent constant as in the Berkeley experiment, together with a temperature dependent contribution at the lowest temperatures. In all cases, the effective viscosity is reduced below that of the bulk Fermi liquid.

According to the results of Højgaard–Jensen *et al.*,[55] (we also note that a qualitatively similar result was obtained independently by Jaffe[71]) the viscosity can be best parameterized in terms of two scaled quantities. The effective viscosity η_{eff} is scaled by the value of the viscosity at a mean free path equal to the characteristic cell size, d which leads to $\eta_d = n p_F d/5$ (cf. Eq. (177)). The temperature can be scaled to the value of the temperature, T_d at which the mean free path λ_η is equal to d. Fig. 15(a) shows $\eta_d/\eta_{\mathrm{eff}}$ plotted against $(T/T_d)^2$. The temperature scale is identical to Kn^{-1}. Under such a scaling, the effective viscosity is not expected to depart from the (linear) slip behavior until the Knudsen number is above about 0.5. In the experiment, the viscosity showed a departure away from the expected behavior at a lower Knudsen number (~ 0.1). Also, in Fig. 15(a) Parpia and Rhodes were able to observe a significant decrease in the effective

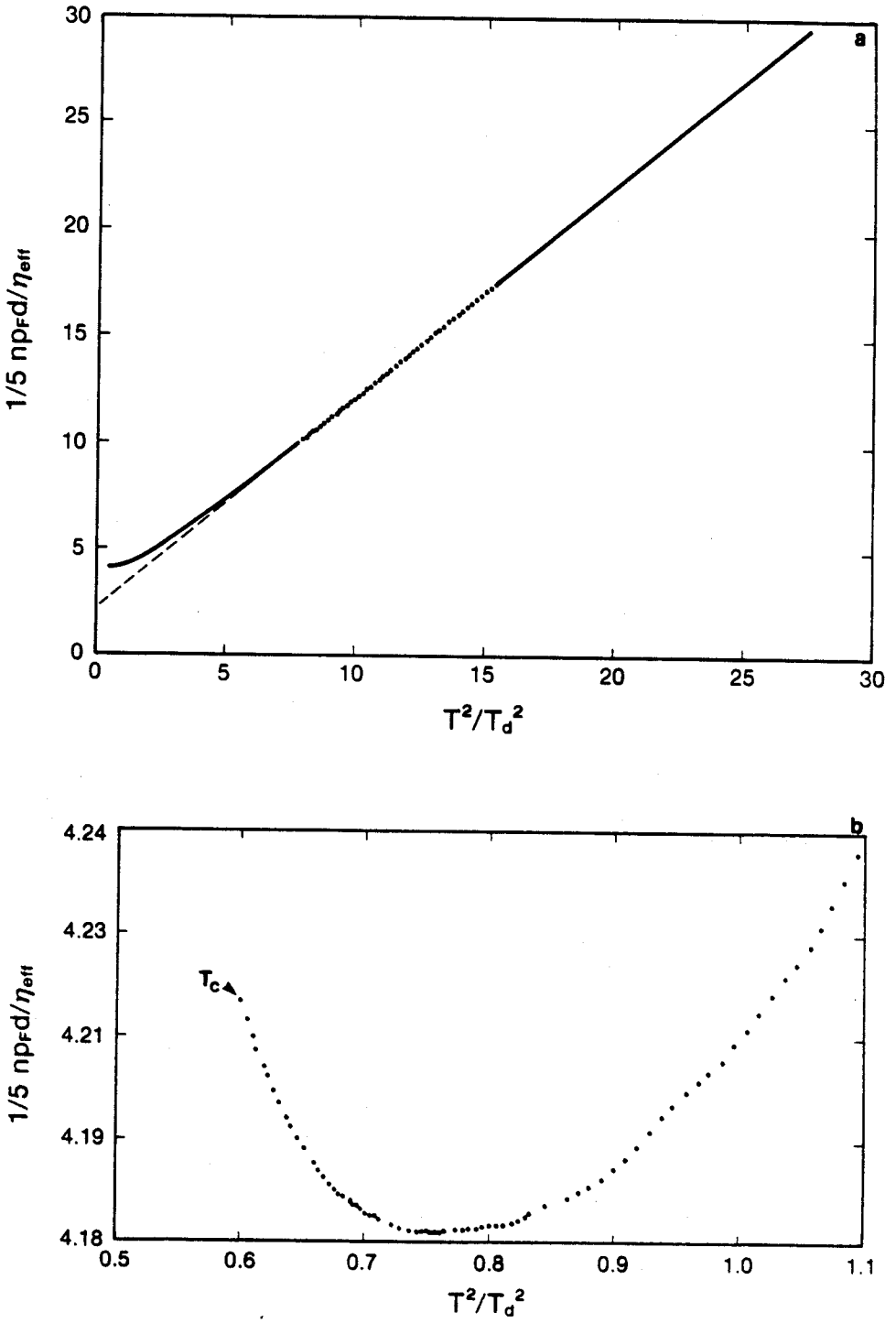

Fig. 15. (a) Plot of the inverse effective viscosity scaled to the value of the viscosity for a mean free path equal to cell height. This quantity is plotted against a dimensionless temperature squared where T is scaled to the temperature at which the mean free path is equal to the cell height. Experimental data—solid black line and data points plotted along with the extrapolation of the high temperature data that shows the first order slip correction—the dashed line. The intercept of this line is a measure of the slip and is found to be about 60% of the theoretical value for diffuse scattering.[55] In (b), the Knudsen minimum is shown, and is displaced to 0.75 $(T/T_d)^2$ as compared to the expected value of 0.5. The horizontal scale corresponds to Kn^{-1}. Data from Parpia and Rhodes.[70]

viscosity before the cell passed into the superfluid phase. This decrease is eventually responsible for the Knudsen minimum (Fig. 15(b)), below which the effective viscosity decreases as the mean free path increases. The Knudsen minimum is a manifestation of slip and higher order finite size effects. The inverse viscosity is expected to diverge as the mean free path increases, but due to thermometry problems the viscosity was not measured in the superfluid, which in any case makes the analysis somewhat more complicated.

The value of the temperature independent offset measured by Parpia and Rhodes is different from that calculated for purely diffuse scattering. It implies a scattering probability that is skewed toward backscattering—thus termed "superdiffuse." Since the surfaces were epoxy that was set onto polished aluminum and released from the aluminum surface through a NaOH etch, it is possible that the surface was pitted at some microscopic level after release and thus the scattering may have been altered away from the expected diffuse behavior. The ratio of the measured slip length to the theoretical value is 0.6. This is equivalent to superdiffuse scattering parameter, $t = -0.25$ (see Eq. (126)), and is comparable to the values of the slip parameter measured in the smallest tubes of the Berkeley experiment.

Thus these two (Berkeley & Texas A&M) experiments show qualitative agreement with the results expected of Fermi liquids in the presence of slip. However, both experiments see a reduction in the slip below that expected for the case of purely diffuse scattering in the Knudsen regime. In addition, the experiment at Texas A&M showed that higher order correction terms seem to be important at smaller mean free paths than expected and contribute to the observation of a Knudsen minimum.

In both of these experiments, the ^{3}He was in the well clamped regime. In the mechanical oscillator, the real and imaginary parts can be related to the period and the dissipation of the oscillator (cf. Eqs. 145–148). For the torsional oscillator experiments the primary quantity that is measured is the dissipation. When the frequency and geometry are such that the fluid is unclamped, the response of the system is described as a surface impedance rather than as Poiseuille flow. Experiments done by Eska *et al.*[62] on the attenuation and sound velocity of first sound were the first to probe this regime and observe the effects of slip.

In this experiment, Eska and coworkers used mylar transducers to excite the sound modes at frequencies between 40 kHz and 300 kHz. The cylindrical resonator had walls whose roughness was less than 9 μm and a periodicity of 50 μm due to machining. The Q of the resonance was on the order of 1000 at high temperatures and was dominated by the properties of the mylar film. Upon application of a pulse, the decay of the sound field

was measured and the attenuation calculated. In the hydrodynamic limit, the attenuation can be derived from Eq. (166) and is given by

$$\alpha(\omega) = \frac{2\eta\omega^2}{3\rho c_1^3} + \frac{\omega\delta}{2Rc_1} \tag{184}$$

with c_1 being the first sound velocity, δ, the penetration depth and R is the radius of the resonator. The damping was dominated by the second term which is related to scattering from the walls. The presence of the walls and the higher experimental frequency, leads to a change in the first sound velocity from the bulk value, c_∞. Thus

$$c_1 = c_\infty \left\{ 1 + \mathrm{Im}\left[\frac{2\omega\eta}{3\rho c_\infty^2 (1 - i\omega\tau_\eta)} + \frac{Z_\perp(\omega)}{\omega\rho R} + \frac{\omega}{4\rho c_\infty} \frac{\rho^n}{\rho} X(\omega) \right] \right\} \tag{185}$$

$Z_\perp(\omega)$ is the complex acoustic shear impedance, while $X(\omega)$ is an additional term due to the cylindrical cavity

$$X(\omega) = \frac{\eta}{1 - i\omega\tau_{\eta\perp}} \left[1 - \frac{8L}{(\pi n)^2 R} + 2\left(\frac{L}{\pi n R}\right)^2 \right]$$

Here n is the index which counts the harmonics. The second term in Eq. (185) arises from zero-sound corrections and the third and fourth terms take into account wall effects. c_1 is affected by δ/R corrections and slip enters in as a correction to the sound velocity

$$\Delta c_s = c_\infty \frac{8}{15} \frac{\lambda}{R} \tag{186}$$

There are more terms for the effects of zero sound that enter into the slip. Thus the additional shift in sound velocity

$$c_2 = \frac{\eta\omega^2\tau_\eta}{\rho c_\infty [1 + (\omega\tau_\eta)^2]} \left(\frac{2}{3}\lambda_1 + \frac{1}{4}\lambda_2 \right) \tag{187}$$

These results can be compared to the experimental sound velocity below about 5 mK. In Fig. 16, the hydrodynamic limit (dashed line) shows the T^{-1} correction to the sound velocity due to ordinary hydrodynamics. The presence of slip (dashed-dotted line) and finally the inclusion of zero sound effects together with slip are shown as the solid line. Thus, even in a relatively open geometry, slip is seen to play a significant role in the

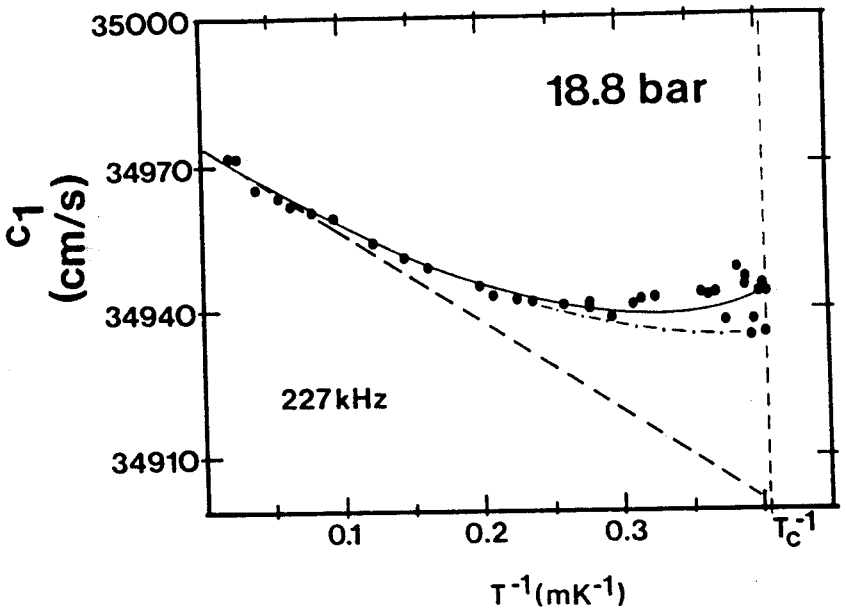

Fig. 16. The first sound velocity c_1 vs. temperature in normal liquid ^{3}He at 18.8 bar. The expected result for a bulk system in the hydrodynamic limit (where the ratio of the viscous penetration depth to the resonator radius is not negligible) is shown as the dashed line. When slip contributions are included, the temperature dependence shown as the dash-dotted line is expected. The solid line is the expected temperature dependence when effects due to the finite frequency (transition toward zero sound) are included. Data shown are from Eska *et al.*[62]

modification of the sound velocity due to the influence of the interaction of the sound with the walls of the cell.

The results of Carless *et al.*[72] using a vibrating wire viscometer are interesting because they show that slip does not play a part in many (particularly vibrating wire) experiments. Slip is introduced into the equations of motion by including the boundary condition $v_s - u_s = \zeta_0 \partial v_s / \partial r$ (cf. Eq. (106)), where ζ is a slip length, v_s is the fluid velocity which may differ from the wire velocity u_s. Here, the response of the vibrating wire can be divided into its real (c_0) and imaginary (c_0') components. The in-phase (real) component is almost entirely unaffected by the presence of slip. The extent of this correction to c_0' is seen (Fig. 3 in Ref. 72) to be almost negligible in relation to the effect of finite size, $b/a = 65$, where b is the radius of the channel and a is the wire diameter.

Another experiment carried out at Texas A&M and reported on by Einzel and Parpia[58] mainly concentrated on results obtained in the superfluid. The oscillator in this experiment had a characteristic size of $d = 135\ \mu$m. Because of the larger separation between the plates (compared to the earlier experiment by Parpia and Rhodes), higher order correction terms to the viscosity were not so evident. However, even this experiment

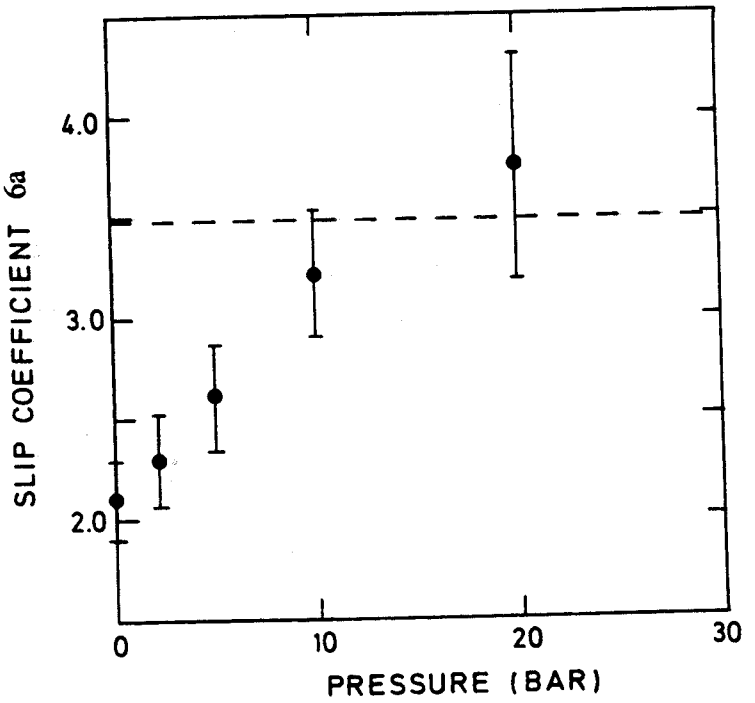

Fig. 17. The pressure dependence of the slip parameter, 6a. The value based on entirely diffuse scattering is shown as the dashed line. The pressure dependence is not understood. The data points were obtained at Texas A&M, and were reported on in Ref. 58.

showed a small deviation from the first order slip correction. As in the earlier experiment, the first order correction was parameterized by

$$S(T) = 1 + 6\frac{\zeta_0}{d} = 1 + 6a\frac{\lambda_\eta}{d} \tag{188}$$

The experiment found 6a to be 2.1 at low pressure increasing to 3.7 at high pressure (Fig. 17). The first order correction term showed a systematic increase towards the theoretical value 3.48 for diffuse scattering, as the pressure was increased, although the precision of the experiment became smaller at elevated pressure. Similar results have been recently observed in a very different experiment performed in the unclamped limit by the group of Nakagawa *et al.*,[73,74] though in the light of the next section which primarily discusses the work of Ref. 19, the pressure dependence may turn out to be an artifact of non-Fermi liquid behavior of liquid ^{3}He.

7.1. Non-Fermi Liquid Behavior of Pure ^{3}He

In several different experiments (vibrating wire, and torsional oscillators) carried out in a number of geometries, there have been consistent

reports of a viscosity that does not behave as T^{-2}, expected of Fermi liquids. This section is written to summarize the data, and also to evaluate in a qualitative manner the consequence of such non-Fermi liquid behavior on the effective viscosity.

The first indications that there were possibly some deviations from the expected T^{-2} behavior came after the thermometry was placed on a better footing by the work on the melting curve of ^{3}He[64] and platinum thermometry. Carless *et al.*[72] using a vibrating wire found that the inferred viscosity (after accounting for corrections due to finite size and slip) was best expressed as

$$\eta T^2 = \frac{1}{A + B/T^2} \tag{189}$$

where A and B are positive constants. Thus the apparent viscosity does not increase as fast as it should under the assumption of Fermi liquid theory. The value for B varies from 0.04 P^{-1} at 0.1 bar to 1.45 P^{-1} at 29 bar. These results are shown in Fig. 18. Similar results (though with a different

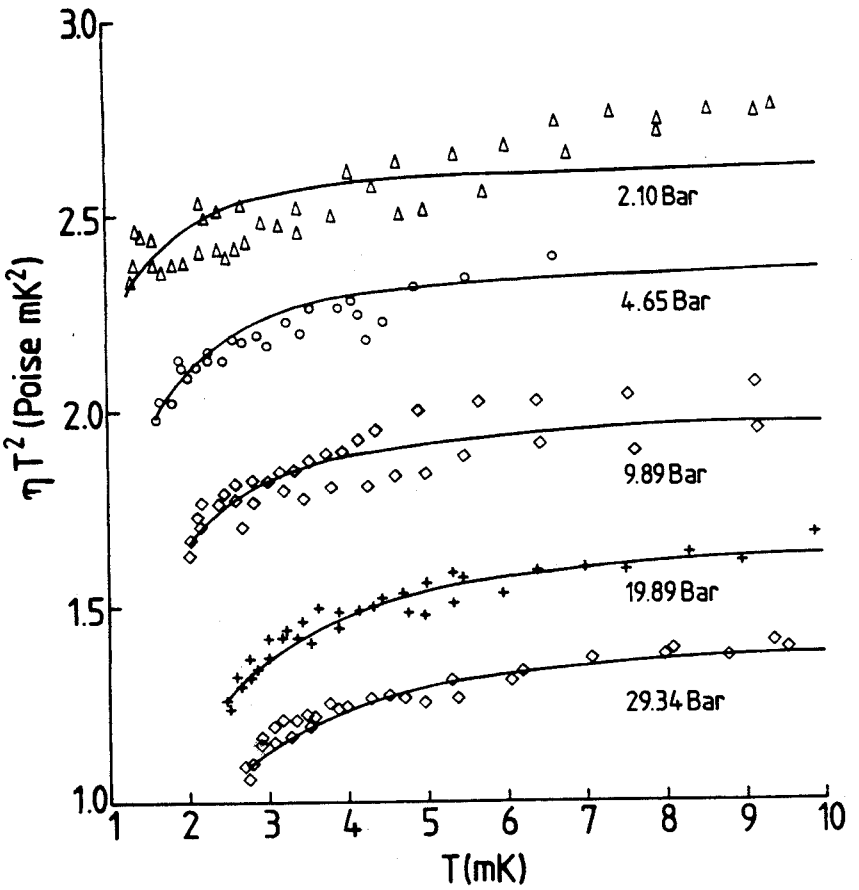

Fig. 18. Experimental values of ηT^2 as a function of T for various pressures. Data was taken with a vibrating wire and published by Carless *et al.*[72] The solid curves are fits to a non-Fermi liquid like viscosity.

fitting form and which will be discussed later) were seen at 5 bar by Nakagawa *et al.*[74] and more recently reported by the same group[19] at a number of pressures between 0 bar and 29 bar. Thermometry is most likely not a factor in these experiments unless the discrepancies reflect a difference in the thermal gradient between the thermometer and experimental cell, because thermometry errors would produce a constant B that would be pressure independent. A thorough discussion of the issues can be found in Carless.[72] The observation of these deviations from the Fermi liquid behavior were also seen in a torsional oscillator experiment where the ^{3}He was confined to a 105 μm cavity (see Fig. 5 of Ref. 75). In this result, Hook and co-workers note that B can be forced to zero if the slip length is increased to $1.5\lambda_\eta$, which is unlikely. This adjustment would be inapplicable to the results of the vibrating wire experiments. So it is unlikely that this unexpected behavior is an artifact.

The experiment by the Osaka City University group[19] was the first comprehensive attempt to examine the possibility of non-Fermi liquid behavior of ^{3}He. Their cell consisted of a torsional oscillator with a 11 mm diameter x 6mm high Stycast 1266 body immersed in the liquid ^{3}He. The surface roughness was not measured. At all the pressures that they carried out experiments at, they observed a viscosity that decreased below the expected T^{-2} behavior (Fig. 19). At 21 bar, the viscosity that they measure shows remarkable agreement with the Manchester results (inset to Fig. 19). They found that the viscosity could be best fitted to a form different from that suggested by Carless *et al.* which yields a dependence linear in T:

$$\eta T^2 = \frac{1}{A - BT} \tag{190}$$

and which gave larger values of A and B. In addition to this dependence, they saw a further departure from the T^{-2} behavior. They were able to obtain an excellent fit for this residue using the theory of Emery[18] with parameters that fell within limits proposed by Emery.

The consequences for our understanding of the properties of ^{3}He are significant if the viscosity and collision rate show non-Fermi liquid behavior, particularly well below T_F and also if fluctuations do play such a large role in the behavior near T_c. Greywall's temperature scale[64] relies on the assumption that the specific heat is Fermi-liquid-like and linear in T. Clearly the other transport parameters should also reveal deviations, and in fact the zero sound attenuation which involves similar collision processes to the viscosity should display a corresponding non-T^2 behavior extending to $2T_c$ and beyond. A fluctuation precursor effect on zero sound

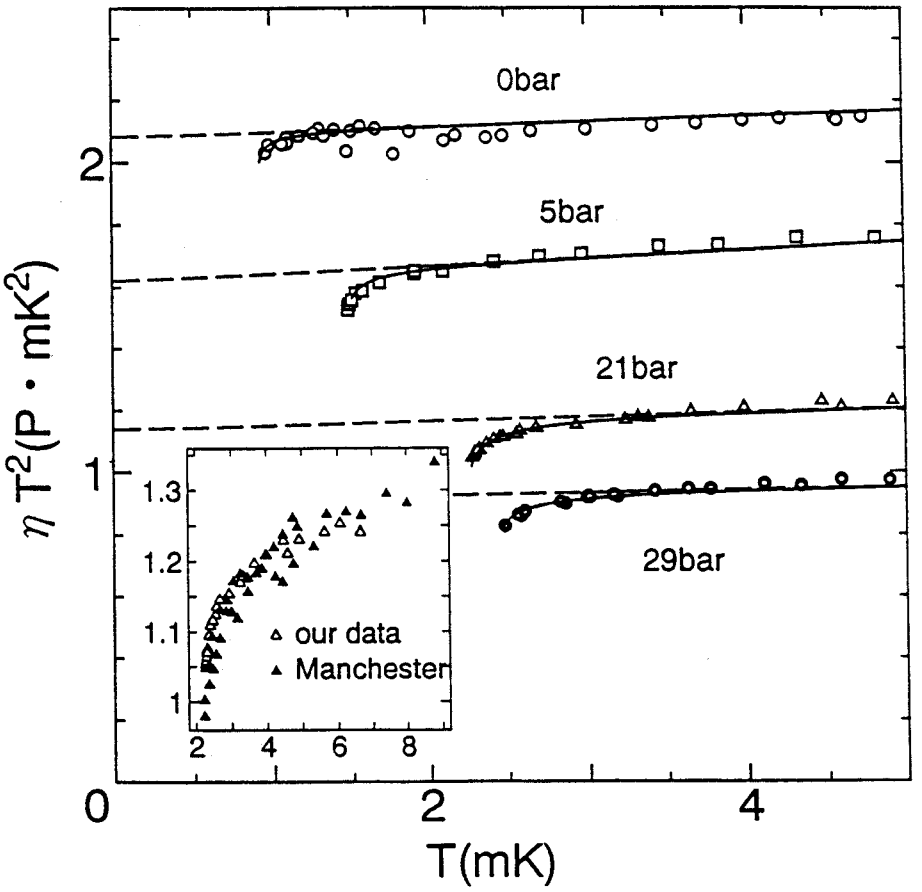

Fig. 19. The experimental values of ηT^2 as a function of T for various pressures. This data was taken with a large torsional oscillator, operating in the unclamped limit and published by Nakagawa *et al.*[19] The solid curves are fits to the theory by Emery based on fluctuations above T_c.[18] The dashed lines are fits to the non-Fermi like viscosity behavior found by Carless *et al.*,[72] whose data at 21 bar is compared to that of Nakagawa *et al.* in the inset.

attenuation was observed by Paulson and Wheatley,[76] but this effect was confined to a few percent above T_c.

The upshot of the non-Fermi liquid like behavior is that the discrepancy of the position of the Knudsen minimum,[70] as well as the apparent need for higher order correction terms as evidenced by the departure of the viscosity from the first order correction at relatively small Knudsen numbers, may be due (in part) to this deviation from Fermi liquid behavior. On one hand, the deviation from Fermi liquid behavior seems to be least pronounced at saturated vapor pressure (see Figs. 18 and 19), so it would seem that non-Fermi liquid contributions would not dominate the measurements at this pressure. Putting it differently, in the experiment by Parpia and Rhodes,[70] the effective viscosity itself was seen to decrease above T_c, whereas in these nearly bulk geometries, the observation points towards a viscosity that does not increase as fast as T^{-2}. On the other hand, it is possible that the

pressure dependence of the slip intercept is a consequence of essentially force-fitting the viscosity to a T^{-2} law which would produce a slightly smaller slope and a larger intercept in figures comparable to Fig. 15.

A caveat should be expressed at this point, particularly with regard to oscillator experiments (including those by the authors of this review), that involve metallic components. Metals have a surprisingly strongly temperature dependent mechanical Q at low temperatures. Thus background measurements have to be carefully carried out on empty cells (see Ref. 70). Such a background measurement is only applicable at low pressure, so results at high pressures, where torsion tubes may be hydrostatically stressed, may have to be carried out with ^{4}He as a medium.

The possibility of non-Fermi liquid behavior or fluctuations at temperatures near T_c is interesting and may have far reaching implications. It is possible that some of the discrepancies noted in the previous section between theory and experiment may have their origin in this unexpected but fascinating behavior.

7.2. Summary of Experiments in the Normal State

Experiments performed in the normal fluid all show qualitative agreement with the theoretical expectations. Quantitative agreement is lacking at low pressure, while there appears to be better agreement at higher pressures for the first order correction to the hydrodynamics, though this may be fortuitous due to the onset of fluctuations or non-Fermi liquid effects. Also, at saturated pressure, the temperature dependent departure of the effective viscosity from the bulk T^{-2} dependence occurs at a smaller value of the Knudsen number than expected, and in addition, the Knudsen minimum appears to be shifted to a higher temperature than expected theoretically.[55] This latter effect corresponds to (in a sense) more slip than expected from the theory. Thus one has two apparently inconsistent results. If we parameterize the viscous behavior of the ^{3}He in terms of slip then one can express the larger measured effective viscosity in terms of a certain amount of backscattering. Therefore, the observed behavior i.e. less slip due to backscattering and the presence of higher order correction terms to slip behavior may possibly occur in a combination, the origin of which is not presently known. A new experiment observed a non-Fermi liquid behavior of the viscosity and also points towards fluctuations as contributing to a non-T^{-2} viscosity. Such behavior may in principle be able to account for the pressure dependence of the slip coefficient. However, this non-Fermi liquid behavior (or fluctuations) should also be manifested in other transport properties which should be examined critically. More detailed experiments of zero sound using the new temperature scale should also

reveal the existence of non-Fermi liquid behavior. In all experiments, it will be necessary to be able to adequately characterize the surface scattering properties of the experimental apparatus, and in experiments using metallic structural parts, the low temperature dependence of the mechanical Q should be measured at a range of pressures.

8. EXPERIMENTS IN SUPERFLUID ^{3}He

Very early in the development of the understanding of transport in the superfluid phases of ^{3}He, it was predicted that the viscosity decrease of the normal fraction, $(1-\eta/\eta_c)$, should vary approximately as the gap energy close to T_c,[39] and that there should be a shallow minimum in the viscosity[77–81] which would then eventually attain a zero temperature result[40] of about 0.2 of the value at T_c.

Experiments were rapidly able to confirm the former dependence, at least arbitrarily close to T_c[29] but the low temperature viscosity measured in a torsional oscillator apparatus having approximately 94 μm thick slab of ^{3}He, showed a behavior where the viscosity appeared to radically decrease away from the 0.15 η_c plateau at about 0.8 T_c[41] (the so-called droop). These observations were reported together with the first order corrections for slip at the surface, assuming diffuse boundary conditions.[41] However, in these intermediate sized geometries, the first order correction for finite size, namely slip, is insufficient to explain the large departure away from the expected bulk viscosity. In the superfluid, as can be seen from Fig. 5 the mean free path first decreases near T_c before it starts to increase almost exponentially. Below 0.6 T_c, the slip approximation is no longer sufficient, but higher order correction terms have to be included (see Fig. 10). Also, at temperatures below 0.6 T_c the depression of the order parameter near the surface results in the growing importance of Andreev scattering processes, and as a consequence, the slip length increases beyond the value expected for diffuse scattering alone with higher order corrections taken into account. This quantum slip effect was discussed by Einzel *et al.*[82] in which they were able to satisfactorily explain the departure of the effective viscosity from the bulk value using a description valid at arbitrary Knudsen numbers incorporating both diffuse and Andreev scattering from the surface. The many corrections and their relative importance introduced to account for finite size effects can be appreciated by examining Fig. 20. The bulk viscosity as calculated by Einzel[35] can be compared to the uncorrected data for the effective viscosity (dots). Curves 1, 2 and 3, show the results obtained for diffuse scattering if higher order terms are included but if no Andreev scattering is present (1); if Andreev scattering from a step-like profile of the order parameter is invoked (3) and for Andreev scattering if

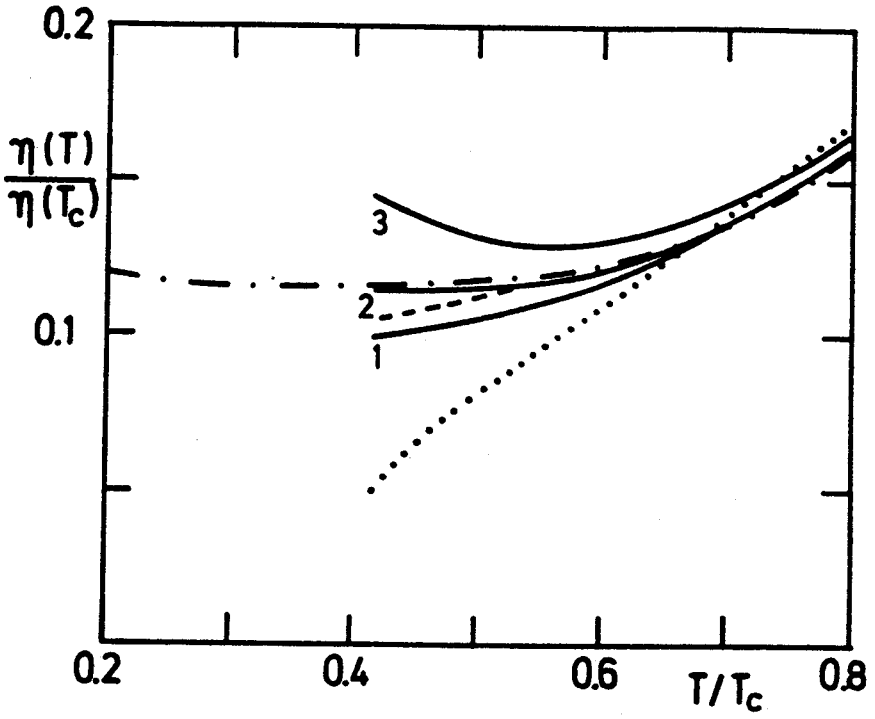

Fig. 20. The reduced viscosity at 30 bar plotted against reduced temperature. The data (dots) is taken from Archie *et al.*[41] The experimental points display the "droop" from the expected theoretical results for bulk ^{3}He (Refs. 50, 77–82). The solid curves show the effect of Andreev scattering after all the higher order finite size corrections are included. Curve 1 shows the result of purely diffuse scattering, curve 2 the effect of including Andreev scattering from an order parameter variation near the wall that varies on the length scale of the coherence length, and curve 3 the effect of a purely step like variation of the order parameter. The dash - dotted line is the theoretical result for bulk helium ^{3}He-B as calculated by Einzel.[35] The dashed line includes the same profile for Andreev scattering as in curve 2, but including only the first order (slip) correction for finite size. For details we refer to Ref. 82.

the order parameter is allowed to vary smoothly over a length scale of the order of the coherence length (2). The dashed line should be compared to line 2, since it includes Andreev scattering from the same order parameter profile, but includes only first order (slip) corrections. The reader is referred to Eq. (128) and the discussion preceding and following it.

A comparison of the expectations of bulk viscosity and experimental corrections due to finite size effects and slip were tested in a systematic manner by the experiments carried out by Carless *et al.*[83] in the superfluid. They measured the response of a vibrating wire oscillator and they contrasted this behavior to data obtained with a torsional oscillator with a spherical cavity for the helium. The latter set of data was taken by Zeise and co-workers at Cornell.[84] In both these experimental geometries, the presence of diffuse scattering and slip has a rather small effect on the effective viscosity. The characteristic dimension of the fluid container is larger

than the viscous penetration depth, δ. Thus, the fluid is not in the clamped regime at any temperature in the course of the experiment.

The effect of finite size is made most apparent in Fig. 21 taken from Carless *et al.*[83] In this figure the results of Archie *et al.*[41] including first order slip corrections are compared to those of the spherical oscillator and the vibrating wire. The vibrating wire experiments corrected for finite compressibility (readers are referred to the paper by the Manchester group[83])

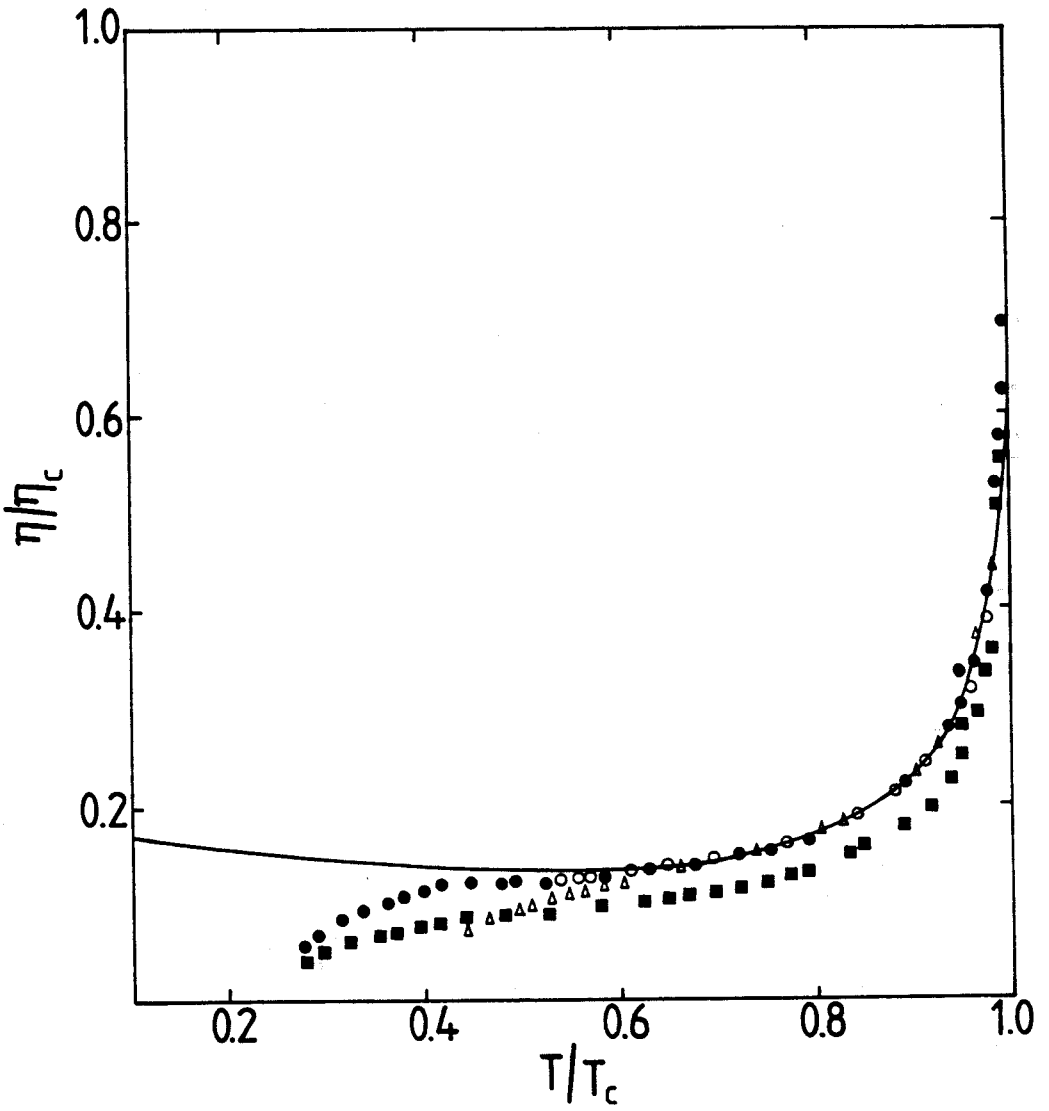

Fig. 21. The reduced viscosity at 19.9 bar obtained with a vibrating wire (solid squares) and corrected for compressibility of the superfluid fraction (solid circles). The corrected vibrating wire data agrees well with the results obtained with a spherical viscometer (open circles), with radius greater than the viscous penetration depth. The triangles are data from torsional oscillator with only slip corrections introduced (see Fig. 20). None of the data is corrected for Andreev scattering or for terms to higher order than the slip result. The solid line is the theoretical plot due to Ono *et al.*[77] Data are from Carless *et al.*[83]

of the fluid agree remarkably well with the spherical oscillator. Both experiments are in good agreement with the theoretical result of Ono *et al.*[79] down to about 0.6 T_c. In contrast, the data from the more restricted geometry deviates from the other two experiments (and the theory) progressively as the temperature is lowered. The Knudsen regime corrections (accounting for all orders of λ/δ) and quantum slip corrections for the spherical oscillator and the vibrating wire have never been calculated, but it is unlikely that these computations will be carried out because they are unlikely to provide information that is different from that revealed in the next series of experiments.

Rather than probing the hydrodynamics in the unclamped regime, where slip effects are generally small, Einzel and Parpia carried out an experiment in the regime where finite size effects would dominate the measured viscosity. The experimental parameter space probed extended down to about 0.25 T_c at various pressures with a torsional oscillator with a height $d = 135\ \mu$m. The results are shown in Fig. 22. In these experiments at the lowest pressure and temperatures, the viscous mean free path grew to be as large as 1 cm corresponding to a Knudsen number of about 70, and at 0 bar the effective viscosity had decreased to almost 3 orders of magnitude smaller than the expected bulk result. The theoretical description developed by Einzel includes the effects of slip and quantum slip, which together within bounds set by diffuse scattering alone (line marked 1) and Andreev scattering from a step like order parameter profile (line marked 2), provides an adequate explanation for the decreased effective viscosity observed in the experiments deep in the superfluid B phase except perhaps at the lowest pressures. It is important to remember that thermometry at these low temperatures may play a role and further that surface roughness effects were never properly accounted for. Thus, at this juncture, the agreement between theory and experiment must be regarded as being excellent.

In the superfluid B phase, the analogous U tube relaxation experiment to that carried out in the normal phase by Eisenstein and Packard,[85] seemed to imply that there was always some dissipation present in the superfluid. Only the superfluid flows in the U tube experiment since the normal fluid is clamped. However, the free surfaces also rise and fall and these imply motion of the normal component as well. Similar arguments to those put forward here were presented by Hall and Hook in their review.[86] Brand and Cross[87] showed that there must be a conversion of pure superfluid to normal fluid near the free surface. The boundary condition at the surface states that $v^s = v^n =$ velocity of the surface. They then show that conversion to pure superflow takes place within a distance $(\rho^2\zeta_3/\eta_{\text{eff}})^{1/2} d$ from the surface. The separation, d of the annular region provides the characteristic size, and ζ_3 is the second viscosity. The pressure difference

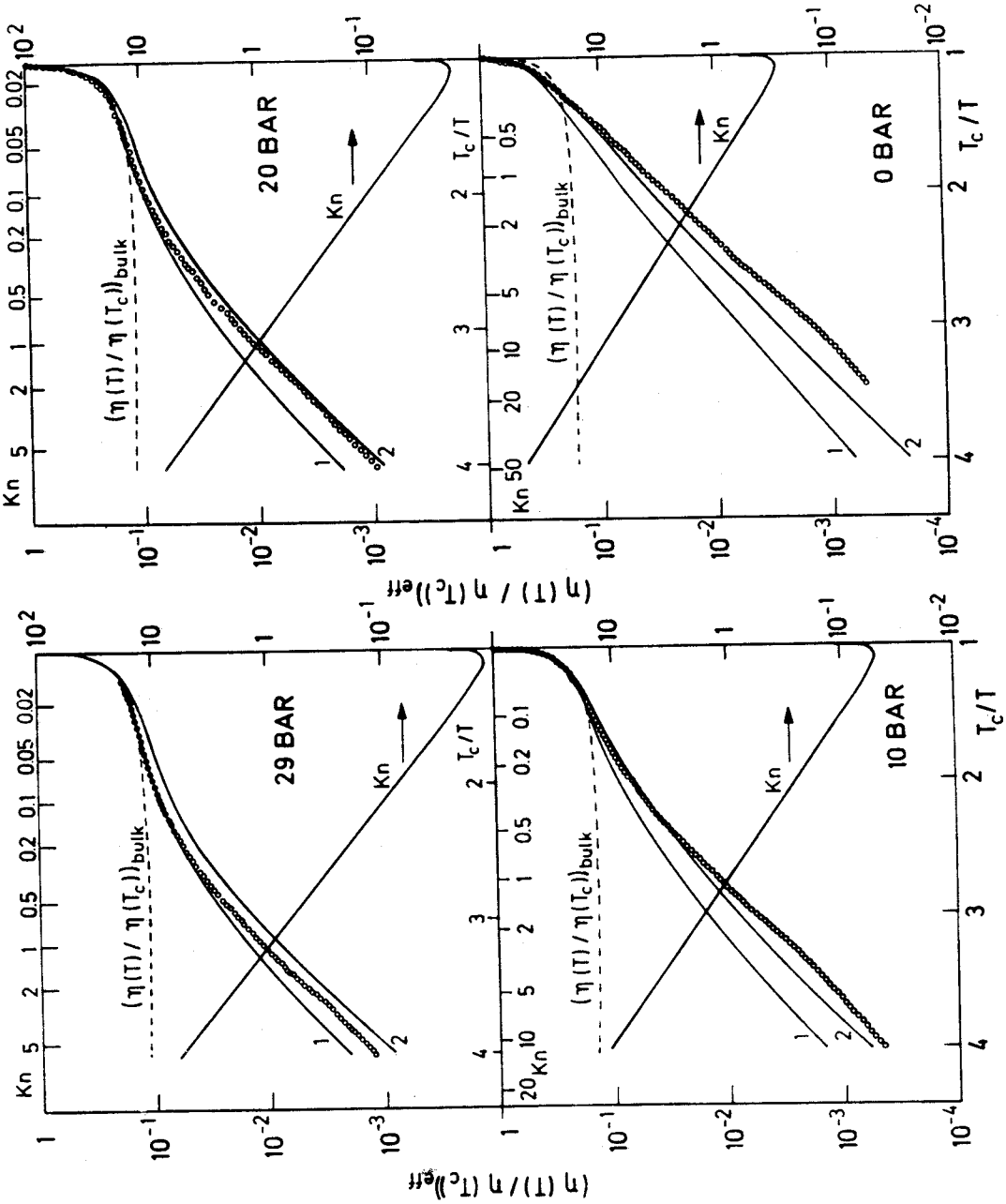

Fig. 22. The effective viscosity as a function of T_c/T for data obtained at 0, 10, 20 and 29 bar. The solid lines are the limits for diffuse scattering alone (1) and diffuse plus Andreev scattering from a step variation of the order parameter (2). The figure is from Ref. 58.

$2\rho g x$ is due to a height difference $2x$, that drives the superflow between the two reservoirs. This pressure difference is then reduced by twice the pressure head across these conversion regions, and this leads to a finite contribution to the damping coefficient measured in the Berkeley experiment.

$$\ddot{x} + 2L\dot{x} + \omega_0^2 x = 0 \tag{191}$$

The damping term, L is given by

$$L = \frac{\rho^s}{\rho}\frac{a}{A}\frac{1}{ld}\sqrt{\zeta_3 \eta_{\text{eff}}} \tag{192}$$

l and a are the length and area of the flow channel connecting the two reservoirs, and A is the area of the reservoirs. The oscillation frequency ω_0 of the U-tube is given by

$$\omega_0^2 = \frac{\rho^s}{\rho}\frac{a}{A}\frac{2g}{l} \tag{193}$$

but L (cf. Eq. 192) turns out to be so large that the system is overdamped. The calculation of Brand and Cross ignored the slip correction within the annular region. The original Brand and Cross results are shown as the upper full lines labeled 1–3 in Fig. 23. A calculation which accounts not only for slip in the reservoirs but which is valid for arbitrary Knudsen numbers by Einzel[88] can explain the observed maxima in the U tube relaxation parameter L. The results are shown as curves 1a–3a in Fig. 23.

The effects of slip also play a central role in the dissipation observed in fourth sound experiments in superfluid ^{3}He. In these experiments, the fluid is constrained in pores of a material whose characteristic size is smaller than the viscous penetration depth, and also the bulk mean free path exceeds the mean pore diameter by a substantial amount. Therefore these experiments are carried out deep in the Knudsen regime where the ratio of the viscous mean free path to the pore diameter is very large. Consequently, the assumption that the normal fluid is entirely clamped is incorrect and the finite motion of the normal fluid leads to a radical reduction in the Q of the fourth sound resonances. This can be qualitatively understood by recalling the results of Parpia and Rhodes where the effective viscosity and thus the damping were seen to decrease substantially as the Knudsen number increased. The actual calculation cannot be expected to provide exact results since the pores are not uniform and the tortuosity factor must also play a role. Additionally, unlike in the case of the torsional oscillator, whose geometry can be approximated to two parallel plates, the

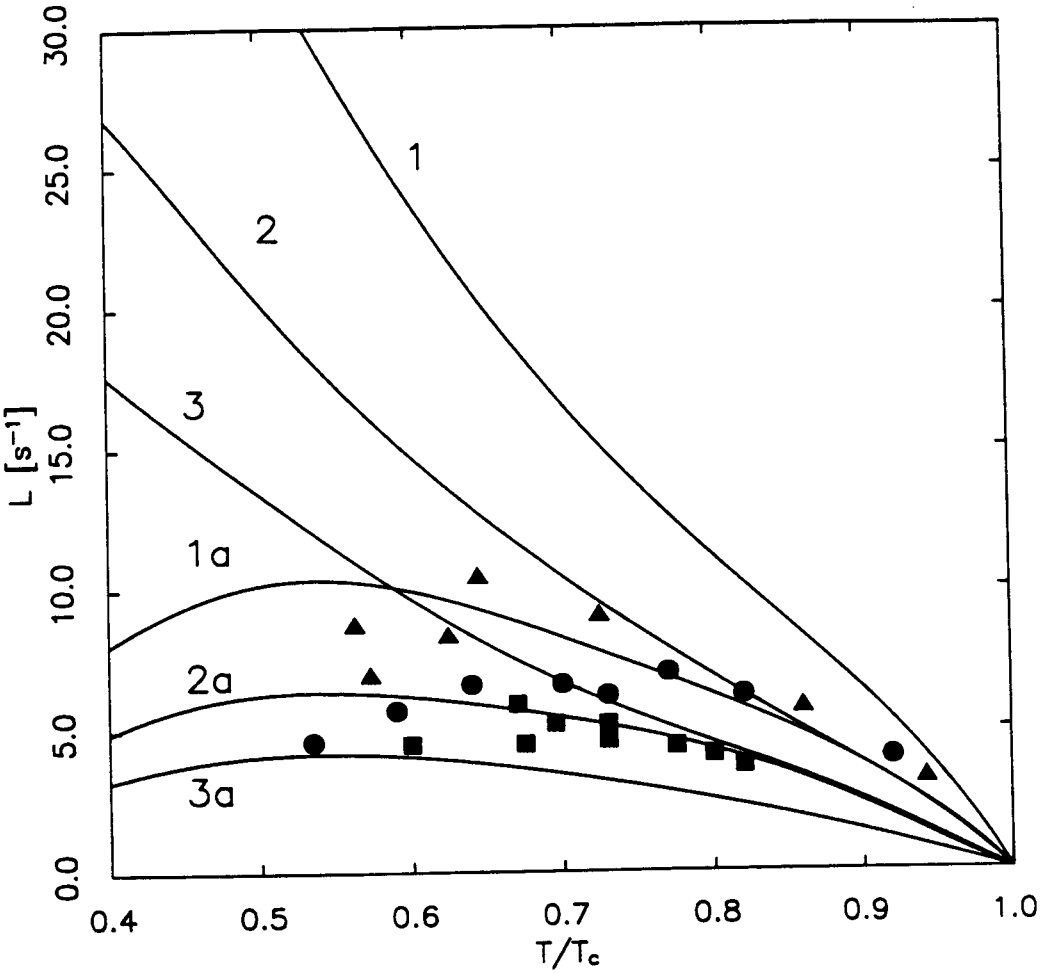

Fig. 23. Values of the damping coefficient in the Berkeley U-tube experiment,[85] for a 227 μm tube (triangles); for a 126 μm tube (circles); and for a 102 μm tube (squares). The solid lines labeled 1, 2, 3 are the results of Brand and Cross[87] for the 227 μm, 126 μm, and 102 μm tubes respectively. The inclusion of contributions to slip and even Knudsen flow in the reservoir produces the lines 1a, 2a and 3a for the same diameters.[88]

effective viscosity in the long mean free path limit in a cylindrical geometry decreases to a finite, geometry dependent value.[89] For issues related to fourth sound and slip (though not including discussions on higher order corrections) the reader is referred to the results following Eq. (154).

Within these constraints, using the slip approximation, Einzel has calculated that the Q in experiments carried out at Cornell[67] and at Rutgers[68] should have been reduced to on the order of 100, while the experiments were about a factor of 2 smaller. However, the theoretical description adequately accounts for the difference between the Q's observed for pure ^{4}He in the same cells. Table II gives a comparison of the calculated and experimental values.

TABLE II

Parameters for Fourth Sound and Slip. Here R Denotes Mean Pore Diameter, Q_4^{exp}, the Experimental Value of the Fourth Sound Q. Q_4^{vol} Is the Expected Value of Q Based on the Second Viscosity, Q_4^{surf} Includes the Effects Due to Viscous Damping at the Surface (Hydrod.) and Effects Due to Slip

Authors	PRESS. (BAR)	T/T_c	ω $10^3\,s^{-1}$	R μm	Q_4^{exp}	Q_4^{vol}	Q_4^{surf} hydrod.	slip
Yanof & Reppy Chainer	22.8	0.95	4.6	1	65	11,500	1770	215
Morii KoJima	20.6	0.86	3.8	0.5	35	2,400	2440	113

8.1. Summary of Experiments in the Superfluid Phase

In the superfluid phases, experiment and theory show a substantial degree of agreement. The experiments span the range of very large Knudsen number (such as those reported on by Einzel and Parpia) and low temperatures. Here, in addition to finite size effects, Andreev scattering plays a significant role. Eventually finite size effects are always seen to be important for the interpretation of the experimental results, regardless of geometry. The theory is also able to account for the behavior observed in U tube oscillation experiments where in addition to the slip at the surfaces of the U-tube, normal-fluid to superfluid conversion at the free surface plays a significant role in understanding the damping of the oscillation. Finally, the role of slip effects is seen to be important in quantitatively understanding the Q of fourth sound resonances of ^{3}He in porous media.

9. MIXTURES OF ^{3}He AND ^{4}He

Mixtures of ^{3}He and ^{4}He are particularly interesting to study since about 2 layers of the ^{4}He component are preferentially coated on the walls. This inert layer leads to a suppression of magnetic coupling between the surface and the ^{3}He but apparently induces relatively little change in the scattering of the ^{3}He quasiparticles. As more ^{4}He is added, it builds on this inert layer. Relatively little is known of the ^{3}He concentration in the film of ^{4}He due to the presence of the bulk ^{3}He. It is known that when ^{3}He is added to pure ^{4}He films, there are states occupied by ^{3}He within the ^{4}He film.[90] Thus, eventually the study of scattering from the pure ^{3}He-film interface may provide additional insights into the properties of the mixture film.

The earliest experiments by Betts and coworkers[91] carried out on mixtures are described by Hall (Fig. 24).[92] These were carried out using a torsional crystal oscillator with a resonant frequency of 40 kHz. There was a large annular region around the oscillator, so that the experiments were carried out in the unclamped regime. At the lowest temperatures, the mean free path was on the order of the viscous penetration depth. Experiments were done both with pure ^{3}He and various mixtures of ^{3}He and ^{4}He. The viscosity of pure ^{3}He and ^{3}He as varying amounts of ^{4}He were added are plotted in this figure. The Sussex group found that at some temperature there was a clear departure of the inferred viscosity from the T^{-2} behavior and that this temperature increased with the concentration of ^{4}He. The viscosity eventually regains the T^{-2} behavior at sufficiently low temperatures, but the coefficient of the effective viscosity, ηT^2, was reduced by two orders of magnitude at the highest ^{4}He concentrations. For all concentrations, the effective viscosity was smaller as the ^{4}He content increased.

Although the results of this experiment were never fully explored, a simple picture was put forward to account for this remarkable behavior. Hall[92] proposed that since the difference in chemical potentials $\mu_3 - \mu_4$ must be independent of distance from the wall, x, the result is a $1/x^3$ barrier for ^{3}He excitations. This barrier has a height of 0.3 K at 10 Å from the wall. Thus classically, there should be no momentum exchange across the intervening ^{4}He layer with the wall. If one models the "barrier" by a WKB potential with a cut off at about 5–10 Å from the wall, a penetrability of 1% is achieved, neatly explaining the reduction in momentum transfer. Accordingly, the decrease in the effective viscosity observed was interpreted as a change in the specularity of the scattering induced by an intervening ^{4}He layer which appeared below a certain temperature compatible with phase separation in the concentrated mixture.

Experiments were also carried out in the unclamped regime using a transversely oscillating AT cut quartz transducer. Lea *et al.*[93] measured the transverse acoustic impedance at 20.5 MHz in liquid ^{3}He–^{4}He mixtures from 0.05 to 1 K at various concentrations of ^{4}He. They found a remarkable consistency of their results for these various concentrations (Fig. 25), in which they observe a temperature dependent diffuse scattering factor α (where $\alpha = 1 - s$, Eq. (112)) to vary from 0.3 at low temperatures to nearly 1 at high temperatures. They hypothesize that this large a diffuse scattering factor is plausible because of the surface roughness introduced by the gold evaporated on the quartz surface. The temperature dependence of the specularity was attributed to the reflection properties of the barrier as calculated by Hall.[92] A fit to this model was not particularly satisfactory and was unable to reproduce the nearly diffuse scattering observed at high temperatures. By examining the contribution of 2D surface rotons at the

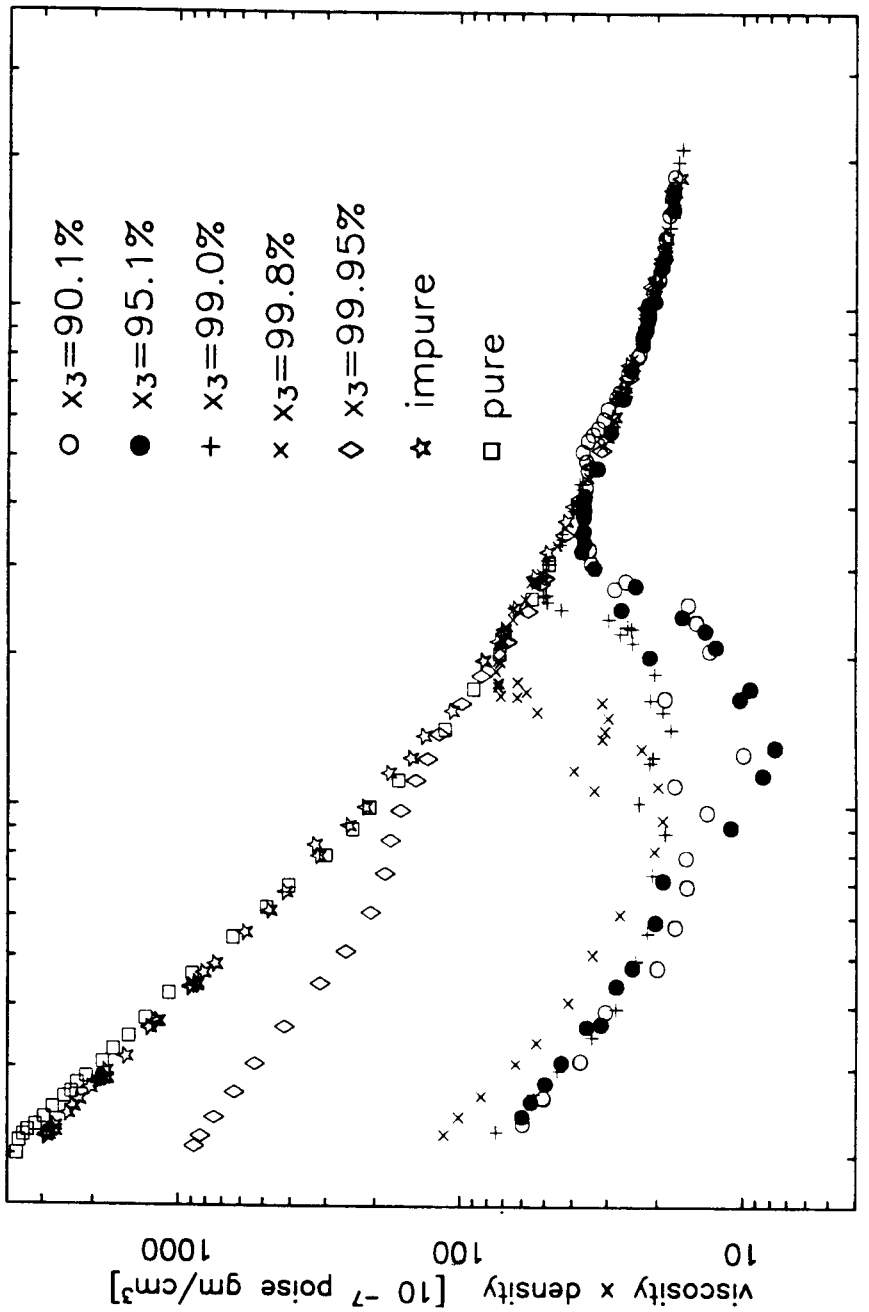

Fig. 24. Values for $\eta_{eff}\rho^n$ obtained[91] for various concentrated solutions plotted against the temperature. In all cases the effective viscosity decreases dramatically at temperatures below phase separation and then follows a T^{-2} dependence paralleling the Fermi liquid behavior. This was the first indication that the presence of a ^{4}He rich boundary layer is a specular scatterer of quasiparticles. The plot is a modified version of one in Ref. 92.

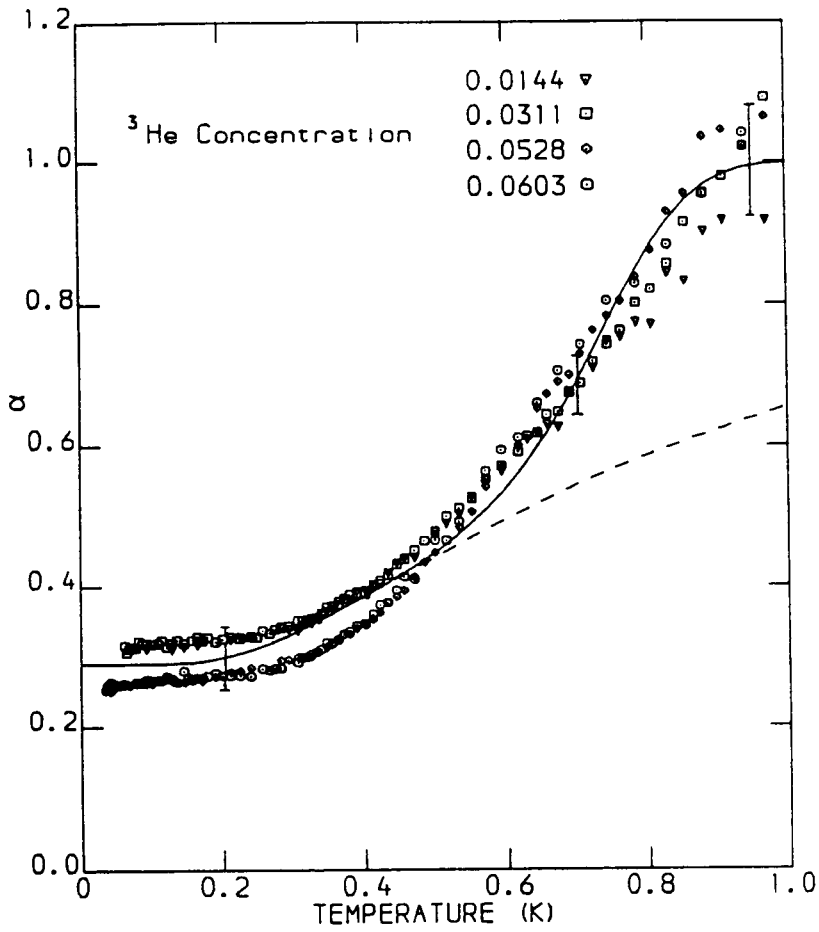

Fig. 25. The diffusivity coefficient $\alpha = 1 - s$ plotted against the temperature in Kelvin for the reflection of quasiparticles from gold plated quartz surfaces. The dashed line corresponds to diffuse scattering of quasiparticles with energy greater than 1.2 K convoluted to the residual roughness of the surface. A better fit is obtained when the interactions of quasiparticles together with interfacial rotons is taken into account, with the roton gap of 5.85 K. This yields the solid line shown in the figure. The data and fits were reported by Lea *et al.* in Ref. 93.

interface, they were able to obtain a good fit to the data taking into account the smaller energy gap of the 2D surface rotons (5.85 K) compared to those in bulk. The fit that they obtain using both mechanisms (the barrier at the surface due to exclusion of ^{3}He from the walls, and the roton contribution) seem to give good agreement with experiment as shown in Fig. 25. For details of the fit, we defer to the original publication.[93]

Experiments carried out in saturated mixtures at very low temperatures continued to show rather curious behavior (Fig. 26). Guenault *et al.*[94] used a vibrating wire to probe the viscosity of the 6.4% solution down to 0.4 mK. They found that the response of the wire deviated strongly from

the result expected under conditions that include slip at a diffusely scattering surface. In order to extract the viscosity—which Guenault *et al.* did not do—both the in-phase and out-of-phase signal voltages have to be deconvoluted. Instead, Guenault *et al.* display their data in terms of the frequency shift ($\Delta f_1/f_0$) and resonance width ($\Delta f_2/f_0$).

$$\frac{\Delta f_1}{f_0} = \frac{\rho}{2\rho_w} + \frac{\rho^n}{2\rho_w}(k-1)$$
$$\frac{\Delta f_2}{f_0} = \frac{\rho^n}{\rho_w} k' \tag{194}$$

where k and k' are as defined by Stokes,[95] and depend on the ratio of the wire radius, a to the viscous penetration depth, δ. ρ_w refers to the density of the wire. The first equation represents the contribution of the fluid to the inertia of the wire and the second equation the dissipation as characterized by the width of the resonance Δf_2. As Guenault and Pickett point out,[96] to qualitatively understand the behavior, one should consider the response of the wire vibrating in a fluid of zero mean free path. Since η is zero, the only contribution that the fluid makes is to the inertial term which shows a shift due to the volume of fluid displaced as the wire moves ($k=1$, $k'=0$). As the viscosity increases, more fluid moves with the wire, and this is accompanied by dissipation ($k<1$, $k'>0$). This is the Stokes result, with ($k'=k$) and is shown as the line marked "A" in Fig. 26. The effect of slip is to modify the boundary condition, and these corrections enter into the Stokes equations through a parameter β,[55]

$$\beta = \frac{\zeta_0}{a}\frac{1}{1+\zeta_0/a} \tag{195}$$

The results of the slip correction are shown as the curve "B" whose region of validity is limited to temperatures above 3 mK or when the mean free path is less than the wire diameter and $\beta \ll 1$.

To understand why the response of the wire bends back onto itself, it is useful to examine the limit of infinite mean free path. The dissipative term (Δf_2) is proportional to the force on the wire and the force is proportional to the velocity. Consider the motion of a wire of unit length, and radius a, moving with velocity v as it encounters quasiparticles of density n, and group velocity v_g. On the leading side, the wire intercepts $a(v_g+v)\,n$ particles per unit time and on the trailing side $a(v_g-v)\,n$ particles. Each collision leads to a momentum transfer of order $2p_F$ with the wire. Thus the force on the wire is $F=-Anp_F av$ where A is a constant, and is proportional to and in phase with the velocity, so there is no contribution to Δf_1.

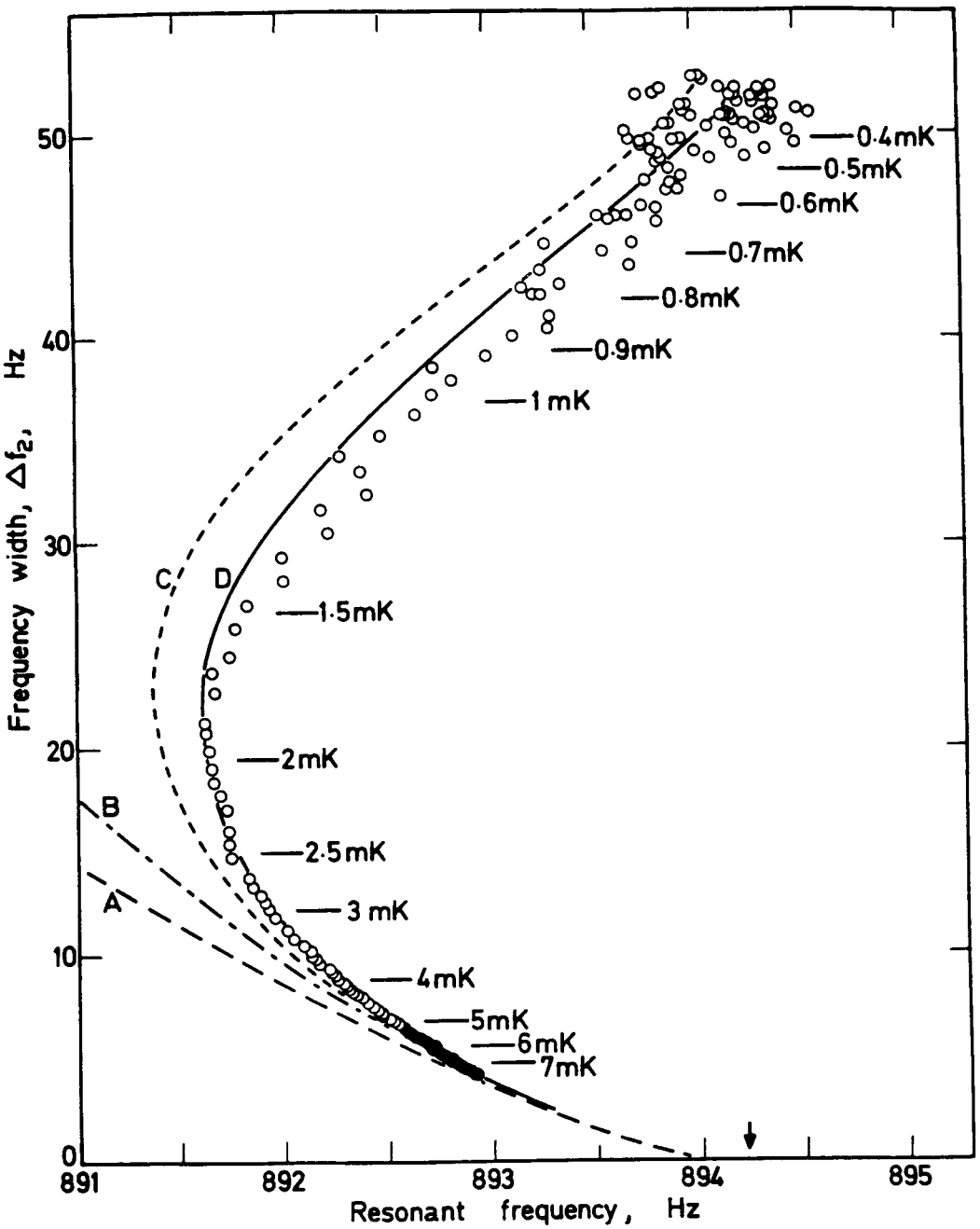

Fig. 26. A plot of the frequency shift Δf_1 against the resonance width Δf_2. Δf_1 represents the additional inertial mass coupled to the wire. With lower temperature, both the inertial and dissipative terms increase as the viscous penetration depth increases. This is the Stokes functional form shown as curve "A." In the presence of slip there is less mass coupled to the wire and thus Δf_1 is lower than the Stokes case (B). When λ becomes comparable to the experimental size, the Stokes description is not valid. In the extreme long mean-free path limit, the force (on the wire) is proportional to the wire velocity, thus affecting the damping but not the inertia, and causing the response to bend back to the vacuum period with additional dissipation. "C" includes a fit accounting for the finite compressibility of the liquid. Curve "D" shows the result of an empirical modification to the form of β (Eq. 195) used in curve "C," details of which can be found along with the data in the paper by Guenault *et al.*[94]

Consequently, there is finite dissipation, without additional inertia in this limit. Thus the infinite mean free path and zero mean free path points should both occur at the same frequency, with the long mean free path contributing a finite amount of damping. The extent and shape of the Δf_1 vs. Δf_2 curve then depend on the details of scattering from the surface.

Carless *et al.* calculated the corrections (curve marked "C") that would have to be included to account for the hydrodynamics of a vibrating wire in helium. In addition to contributions that account for the compressibility of the fluid, Carless *et al.* use a different equation for β to interpolate between the zero and infinite mean free path limits

$$\beta = \frac{\zeta_0}{a} \frac{1 + \alpha(\lambda/a)}{1 + \lambda/a} \tag{196}$$

where α is a constant of order 2. In the results plotted by Guenault *et al.*, they found that the description provided by Carless *et al.* was not sufficient to correct for the observed behavior. Instead they had to allow for a still greater correction (by about 30%) to account for the data (see curve "D" in Fig. 26). While there is no current understanding of the origin of this discrepancy, it is possible that since the corrections of Carless *et al.* were carried out for pure ^{3}He and this is entirely a dilute solution, then there may be additional corrections due to Fermi liquid factors. Further, the analysis neglects any variation in the concentration profile away from the wire, and this may play a role in the smaller momentum coupling to the fluid from the wire in a manner similar to the argument presented by Hall to understand the result of Betts *et al.*

The early experiments of Betts *et al.* showed that when surfaces were coated with a solution of ^{4}He (perhaps with ^{3}He impurities in it), that the momentum transfer was strongly impeded, leading to a specularity induced presumably by the presence of the intervening layer of ^{4}He acting as a barrier to the incoming quasiparticles. An experiment by Freeman and Richardson[97] was the first to observe that the momentum transfer is radically affected by the superfluidity of the ^{4}He film layer. The experimental configuration consisted of a stack of mylar plates separated by polystyrene spheres. Enough ^{4}He was used to coat the surfaces so that there was a film of ^{4}He fluid on the surface of the mylar plates. As the temperature was lowered, the mechanical oscillator showed the progressive coupling of the ^{3}He contained within the plates. At some temperature [190 mK and 80 mK in Fig. 27] the intervening film of ^{4}He passed into the superfluid phase, and the result was a strong decoupling of the moment of inertia of the ^{3}He from the mechanical oscillator. This experiment demonstrated that the superfluidity of the intervening ^{4}He layer increases the specularity of a surface,

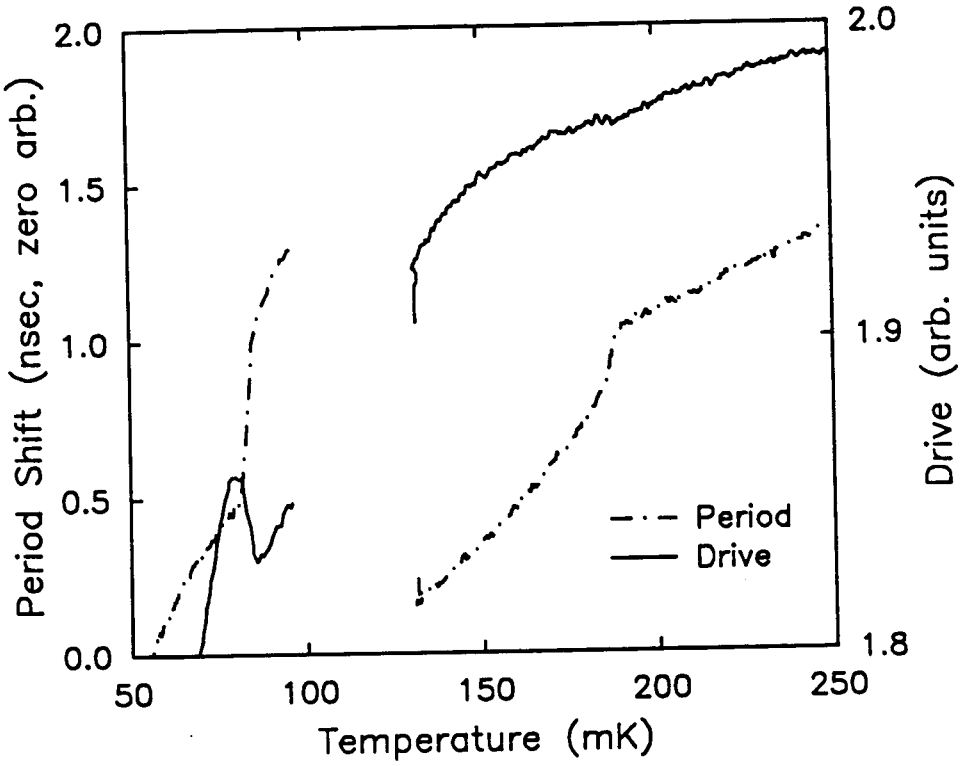

Fig. 27. The torsional oscillator period signal (Dash-dot line) obtained by Freeman[97] showing the large decrease in the fluid inertia coupled to the pendulum due to an increased slip (due to change in specularity) induced by the onset of superfluidity of the ^{4}He film. A small increase in the dissipation (solid line) is also seen due to the unlocking of the fluid. The lower temperature data was obtained at 29.3 bar, while the higher temperature data was measured at 8.7 bar. The amount of ^{4}He in the cell was constant, and the different onset temperatures are thought to reflect the pressure dependence of the solubility of ^{4}He, the pressure dependence of the inert layer, and possibly the rearrangement of the amount of ^{4}He in the fill lines and heat exchanger.

and the momentum transfer is affected by the state of the intervening ^{4}He. While there were not any possible conclusions about the applicability of the explanation provided by Hall, certainly this experiment demonstrated that superfluidity of the ^{4}He component adds to the specularity.

Concurrently with Freeman's experiment, the results of Ritchie, Saunders and Brewer[98] provided more puzzling data on the scattering properties of superfluid ^{4}He coated surfaces and mixtures of ^{3}He and ^{4}He. This experiment consisted of a hollow cylinder machined from Stycast 1266 epoxy and operated at its torsional resonance at about 1.8 kHz. Since the fluid within it was unclamped, the experiment measures the transverse impedance (see Eq. (7), (150) and (182)).

$$Z_\perp(\omega) = X(\omega) + iY(\omega) \tag{197}$$

Both the real and imaginary parts of the complex response were measured (see Fig. 28). For pure ^{3}He, the real and imaginary parts should be proportional to one another. When the ratio of these was calculated, it was found to be close to 1, and nearly temperature independent, in conformity with theoretical expectations. Upon adding ^{4}He the ratio decreased dramatically, with less fluid being coupled to the oscillator (Y/X decreased), and the absolute values of both of the real and imaginary terms decreased. The real and imaginary terms were both relatively temperature independent. In this experiment, the effective viscosity of the helium decreased by about a factor of two upon adding 3 to 4% ^{4}He. Estimates that included a large degree of specular scattering were not able to explain the result since this should exhibit some temperature dependence which seemed to be lacking in these experiments.

Einzel, Panzer, and Liu[60] recognized that the surface scattering could be radically affected by the mesoscale features on a surface. If the scattering is in the highly specular regime such as that induced by surface superfluid ^{4}He, then the slip length may become extremely large, while the mean free path in the normal ^{3}He may still be small enough compared to d the width of the flow channel, to apply hydrodynamics. If the surfaces of the boundaries are rough with some mesoscale curvature, then the slip length can be bounded from above in the presence of specular scattering. They modeled the surface corrugation by assuming a periodic variation of the height with a periodicity of order $1/q$, and a dimensionless height parameter, κ, given by $\kappa = h_0 q$. The results of this calculation are summarized in Fig. 29. As the mean free path increases (for example with lower temperatures), in the absence of mesoscale roughness the effective slip length ζ_{eff} will also increase without bound (dashed line in Fig. 29). If there is mesoscale roughness, ($\kappa > 0$) the actual slip length can be limited to being on the order of the periodic modulation when the product $q\zeta_0$ is very large. Thus, depending on geometry and the variation of ζ_0 with temperature, radically different behavior from the pure specular result (Eq. (112)) may be manifested in an experiment. Einzel *et al.* found that by assuming a periodicity of 1.8 μm, and a height of the surface roughness features of 1 μm, the slip length would be limited to about 6 μm. They found this to be a reasonable approximation to the data of Ritchie, Saunders, and Brewer. Wang and Yu[99] adopted a different approach to develop a model to explain the results of this experiment. They considered the impedance of a thin boundary superfluid ^{4}He layer in series with the liquid ^{3}He. With this approach they attributed the momentum exchange mechanism across the superfluid layer to the presence of vortex lines in the ^{4}He film. Without the construction of a special surface with a well characterized roughness, it is difficult to assess which of the contributions (vortex lines or mesoscale

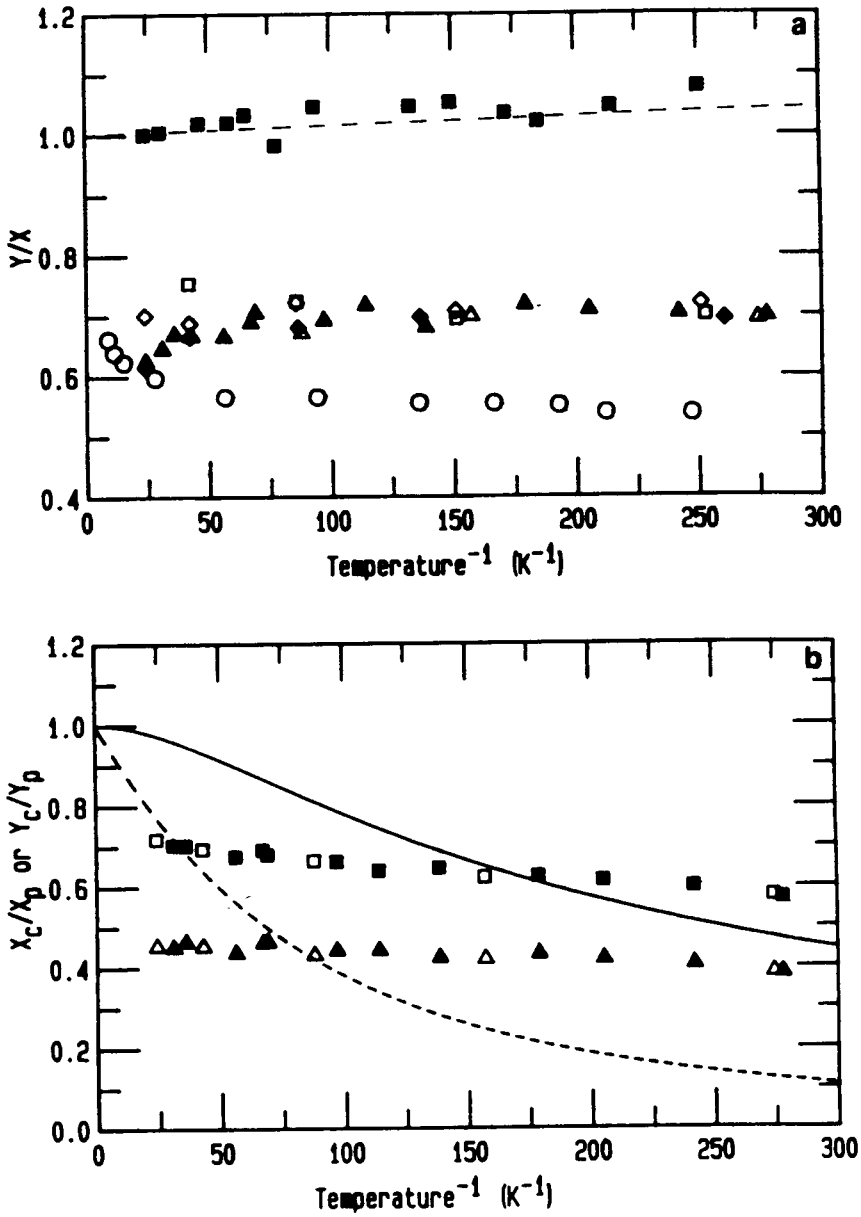

Fig. 28. (a) Measured value of the inertial term (Y) divided by the dissipative term (X) against the inverse temperature. Filled squares, pure ^{3}He; open squares, $x_4 = 0.005$, open diamonds, $x_4 = 0.01$, filled diamonds, $x_4 = 0.02$, open triangles, $x_4 = 0.03$, filled triangles, $x_4 = 0.04$, circles $x_3 = 0.0514$. The dashed line represents the theoretical result for pure ^{3}He. When ^{4}He is added, the inertial term decreases more rapidly than the dissipative term. (b) The ratios X_c/X_p and Y_c/Y_p, (the subscript refers to a concentration) vs. the inverse temperature. X_c/X_p: ($x_4 =$ 0.03—open squares, $x_4 = 0.04$—filled squares); Y_c/Y_p: ($x_4 = 0.03$—open triangles, $x_4 = 0.04$—filled triangles). The curves show the result for slip theory with a specularity of 0.975 for X_c/X_p (solid line) and Y_c/Y_p (dashed line). The temperature dependence does not replicate the experimental result. The results are from Ref. 98.

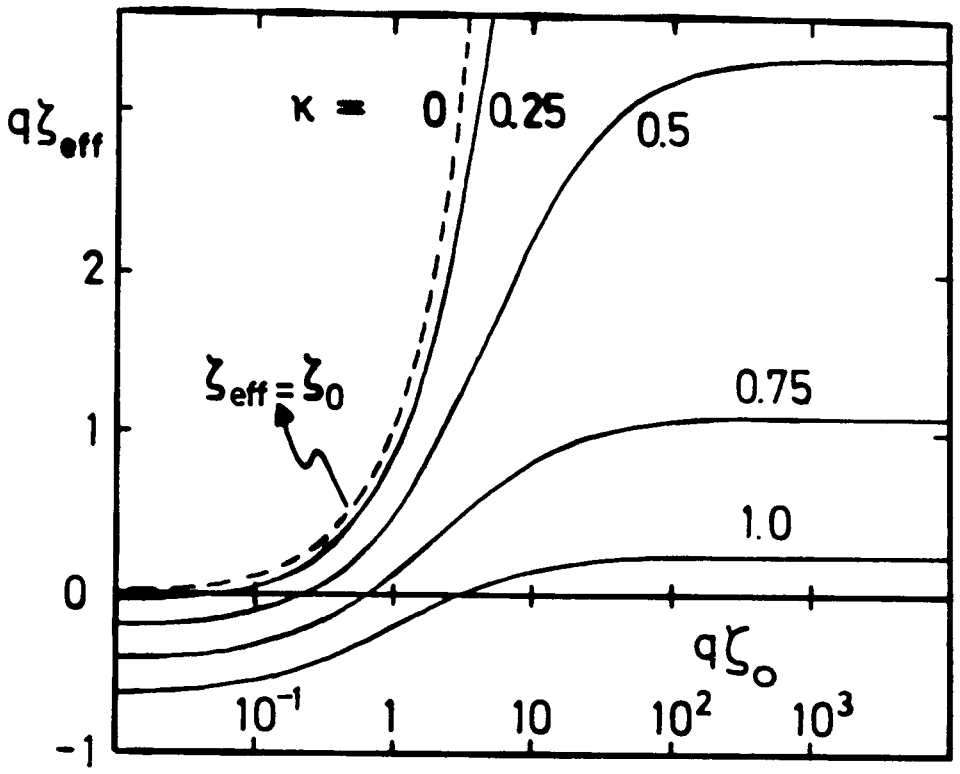

Fig. 29. The effective slip length ξ_{eff} for a cosine surface profile plotted against ξ_0 where ξ_0 is the microscopic slip length given by $a\lambda_\eta$. If there is no mesoscale curvature, the slip length $\xi_{\text{eff}} = \xi_0$ and is shown as the dashed line. Solid lines show results for surface corrugations $\kappa = 0.25$–1.0, where $\kappa = qh_0 = h\ \Lambda$. For surface corrugation where $\lambda_\eta q \ll 1$ the slip length can be negative. In the case of large scale corrugations, with wavelengths smaller than λ_η, the slip length can be much reduced (the flattening seen for $q\xi_0 > 10$). Such behavior can qualitatively model the results obtained in the Ritchie, Brewer, and Saunders experiment[98] but cannot explain the lack of temperature dependence. The plot is taken from Ref. 60.

roughness) dominate the momentum transfer process at a ^{4}He covered surface.

Vibrating wire measurements carried out in Bayreuth by König and Pobell[100] also took into account the effects of finite slip. They included the effects of slip in both the real and imaginary response functions and, were able to extract the viscosity after correcting for slip. In these experiments (for example for a 0.98% mixture at three pressures) they found a plateau-like region with a coefficient of viscosity of about 2×10^{-9} poise K^2. They found that the viscosities extracted in this manner were in fair agreement with the theoretically expected values for various dilute solutions. At temperatures below about 2 mK, the mean free path exceeds the wire diameter, and the result is that first order correction terms are not sufficient to provide an adequate hydrodynamic description. (This effect is similar to that observed for pure ^{3}He and which was discussed along with Fig. 20, in

the case of the torsional oscillators.) Therefore, the apparent viscosity shown in Fig. 30 shows a decrease below the expected T^{-2} behavior.

Experiments on films of ^{3}He carried out by Steel and coworkers[101] measured the superfluid transition temperature with and without a coating of superfluid ^{4}He on the surface. When the onset of film flow was measured for pure ^{3}He films, they found that the transition temperature was suppressed to almost 0.6 of the bulk value for their thinnest film. They also found that the ratio of the film to bulk transition temperatures, T_{cf}/T_{cB}, varied as d^{-2}, where d is the film thickness. This result was in agreement with a calculation by Fetter and Ullah.[102] Following on the Freeman and Richardson experiment,[97] they observed that when the surfaces were coated with even a single monolayer of ^{4}He, that the transition temperature of the ^{3}He film was restored to the value of the bulk superfluid at saturated vapor pressure.

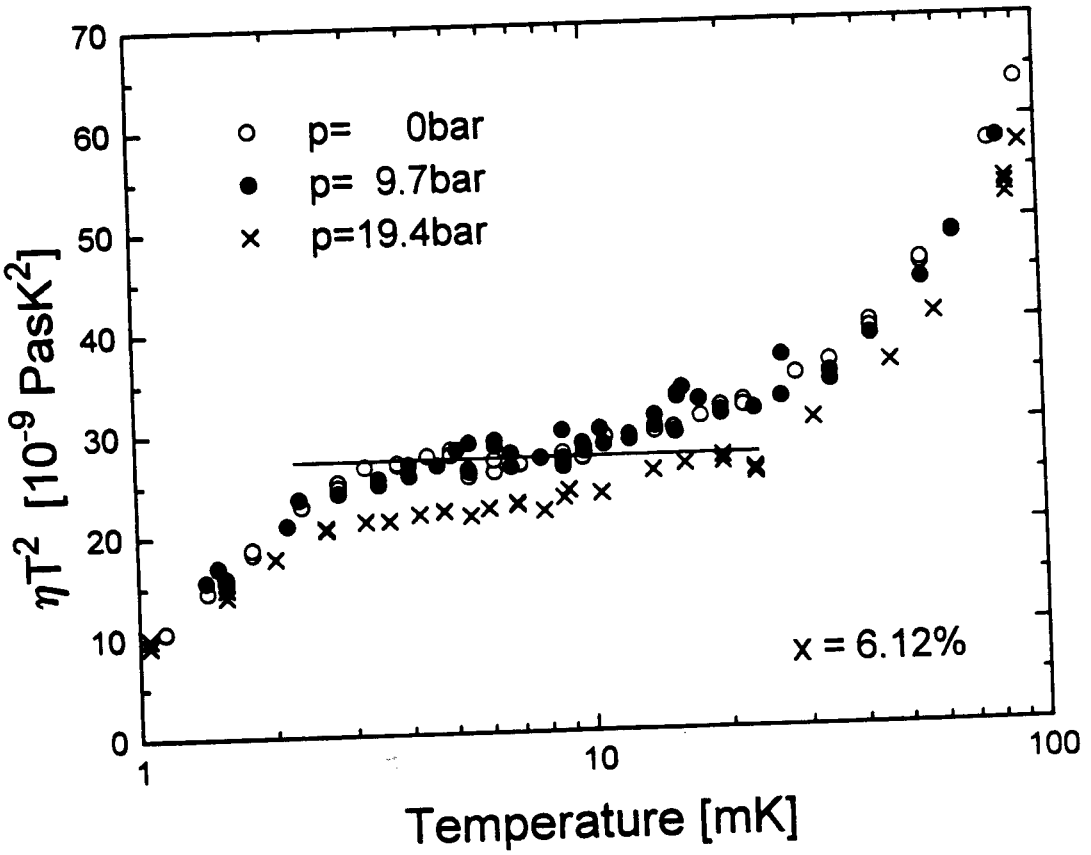

Fig. 30. The effective viscosity of the dilute solution (obtained by König and Pobell[100]), showing the expected T^{-2} behavior down to low temperatures. The decrease in the effective viscosity at very low temperatures is related to the mean free path exceeding (at 2 mK) the wire diameter. Thus, additional correction terms beyond the first order slip correction would have to be introduced to account for the observed behavior.

Tholen and Parpia[103] investigated the scattering properties of a highly polished silicon substrate. Two plates of silicon formed the confining surfaces of a parallel plate viscometer. With pure ^{3}He they found that the viscosity exhibited a temperature dependent specularity that varied from about 0.4 at 10 mK and decreased as the temperature was lowered. Although no explanation was provided for this effect, they also found that the specularity was not altered when the surfaces were coated with a single monolayer of ^{4}He but that the specularity increased when the ^{4}He (in the superfluid state) coated the surfaces to 2 layers. Further increases in ^{4}He coverage resulted in a rapid increase in the specularity of the system till at 9 layers there appeared to be close to saturation with a specularity of greater than 90%. The effective viscosity showed a continuous decrease away from the pure result as the ^{4}He was added. In Fig. 31(a) the results on the effective viscosity as the ^{4}He content was increased are shown. In Fig. 31(b) the temperature dependent specularity value is shown. The temperature dependence remains an unknown in these experiments. Finally, in Fig. 31(c), the specularity factor at 3 mK is shown, illustrating the onset of specularity presumably induced by superfluidity of the surface ^{4}He. Other than the temperature dependence of the specularity, the picture seems to be in reasonable conformity with the model put forward by Hall to explain the increased specularity observed by Betts and coworkers in the early Sussex experiments.

Tholen and Parpia also found in a separate experiment,[104] that the diffuse scattering result could be regained when the surface ^{4}He was solidified by the application of pressure. Thus, once the surface layer is solidified, quasiparticles scatter off from the solid ^{4}He surface much as they would from a surface before ^{4}He is added. These results were obtained by studying the superfluidity of the ^{3}He contained within pores of silver sinter. The boundary condition being relaxed from diffuse towards specular results in a reduction of the suppression of the order parameter near a surface, and thus the superfluid fraction may be used to infer the specularity of the scattering at the surface. These results show that the magnetic state of the solid ^{3}He at the surface probably has little to do with the boundary condition at the surface.

A very comprehensive series of experiments on porous powders was carried out a little later by the Osaka City University Group consisting of Kim, Nakagawa, Ishikawa, Hata and Kodama and Kojima.[105] Using a fourth sound technique they found a different pressure dependence to that observed in Ref. 104 (as well as the absence of the hysteretic solidification seen in Ref. 104). Using several powdered samples that acted as superleaks, they found that the specularity of the surface layer increased for coverages of between 1 and 2 layers and appeared to be nearly complete at 3 layers for the Ag sinter, and the 3 μm and 1 μm alumina powders, while the

smallest powders (0.3 μm) continued to show substantial suppression of the superfluid fraction at this coverage.

9.1. Summary of Experiments on Mixtures of ^{3}He and ^{4}He

In general then, the results in the mixtures show that there is substantial agreement between the theoretical expectations and experiment. There are still some questions related to details of the momentum transfer

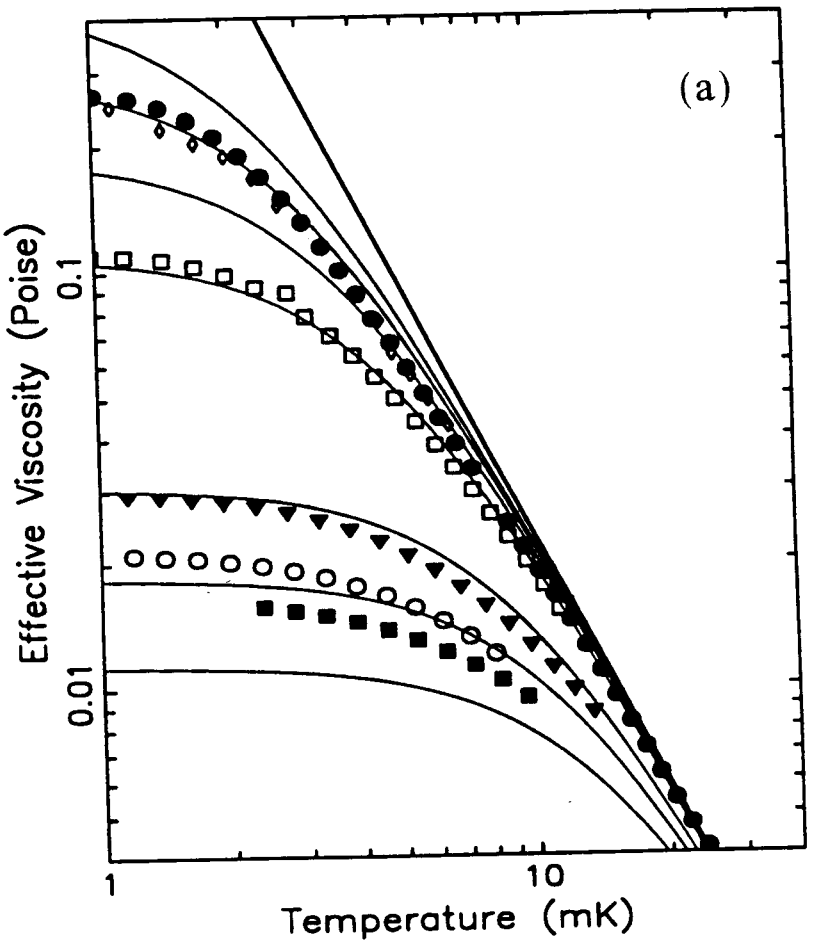

Fig. 31. (a) Data on the effective viscosity obtained by Tholen and Parpia[103] for a parallel plate torsional oscillator with a 57 μm gap. The solid lines from top to bottom correspond to no slip, ($\eta_{\rm eff} = \eta$, purely diffuse scattering ($s = 0$), $s = 0.2$, 0.4, 0.6, 0.87, 0.92, and 0.97. Solid circles correspond to pure ^{3}He; open diamonds to 20.8 μmol/m^2; open squares to 30 μmol/m^2; filled triangles to 39.2 μmol/m^2; open circles to 57.7 μmol/m^2; and filled squares to 115 μmol/m^2 (approximately 9 layers). (b) The calculated specularity values corresponding to the data in Fig. 31(a); the open stars correspond to the 86.6 μmol coverage not shown in Fig. 31(a). The origin of the temperature dependence is not known. (c) The specularity taken from Fig. 31(b) at 3 mK is plotted as a function of the ^{4}He coverage. The solid line is a guide to the eye.

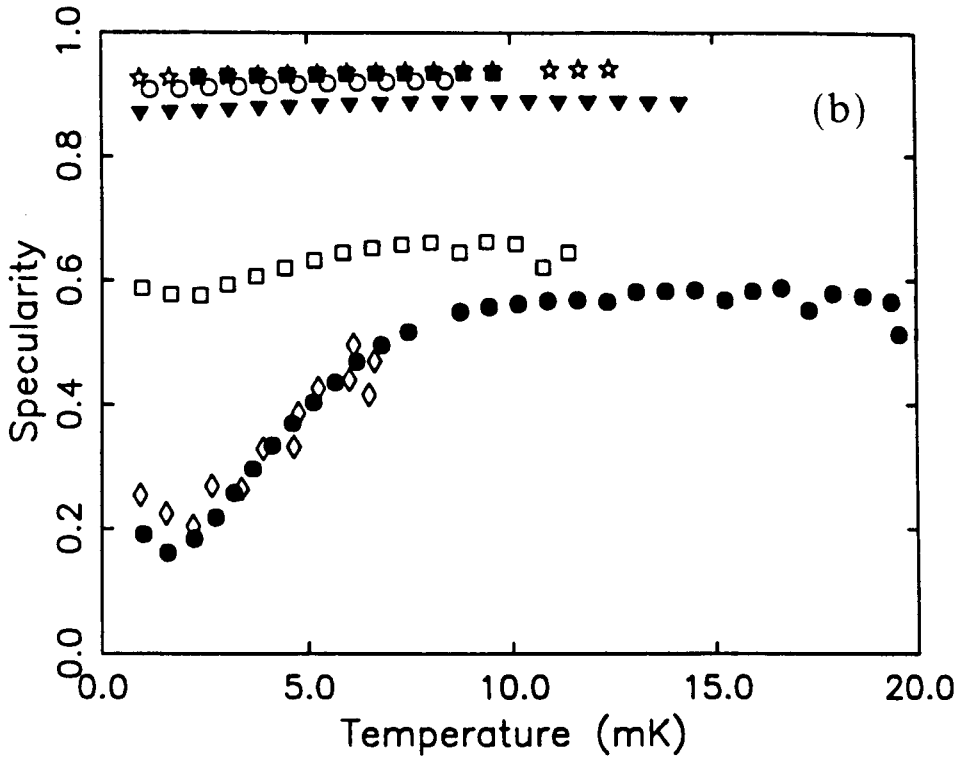

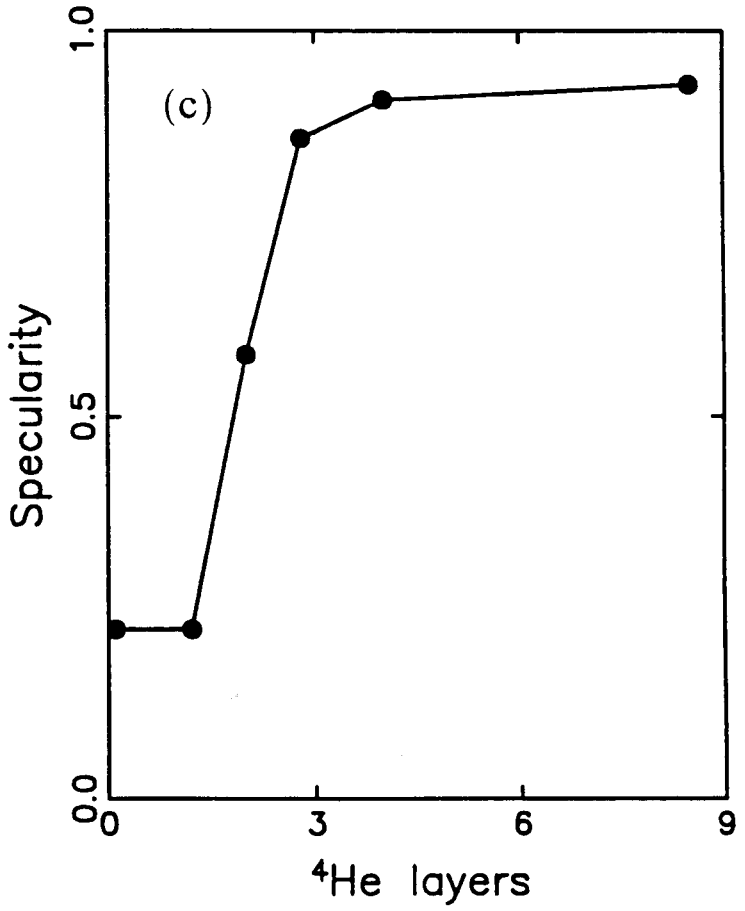

Fig. 31 (*Continued*)

mechanism across the ^{4}He boundary layer, as well as the temperature dependence of the experiments performed by Ritchie and coworkers.

10. EXPERIMENTS IN SUPERFLUID ^{4}He

As already discussed in section 2, in pure ^{4}He, there are two sets of excitations, the phonons and the rotons. Each has their own mean free path and thus each component has to be considered separately for slip corrections. In this section we summarize the study of the viscosity of ^{4}He as reported on in two works.

Lea, Fozooni, and Retz[106] carried out measurements of the complex acoustic impedance at frequencies of 20.5, 34.1 and 47.8 MHz. They measured the Q and resonant frequency of a shear mode quartz crystal resonator that was directly immersed in the liquid. The temperature dependence of the viscosity was deduced from the impedance, using tabulated values of the normal fluid density. In this experiment, $\omega\bar{\tau} > 1$ and also the mean free path of both phonons and rotons greatly exceeds the viscous penetration depth. Thus the experiments are carried out in the non-hydrodynamic or collisionless regime, where $\omega\bar{\tau} > 1$ which gives rise to relaxation effects and $\lambda_\eta/\delta > 1$ which gives rise to non-local behavior. In this collisionless regime where there is no local equilibrium, the concepts of viscosity and penetration depth are inappropriate.

In the hydrodynamic regime where $\omega\bar{\tau} < 1$ and $\lambda_\eta/\delta < 1$, the complex pedance is written as $Z_\perp(T) = R(T) - iX(T) = (1-i)(\omega\eta\rho^n/2)^{1/2}$. The presence of liquid helium decreases both the Q and the resonant frequency ($\omega = 2\pi f$) of the quartz crystal oscillator by:

$$Q_{\mathrm{He}}^{-1} = \frac{4R(T)}{n\pi R_q}; \qquad \Delta f = \frac{2fX(T)}{n\pi R_q} \tag{198}$$

where R_q is the transverse acoustic impedance of the quartz, and n is the harmonic number of the resonance. Lea, Fozooni, and Retz define two viscosities η_1 and η_2 that are derived from the real and imaginary part of the complex surface impedance in analogy to Eq. (7)

$$\eta_1(T) = \frac{2}{\omega\rho^n(T)} R^2(T); \qquad \eta_2(T) = \frac{2}{\omega\rho^n(T)} X^2(T) \tag{199}$$

These terms can be analyzed to yield the effective viscosities. The viscosities η_1 and η_2 strongly deviate at low temperatures in the non-hydrodynamic limit from those obtained by a vibrating wire viscometer in the hydrodynamic limit. The data are shown in Fig. 32. For $T > 1.6$ K, the

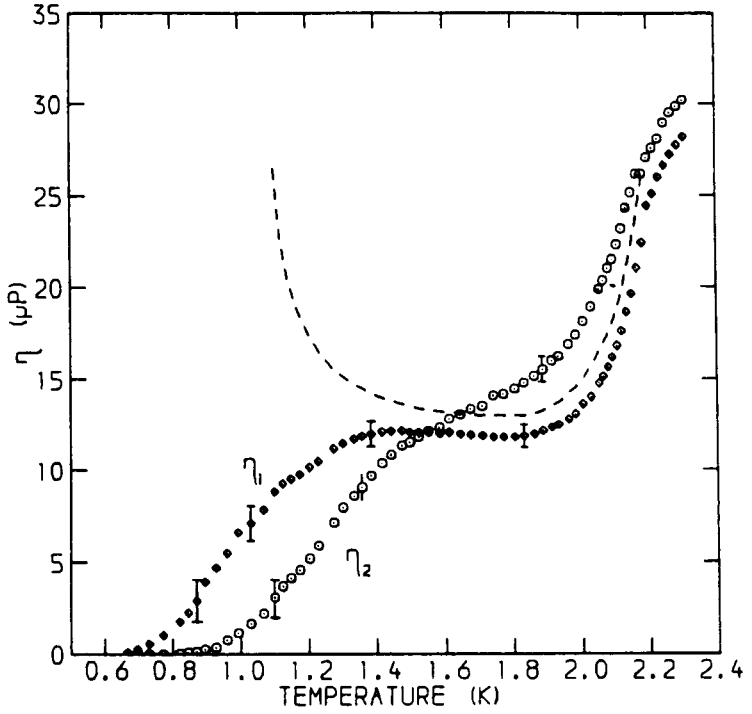

Fig. 32. The viscosity of ^{4}He plotted as η_1 and η_2. η_1, η_2 are determined from the real and imaginary parts of the transverse impedance of a 34.1 MHz crystal. The dashed line is the result obtained using a vibrating wire viscometer. At frequencies used in this experiment $\omega\tau > 1$ for temperatures below 1.6 K. Also, $\lambda_\eta/\delta > 1$ producing non-local effects. The small maximum in η_1 is the result of the rapid increase in phonon viscosity. The data shown were obtained by Lea, Fozooni, and Retz.[106]

experiments are in the hydrodynamic regime with mean free paths for both phonons and rotons being smaller than the viscous penetration depth. In this regime, the agreement between these high frequency measurements and the results obtained at low frequency with vibrating wires or oscillating disc experiments is excellent. However, at lower temperatures, instead of the rapid rise in phonon viscosity seen in oscillating disc experiments, the viscosity falls rapidly due to non-hydrodynamic effects ($\omega\bar{\tau} > 1$), leaving only a small maximum in η_1. The position of the maximum is used to determine that the fraction of phonons scattered diffusely is about 0.3 or less.

The analysis by Lea *et al.* concentrates on effects in the temperature range below 1.5 K where the assumption is that the viscosity is due to that of a dilute gas of rotons which scatter diffusely from the crystal. It is important to realize that these low temperature results are in sharp contrast to the measurements of Morishita *et al.*[42] to be discussed below. These differences are primarily due to the high frequency regime ($\omega\bar{\tau} > 1$) that the quartz oscillator operates in.

Between 1.2 and 1.5 K, Lea *et al.* identify a plateau region for η_1. In this region they find the roton viscosity to be 12.5 μP in agreement with previous work. For a gas of excitations in the collisionless limit ($\omega\bar{\tau} \gg 1$), the acoustic impedance Π_{xz} is just the momentum flux away from the surface. Thus, from kinetic theory, in the collisionless limit, the transverse surface impedance is given by

$$\lim_{\omega\bar{\tau}\to\infty} Z_\perp(\omega) = \tfrac{1}{4}\alpha_n \rho^n \bar{v}_{ex} \tag{200}$$

where $\bar{v}_{ex}$ is the root mean square velocity of excitations and α_n is the fraction of diffusely scattered excitations.

In helium, excitations in the form of phonons and the rotons are both present in thermal equilibrium. Lea *et al.* argue (following the work of Nadirashvilli and Tsakadze[107]) that the rapid rise in the phonon viscosity seen at low temperatures, is quenched at these frequencies and only a remnant is seen in the weak maximum in η_1 at about 1.4 K. Lea *et al.* then estimate the phonon viscosity only contributes a few percent to the acoustic impedance at low temperatures. Therefore, the high frequency experiments measure the roton contribution at low temperatures.

The two quantities η_1 and η_2 can then be calculated from the measured real and imaginary impedance contributions and the roton density $\rho^n(T)$, and these show a rapid decrease of the roton viscosity in the low temperature collisionless regime. From the Landau-Khalatnikov theory[13] which gives the roton viscosity in terms of the relaxation time for the dominant roton-roton scattering and the scattering rate as given by Roberts and Donnelly,[108] together with expressions for the mean roton velocity and the roton density, Lea *et al.* find that the calculated impedance in the collisionless limit is much greater than the experimentally observed behavior, if the roton scattering is assumed to be diffuse. The effect of finite $\omega\tau$ is to reduce the impedance below this limit. They consider a theory for viscoelastic liquid which allows for relaxation effects but it does not yield a good fit. Finally they employ the work of Borovikov and Peshkov[109] which corrects the hydrodynamic impedance for finite λ_η/δ (The Fermi liquid analogue is Eq. (182))

$$Z_\perp(\omega) = \frac{(1-i)(\omega\eta_r\rho^n/2)^{1/2}}{1+(1-i)\,\beta\lambda/\delta} \tag{201}$$

where δ is given by Eq. (133) with η_r the roton viscosity, and β is the roton slip coefficient. This expression is valid only as a correction to the hydrodynamic regime, but by setting $\beta = 2\pi/5\alpha_r$, the expression reduces to the correct one in the limit of hydrodynamic and collisionless regimes. This

expression then gives reasonable fits to the data of both η_1 and η_2 when $\alpha_r = 1$ (diffuse scattering limit).

Morishita *et al.*,[42] used a vibrating wire with a resonant frequency of 225 Hz. At this low frequency, the viscous penetration depth is much longer than in the previous experiment and so the transition out of the hydrodynamic regime does not occur till about 0.7 K. The signature of the departure from the hydrodynamic regime is a peak in the dissipation vs. temperature. Shown in Fig. 33, curve "A," is the expected result using the Stokes equations[95] for a vibrating wire. This is satisfactory down to about 1.2 K, but then the experimental data consistently falls below the calculated result. They found that the slip corrected[55] effective viscosity deviates substantially from their result shown as curve "B." This is not surprising since it has been seen that the slip condition is not sufficient to describe the behavior in the general situation which includes the long mean free path (Knudsen) limit.

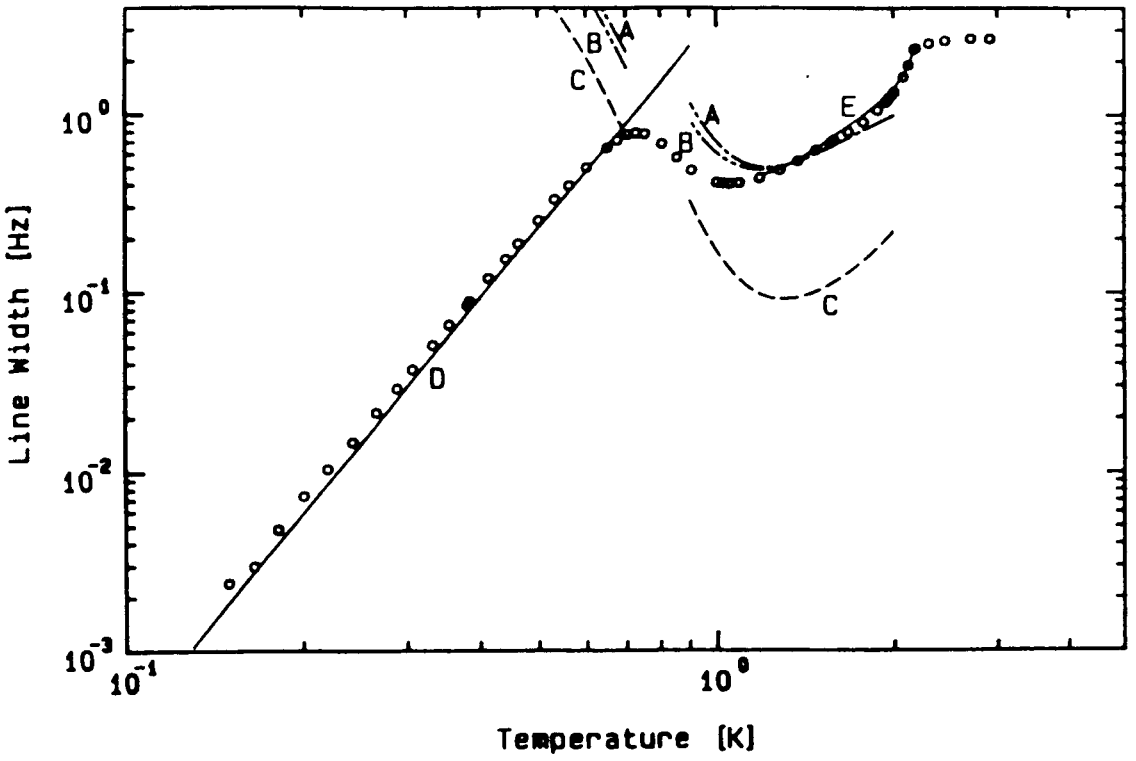

Fig. 33. The behavior of a vibrating wire immersed in pure ^{4}He. The low temperature behavior (Curve D) shows a power law decrease in line width. Below 1.7 K, the only excitations present are phonons whose mean free path $\lambda_p > d$ the wire diameter. The maximum at 0.7 K is due to the transition from ballistic to hydrodynamic behavior ($\omega\tau = 1$ at 0.7 K). Curve A is the result of the Stokes solution to the motion of a vibrating wire and is adequate down to 1.2 K. Including the effects of first order corrections to finite size effects results in B. Curve C is obtained when the variation of the wire velocity along its length (due to the geometry of the vibrating wire) is replaced by an average velocity. The agreement is markedly worse using the average velocity. In curve E, experimental data[110, 111] is used to predict the line width and shows good agreement down to 1.5 K The plot is from Morishita *et al.*[42]

At very low temperatures, phonons are the main excitations in helium-II. The phonon wavelength is much smaller than the wire, and thus the phonons are expected to behave ballistically. In contrast to Lea *et al.*, these experiments are carried out in the limit of low frequency ($\omega\bar{\tau} < 1$) but long mean free paths. Therefore, they calculate the drag force as was done by Guenault and Pickett,[96] and thus obtain an expression for the width of the resonance

$$\Delta f_2 = \frac{2.67}{45\hbar^3 u_1^4 a(\rho_w + \rho^s)} (k_B T)^4 \tag{202}$$

where ρ_w is the wire density, u_1 is the first sound velocity and a the wire radius. Eq. (202) is plotted in Fig. 33 as curve "D."

Morishita *et al.* have shown that the behavior of a vibrating wire immersed in a fluid with very dilute excitations still can be understood rather well. The first order slip correction at the surface is not sufficient to understand the data. However, higher order terms have to be introduced (even though these can only be approached in a phenomenological way) to successfully account for the dissipation in the fluid.

10.1. Summary of Experiments in ^{4}He

These two experiments examine non-hydrodynamic effects that occur in both the roton and phonon excitations under very different limits. In the first experiment that we described, at high enough frequency ($\omega\bar{\tau} > 1$) the roton contribution dominates. However, the phonons are more important in the ballistic limit. In ^{4}He, the characteristic length scales grow to be very long but as in the case of ^{3}He superfluid and the mixtures of ^{3}He and ^{4}He, there appears to be quite a reasonable agreement between the expected results and the actual experiments. In ^{4}He superfluid, there has not been a concerted effort to compare details of the effective viscosity to the expected results of the bulk viscosity. Nevertheless there appears to be strong evidence that the behavior observed in the vibrating wire and in surface impedance measurements are in good agreement with the expected response of the superfluid and its dilute excitations.

11. SUMMARY AND CONCLUSIONS

In this review we have studied theoretical and experimental aspects of finite size effects on the viscosity of the quantum liquids ^{3}He and ^{4}He. In the theory section we introduced viscosity as a dissipative phenomenon, which can entirely be associated with the gas of elementary excitations,

namely the phonons and rotons in superfluid ^{4}He and the Landau- and Bogoliubov quasiparticles, respectively, in normal and superfluid ^{3}He. At sufficiently low temperatures these quasiparticle systems form dilute gases, characterized by low (normal fluid) densities ρ_n^{ex} and long mean free paths λ_η^{ex}. Kinetic theory produces very simple expressions for the normal component's shear viscosity $\eta^{ex} \propto \rho_n^{ex} \lambda_\eta^{ex}$. We argued that λ_η cannot increase to arbitrary high values at low T, but is either bounded by d, the typical dimension of the experimental cell in a low frequency Poiseuille flow experiment or by δ, the viscous penetration depth characteristic of a high frequency surface impedance experiment. If λ_η^{ex} is small (but not negligible) w.r.t. d or δ, we showed that the hydrodynamic viscosity will be renormalized (and in general reduced) by a first order slip correction $\eta_{eff} \propto \eta^{ex}/(1 + a\zeta_0/\max\{d, \delta\})$ with a slip length $\zeta_0 \propto \lambda_\eta$. Mean free path effects on the Poiseuille flow and the surface impedance manifest themselves in different effective viscosities, which we studied not only in the slip regime (small mean free paths) but also in the general case of arbitrary ratios λ_η/d and λ_η/δ. We now summarize the results of comparisons between experiment and theory for the various quantum fluids and different experimental methods.

In the normal state of pure ^{3}He there are a number of puzzles that are unresolved. Firstly, all measurements of the effective viscosity point toward a smaller than expected "super diffuse" slip length at low pressure. Several experiments have observed a pressure dependence of the slip coefficient. This point is as yet questionable, since the recent observation of a non-Fermi liquid viscosity opens up the possibility that the slip parameter does not vary as much as was previously thought. The temperature at which the Knudsen minimum is seen is higher than the theory predicts. The temperature dependence of the slip measured in the experiment on polished silicon, is also unresolved. While many of these experiments may well be dominated by details of surface preparation, it is clear that the picture is as yet incomplete. The possible non-Fermi-liquid behavior of the viscosity particularly below about $2T_c$ has to be considered, and should be carefully examined using other techniques such as zero sound and by measurement of other transport properties. Clearly the origin of the deviations in early experiments from the expected behavior may originate in non-Fermi liquid properties of ^{3}He or as a result of poorly characterized surfaces. Thus, there continues to be room for new experiments with well characterized surfaces and others which might be specifically designed to probe the properties of bulk normal liquid (with no ambiguities concerned with thermometry). These experiments should examine in detail the roughness dependence of the slip parameter. Other experiments which can differentiate between non-Fermi liquid behavior and the location in temperature of the Knudsen minimum would also be desirable.

In the superfluid phase of ^{3}He, there is rather good agreement between theory and experiment, once the possibility of the transition to Knudsen flow and Andreev scattering are taken into account. However, surface roughness effects have not been studied in detail in this system. Low pressure results still appear to fall outside of the bounds of the theoretical expectation, even when Andreev scattering is accounted for. It is possible that thermometry introduces the dominant error in comparisons between theory and experiment. Slip and other mechanisms (such as the conversion between normal and superfluid components at a free surface) have been able to account for a number of puzzles such as the excess damping in fourth sound experiments and the over damping in U-tube experiments. The fact that the slip can be modified by the addition of ^{4}He superfluid surface layers in many of these geometries has not been used, but, in view of the complexity of and time scales for execution of these experiments, it is unlikely that these variations will be tested soon, except perhaps in the context of superfluid Josephson junctions.

In the case of mixtures, while it is true that vibrating wire experiments appear to yield effective viscosities that are reasonable, it is also important to realize that mesoscale curvature notwithstanding, there is the likelihood that the effects of surface ^{4}He are not understood as evidenced in the experiment by Ritchie and co-workers. These may be related to surface preparation artifacts, but, as in the case of pure ^{3}He, there are still unresolved questions in these experiments. Details of exactly why the specularity is modified by the presence of a superfluid ^{4}He boundary layer, and in fact, the microscopic process by which momentum is transmitted across this superfluid are as yet unknown.

In ^{4}He, the experimental and theoretical investigations have not been as detailed. However, in some respects, the very long mean free paths that can be realized, together with the possibility of adding ^{3}He as an impurity to the ^{4}He as a means of limiting the mean free path imply that ^{4}He may possibly be a fertile testing ground for rarefied gas dynamics. Overall, it is clear from the two experiments that we have discussed, that there is substantial agreement between the experiments and the theory as extended to apply to the non-hydrodynamic regime even though the experiments may well be in the extreme long mean free path limit.

To summarize, for the quantum fluids, ^{3}He and ^{4}He and their mixtures, there is considerable agreement between the experiments and theory. Theory has advanced to be able to account for the effects of mesoscale surface roughness and the consequences of Andreev scattering at boundaries to Fermi superfluids. There are some open questions which still need to be answered. In general, the state of the experimental surfaces is in many cases not well established, and thus in the future, surface preparation and characterization must be viewed as a prerequisite for new geometries.

APPENDIX 1: QUASIPARTICLE RELAXATION RATE OF ^{3}He–B

The energy dependent relaxation rate of Bogoliubov quasiparticles can be written in the form

$$\frac{1}{\tau_k} = \frac{1}{\tau(E_k, T)}$$

$$= \frac{1}{\tau_N(T)} \{I_0(E_k, T) - \gamma_0[I_1(E_k, T) + I_2(E_k, T)] + \delta_0 I_3(E_k, T)\} \quad (203)$$

with $\tau_N(T) = 32\mu\hbar/(\pi k_B T)^2 \langle W \rangle_a = \tau_N(T_c) \cdot (T_c/T)^2$ is the normal state quasiparticle lifetime at the Fermi surface (W is the spin independent normal state scattering cross section). The pressure dependent quantities γ_0 and δ_0 are weighted angular averages of the scattering cross section W. It has turned out that for all practical purposes, the energy dependence of the quasiparticle relaxation rate expressed through the dimensionless functions $I_n(E_k, T)$, $n = 0,..., 3$, can be interpolated well between the exact results of both a low temperature expansion in $k_B T/\Delta$ and an expansion in $(\Delta/k_B T_c)^2$ near T_c. Let us first introduce the abbreviation $x = \Delta/k_B T$. The dimensionless quasiparticle relaxation rates $I_n(E_k, T)$ may be decomposed as

$$I_n(E, T) = J_n(T) + \left(\frac{\xi}{k_B T}\right)^2 K_n(T) \quad (204)$$

The temperature dependent functions $J_n(T)$ have the form

$$J_0(T) = \frac{3}{4\sqrt{\pi}} \frac{(1+2x)^{3/2}}{\exp(x) + a_0 + a_1 x + a_2 x^2 + a_3 x^3}$$

$$J_1(T) = \frac{x^2}{\sqrt{2\pi}} \frac{(\frac{1}{2}+x)^{3/2}}{\frac{13}{10} + x^2} \exp(-x)$$

$$J_2(T) = \frac{x^2}{\sqrt{2\pi}} \frac{1}{(\frac{1}{2}+x)^{1/2}} \frac{1}{\exp(x) + \frac{23}{10}} \quad (205)$$

$$J_3(T) = \frac{3x^4}{\sqrt{2\pi}} \frac{1}{(\frac{1}{2}+x)^{1/2}} \frac{1}{\frac{1}{5}+x^2} \frac{1}{\exp(x) + 1 + \frac{1}{10}x^2}$$

Here $a_0 = -0.5768$, $a_1 = 0.2694$, $a_2 = 0.2900$ and $a_3 = -0.0800$. The temperature dependent functions $K_n(T)$ are found to be of the form:

$$
\begin{aligned}
K_0(T) &= \frac{9}{8\sqrt{2\pi}} \frac{1}{(\frac{1}{2}+x)^{1/2}} \frac{1}{\exp(x)+b_0+b_1 x+b_2 x^2} \\
K_1(T) &= -\frac{5}{8\sqrt{2\pi}} \frac{x^2}{(1+x)^{1/2}} \frac{\exp(-x)}{\pi^2+x^2} \\
K_2(T) &= \frac{3}{8\sqrt{2\pi}} \frac{x^2}{(1+x)^{1/2}} \frac{\exp(-x)}{\frac{127}{150}\pi^2+x^2} \\
K_3(T) &= -\frac{15}{8\sqrt{2\pi}} \frac{x^4}{(1+x)^{1/2}} \frac{\exp(-x)}{(\pi^2+x^2)^2}
\end{aligned}
\tag{206}
$$

where $b_0 = 3.4296$, $b_1 = -3.2148$ and $b_2 = 2.3750$. The accuracy for the result for a transport parameter at intermediate temperature evaluated with Eqs. (204)–(206) depends on the involved energy average of the quasiparticle relaxation time. For example it turns out to be better for the hydrodynamic shear viscosity η (typically a few percent) compared to the diffusive thermal conductivity (at most 8%). In view of the relaxation time approximation described in the text (which is also in the range of a few percent), the accuracy of (204) can be regarded as quite satisfactory.

ACKNOWLEDGMENTS

This article would not have been completed without the support in the form of a travel grant (CRG960127) from NATO, also the support of Deutscher Akademischer Austauchsdienst and the National Science Foundation under DMR-9424137. We would also like to thank the various authors for permission to use the figures, as well as for their efforts to unearth the originals for us. Thanks are due to Professors H. Højgaard Jensen, Dick Packard, John Saunders, Henrik Smith and Peter Wölfle for many enlightening discussions. M. Opel, L. Pollack, and R. Biggar helped in various aspects of the preparation of this manuscript. Finally we would like to thank H. Meyer, F. Pobell, and K. Andres for their encouragement. One of us (JMP) would like to acknowledge the hospitality of the Walther–Meissner-Institute für Tieftemperaturforschung. The authors would like to acknowledge the contributions and suggestions of the referees as well as recognize the significant time commitment that they have put in the refereeing process.

REFERENCES

1. L. D. Landau and E. M. Lifshitz, *Fluid Mechanics*, Pergamon Press, Oxford (1963).
2. K. M. Case, *Ann. Phys. (N.Y.)* **9**, 1 (1960), and references therein.

3. C. Cercignani, *The Boltzmann Equation and Its Application*, Springer-Verlag, New York (1988).
4. D. R. Willis, *Phys. Fluids* **5**, 127 (1962).
5. D. Einzel, H. Højgaard Jensen, H. Smith, and P. Wölfle, *J. Low Temp. Phys.* **53**, 695 (1983).
6. A. Kundt and E. Warburg, *Ann. Physik* **155**, 337 (1875).
7. J. C. Maxwell, *Scientific Papers, Vol. 2*, Dover, New York (1953), p. 704.
8. M. Knudsen, *Kinetic Theory of Gases*, Methuen, London (1950).
9. M. N. Kogan, *Rarefied Gas Dynamics*, Plenum, New York (1969).
10. P. Welander, *Ark. Fys.* **7**, 507 (1954).
11. S. Albertoni, C. Cercignani, and L. Gotusso, *Phys. Fluids* **6**, 993 (1963).
12. For excellent reviews see W. H. Keesom, *Helium*, Elsevier, Amsterdam (1942) and K. R. Atkins, *Liquid Helium*, Cambridge University Press, Cambridge (1959).
13. L. D. Landau and I. M. Khalatnikov, *Sov. Phys. JETP* **19**, 637 (1949).
14. K. S. Dy and C. J. Pethick, *Phys. Rev.* **185**, 373 (1969).
15. H. Højgaard Jensen, H. Smith, and J. W. Wilkins, *Phys. Lett.* **27A**, 532 (1968).
16. David Pines, "Highlights of Condensed Matter Physics," *Proc. of the Int. Sch. of Phys., "Enrico Fermi,"* Course 89, F. Bassani, F. Fumi, and M. P. Tosi (Eds.), North-Holland, Amsterdam (1985), p. 580.
17. C. J. Pethick, *Phys. Rev.* **177**, 391 (1969).
18. V. J. Emery, *J. Low Temp. Phys.* **22**, 467 (1976).
19. M. Nakagawa, A. Matsubara, O. Ishikawa, T. Hata, and T. Kodama, *Phys. Rev. B* **54**, 6849 (1996).
20. K. N. Zinoveva, *Sov. Phys. JETP* **34**, 421 (1958).
21. W. R. Abel, A. C. Anderson, and J. C. Wheatley, *Phys. Rev. Lett.* **7**, 299 (1961).
22. D. S. Betts, D. W. Osborne, B. Welber, and J. Wilks, *Phil Mag.* **8**, 977 (1963).
23. M. P. Bertinat, D. S. Betts, D. F. Brewer, and G. J. Butterworth, *J. Low Temp. Phys.* **16**, 479 (1974).
24. M. A. Black, H. E. Hall, and K. Thompson, *J. Phys. C* **4**, 129 (1971).
25. D. N. Paulson, Ph.D. Thesis, University of California, San Diego, unpublished (1974).
26. T. A. Alvesalo, Yu. D. Anufriyev, H. K. Collan, O. V. Lounasmaa, and P. Wennerstrom, *Phys. Rev. Lett.* **30**, 962 (1973).
27. D. T. Lawson, W. J. Gully, S. Goldstein, J. D. Reppy, D. M. Lee, and R. C. Richardson, *J. Low Temp. Phys.* **13**, 503 (1973).
28. J. C. Wheatley, *Rev. Mod. Phys.* **47**, 415 (1975).
29. J. M. Parpia, D. J. Sandiford, J. E. Berthold, and J. D. Reppy, *Phys. Rev. Lett.* **40**, 565 (1978).
30. J. M. Parpia, D. J. Sandiford, J. E. Berthold, and J. D. Reppy, *J. de Phys.* **39**, C6–35 (1978).
31. D. D. Osheroff, R. C. Richardson, and D. M. Lee, *Phys. Rev. Lett.* **28**, 885 (1972); and D. D. Osheroff, W. J. Gully, R. C. Richardson, and D. M. Lee, *Phys. Rev. Lett.* **29**, 920 (1972).
32. R. Balian and N. R. Werthamer, *Phys. Rev.* **131**, 1553 (1963).
33. P. W. Anderson and P. Morel, *Phys. Rev.* **123**, 1911 (1972).
34. P. W. Anderson and W. F. Brinkman, *Phys. Rev. Lett.* **30**, 1911 (1973).
35. D. Einzel and P. Wölfle, *J. Low Temp. Phys.* **32**, 19 (1978); D. Einzel, *J. Low Temp. Phys.* **54**, 427 (1983); D. Einzel, P. Wölfle, and P. J. Hirschfeld, *J. Low Temp. Phys.* **80**, 31 (1990).
36. Data obtained by J. E. Berthold, R. W. Giannetta, E. N. Smith, and J. D. Reppy, see J. D. Reppy, *Physica* **90 B + C**, 64 (1977).
37. R. T. Johnson, R. L. Kleinberg, R. A. Webb, and J. C. Wheatley, *J. Low Temp. Phys.* **18**, 501 (1975).
38. T. A. Alvesalo, H. K. Collan, M. T. Loponen, and O. V. Lounasmaa, *Phys. Rev. Lett.* **32**, 981 (1974).
39. P. Bhattacharyya, C. J. Pethick, and H. Smith, *Phys. Rev. B* **15**, 3367 (1977).
40. C. J. Pethick, H. Smith, and P. Bhattacharyya, *Phys. Rev. B* **15**, 3384 (1977).

41. C. N. Archie, T. A. Alvesalo, J. D. Reppy, and R. C. Richardson, *J. Low Temp. Phys.* **42**, 295 (1981).
42. M. Morishita, T. Kuroda, A. Sawada, and T. Satoh, *J. Low Temp. Phys.* **76**, 387 (1989).
43. For an excellent review see I. M. Khalatnikov, in *The Physics of Liquid and Solid Helium*, K. H. Bennemann and J. B. Ketterson (Eds.), John Wiley & Sons, New York (1976), p. 1.
44. A. J. Leggett, *Rev. Mod. Phys.* **47**, 331 (1975).
45. P. K. Wölfle, *J. Low Temp. Phys.* **22**, 157 (1976).
46. D. Einzel, Nonhydrodynamic Transport in Normal and Superfluid Fermi Liquids, *Lecture Notes in Physics* **394**, M. J. R. Hoch und R. H. Lemmer (Eds.), Springer-Verlag, Berlin (1991).
47. Y. Nambu, *Phys. Rev.* **117**, 648 (1960)
48. O. Betbeder-Matibet and P. Nozieres, *Ann. Phys. (N.Y.)* **51**, 392 (1969); P. K. Wölfle, *J. Low Temp. Phys.* **22**, 157 (1976).
49. D. Pines and P. Nozieres, *The Theory of Quantum Liquids*, W. A. Benjamin, New York (1966).
50. D. Einzel and P. K. Wölfle, *J. Low Temp. Phys.* **32**, 19 (1978).
51. P. W. Anderson, *Phys. Rev.* **112**, 1900 (1958); N. N. Bogoliubov, V. V. Tolmachev, and D. V. Shirkov, *A New Method in the Theory of Superconductivity*, Consultant Bureau, New York (1959).
52. D. Einzel, P. K. Wölfle, and P. J. Hirschfeld, *J. Low Temp. Phys.* **80**, 31 (1990).
53. A. F. Andreev, *Zh. Eksp. Teor. Fiz.* **46**, 1823 (1964) [*Sov. Phys. JETP* **19**, 1228 (1964)].
54. J. Kurkijärvi and D. Rainer, in *Modern Problems in Condensed Matter Sciences*, W. P. Halperin and L. P. Pitaevskii (Eds.), Elsevier, Amsterdam (1990).
55. H. Højgaard Jensen, H. Smith, P. Wölfle, K. Nagai, and T. Maak Bisgaard, *J. Low Temp. Phys.* **41**, 473 (1980).
56. H. Højgaard Jensen, H. Smith, and P. Wölfle, *J. Low Temp. Phys.* **51**, 81 (1983).
57. D. Einzel, *J. Low Temp. Phys.* **54**, 427 (1984).
58. D. Einzel and J. M. Parpia, *Phys. Rev. Lett.* **58**, 1937 (1987).
59. Weiyi Zhang and J. Kurkijärvi, *J. Low Temp. Phys.* **73**, 483 (1988).
60. D. Einzel, P. Panzer, and M. Liu, *Phys. Rev. Lett.* **64**, 2269 (1990).
61. G. Zwicknagel and C. Toepffer, *Phys. Rev. B* **45**, 8138 (1992).
62. G. Eska, K. Neumaier, W. Schoepe, K. Uhlig, and W. Wiedemann, *Phys. Rev. B* **27**, 5534 (1983).
63. K. Uhlig, private communication.
64. D. S. Greywall, *Phys. Rev. B* **33**, 7520 (1986).
65. H. Kojima, D. N. Paulson, and J. C. Wheatley, *Phys. Rev. Lett.* **32**, 1415 (1974).
66. H. Kojima, D. N. Paulson, and J. C. Wheatley, *J. Low Temp. Phys.* **21**, 283 (1975).
67. A. W. Yanof and J. D. Reppy, *Phys. Rev. Lett.* **33**, 631, 1031(E), (1974).
68. T. Chainer, Y. Morii, and H. Kojima, *J. Low Temp. Phys.* **55**, 353, (1984).
69. J. P. Eisenstein, G. W. Swift, R. E. Packard, *Phys. Rev. Lett.* **45** 1199 (1980); and J. P. Eisenstein, Ph. D. Thesis, Univ. of Calif., Berkely, 1980 (unpublished).
70. J. M. Parpia and T. L. Rhodes, *Phys. Rev. Lett.* **51**, 805 (1983).
71. J. E. Jaffe, *J. Low Temp. Phys.* **37**, 567 (1979).
72. D. C. Carless, H. E. Hall, and J. R. Hook, *J. Low Temp. Phys.* **50**, 583 (1983).
73. O. Ishikawa, M. Nakagawa, A. Matsubara, T. Hata, and T. Kodama, *J. Low Temp. Phys.* **101**, 799 (1995).
74. M. Nakagawa, O. Ishikawa, T. Hata, and T. Kodama, *Physica B* **194–196**, 781 (1994).
75. J. R. Hook, E. Faraj, S. G. Gould, and H. E. Hall, *J. Low Temp. Phys.* **74**, 45 (1989).
76. D. N. Paulson and J. C. Wheatley, *Phys. Rev. Lett.* **41**, 561 (1978).
77. Y. A. Ono, J. Hara, K. Nagai, and K. Kawamura, *J. Low Temp. Phys.* **27**, 513 (1977).
78. P. K. Wölfle and D. Einzel, *J. Low Temp. Phys.* **32**, 39 (1978).
79. J. Hara, Y. A. Ono, K. Nagai, and K. Kawamura, *J. Low Temp. Phys.* **39**, 603 (1980).
80. Y. A. Ono, J. Hara, and K. Nagai, *J. Low Temp. Phys.* **48**, 167 (1982).
81. D. Einzel, *J. Low Temp. Phys.* **54**, 427 (1984).

82. D. Einzel, P. K. Wölfle, H. Højgaard Jensen, and H. Smith, *Phys. Rev. Lett.* **52**, 1705 (1984).
83. D. C. Carless, H. E. Hall, and J. R. Hook, *J. Low Temp. Phys.* **50**, 605 (1983).
84. E. K. Zeise, Ph.D. Thesis, Cornell University, 1981, (unpublished). See also Figs. 5, 8, 9 of Ref. 83.
85. J. P. Eisenstein and R .E. Packard, *Phys. Rev. Lett.* **49**, 564 (1982).
86. H. E. Hall and J. R. Hook, *Progress in Low Temperature Physics, IX*, D. F. Brewer (Ed.), Elsevier, New York (1986).
87. H. Brand and M. C. Cross, *Phys. Rev. Lett.* **49**, 1959 (1982).
88. D. Einzel, 1984 (unpublished).
89. F. Topsøe and H. Højgaard Jensen, *J. Low Temp. Phys.* **55**, 469 (1984).
90. N. Pavloff and J. Treiner, *J. Low Temp. Phys.* **83**, 331 (1991).
91. M. P. Bertinat, D. S. Betts, D. F. Brewer, and G. J. Butterworth, *Phys. Rev. Lett.* **28**, 472 (1972).
92. H. E. Hall, *Proc. of the European Physical Soc., Topical Conf., Haifa 1–4 July, 1974*, C. G. Kuper, S. G. Lipson, and M. Revzen (Eds.), John Wiley & Sons, New York (1975), p. 375.
93. M. J. Lea, P. W. Retz, and P. Fozooni, *J. Low Temp. Phys.* **66**, 325 (1987).
94. A. M. Guenault, V. Keith, C. J. Kennedy, and G. R. Pickett, *Phys. Rev. Lett.* **50**, 522 (1983).
95. G. G. Stokes, *Mathematical and Physical Papers, Vol. 3*, Cambridge University Press, London (1901), p. 38.
96. A. M. Guenault and G. R. Pickett, *Physica* **126B**, 260 (1984).
97. M. R. Freeman, Ph.D. Thesis, Cornell University, 1988, (unpublished).
98. D. A. Ritchie, J. Saunders, and D. F. Brewer, *Phys. Rev. Lett.* **59**, 465 (1987).
99. Chengtai Wang and Lu Yu, *Physica B* **169**, 529 (1991).
100. R. König and F. Pobell, *J. Low Temp. Phys.* **97**, 287 (1994).
101. S. C. Steel, P. Zawadzki, J. P. Harrison, and A. Sachrajda, *Physica B* **165** & **166**, 599 (1990).
102. A. L. Fetter and S. Ullah, *J. Low Temp. Phys.* **70**, 515 (1988).
103. S. M. Tholen and J. M. Parpia, *Phys. Rev. Lett.* **67**, 334 (1991); *Phys. Rev. B* **47**, 319 (1993).
104. S. M. Tholen and J. M. Parpia, *Phys. Rev. Lett.* **68**, 2810 (1992).
105. D. Kim, M. Nakagawa, O. Ishikawa, T. Hata, T. Kodama, and H. Kojima, *Phys. Rev. Lett.* **71**, 1581 (1993).
106. M. J. Lea, P. Fozooni, and P. W. Retz, *J. Low Temp. Phys.* **54**, 303 (1984).
107. Z. Sh. Nadirashvilli and Dzh. G. Tsakadze, *J. Low Temp. Phys.* **37**, 169 (1979); *Sov. J. Low Temp. Phys* **4**, 711 (1978).
108. P. H. Roberts and R. J. Donnelly, *J. Low Temp. Phys.* **15**, 1 (1974).
109. A. P. Borovikov and V. P. Peshkov, *Zh. Eksp. Teor. Fiz.* **70**, 300 (1976); [*Sov. Phys. JETP* **43**, 156 (1976)].
110. E. L. Andronikashvili, *Zh. Eksp. Teor. Fiz.* **18**, 424 (1948).
111. A. D. B. Woods and A. C. Hollis-Hallet, *Can. J. Phys.* **41**, 596 (1963).
112. D. F. Brewer and D. O. Edwards, *Proc. R. Soc. A* **251**, 247 (1959).